Experimental Investigation of An R134a Based Organic Rankine Cycle

by

Shaikh Md Emdadul Hoque

A Thesis Submitted in Partial Fulfillment
of the Requirements for the Degree of

Master of Applied Science

in

The Faculty of Engineering and Applied Science

Mechanical Engineering

University of Ontario Institute of Technology

August 2011

Abstract

This thesis research aims to develop an improved, efficient, low-capacity heat engine, running on an Organic Rankine Cycle (ORC) to generate power. The ORC is driven by low or moderate temperature heat sources, such as; renewable energy in the form of a hot gas derived from biomass/biogas/biofuel combustion streams, waste heat recovery, process heat recovery, etc. The ORC is more suitable and flexible than a conventional steam Rankine cycle, especially when it is applied to low power range. In this research, an extended surface heat exchanger is used to boil the pressurised working fluid, R134a, using a hot air as heat source. The expander used is a scroll type, coupled to a generator, which is able to produce maximum 1.6 kW output. Experimental data of the heat engine are measured under different operating conditions and utilized in the analysis and comparisons. Power generation under various conditions is investigated in order to determine the optimum performance parameters for the heat engine.

The isentropic efficiency of the expander is found to be over 40% and reaches 80% for the improved expansion conditions. For the boiler, it is determined that the overall heat transfer coefficient multiplied with the heat transfer area is around 150 W/K. The energy efficiency of the experimental ORC is around 3% for hot air as the low temperature heat source at about 105^{o}C where exergy efficiency reaches 22%, respectively.

Acknowledgements

It is my pleasure to express my sincere thanks and appreciation to my supervisor, Dr. Ibrahim Dincer, for giving me the opportunity to work on developing a suitable heat engine for a small scale renewable energy generation unit. I was lucky to have his support and guidance for this research throughout the process. He gave me the courage and self confidence to explore and experiment. His confidence in me was a great source of motivation and his guidance and support for me was an extremely valuable resource.

I would like to acknowledge the financial support provided by the Ontario Center of Excellence (OCE) and Cleanfield Energy Inc.

I also acknowledge and appreciate Dr. Calin Zamfrescu's help in completing the test and experiment with new ideas and expertise to improve the project work.

I would like to express my gratitude to the research team player, Janette M. Hogerwaard, Ali Tariq, Kishor Govind Nayar and acknowledge the contributions of Snahungshu Sikder.

Finally, I am thankful to my wife, Tasmin Shafi, and my sons, Behrooz Hoque and Behzad Hoque, for their patience and confidence in me as I complete my Master's Degree in Mechanical Engineering from the University of Ontario Institute of Technology.

Contents

List of Figure Captions

List of Table Captions

Nomenclature

A	Area (m^2)
c	Capacity ratio
C_i	Heat capacity (kW/K)
C_p	Specific heat, (kJ/kg K)
D	Diameter (m)
D_h	Hydraulic diameter (m)
E_i	Correlation factor
Ex	Exergy (kW)
e	Error
F	Correction factor
f	Friction factor
G	Mass velocity (kg/m^2 s)
h	Enthalpy (kJ/kg)
h_i	Convective heat transfer coefficient (W/m^2 K)
I	Current (Amp)
j	Colburn factor
l	Length (m)
k	Conductivity (W/m K)
m	Mass (kg)
$\dot{m}$	Mass flow rate (kg/s)
N	Number
NTU	Number of transfer units
Nu	Nusselt number
P	Pressure (kPa)
Pr	Prandtl number
$\dot{Q}$	Heat transfer rate (J/s)
R	Thermal resistance (m^2 K/W)
r	radius (m)
Re	Reynolds number

s	Entropy (kJ/kg K)
T	Temperature (K,^{o}C)
U	Overall heat transfer coefficient (W/m^2 K)
$\dot{V}$	Volumetric flow rate (m^3/s)
V	Voltage (V); Volume (m^3)
v	Velocity (m/s)
VR	Volumetric ratio
W	Work (kJ)
$\dot{W}$	Work rate (kW)
x	Wall thickness (m)

Greek letters

α	Area ratio
β	Correlation factor
Δ	Difference (m)
δ	Thickness (m)
γ	Correlation factor
ε	Heat transfer effectiveness
η	Efficiency
σ	Area ratio
ϕ	Correlation factor
μ	Dynamic viscosity (kg/m s)
ρ	Density (kg/m^3)
ψ	Exergy efficiency
υ	Volume (m^3)
ζ	Correlation factor
τ	Torque (Nm)
ω	Angular velocity (rad/s)

Subscripts

air	Air
avg	Average
b	Base
blow	Blower
c	Cold fluid
comp	Compressor
cond	Condenser
el	Electrical
evap	Evaporator
exp	Expander
fanning	Fanning fcator
f	Fin
ff	Free flow
fr	Frontal area
gen	Generator
h	Hot fluid
ht	Heat transfer
h.ex	Heat exchanger
I	Current
i	Inlet/inner
in	input
lm	Logarithmic mean
m	Mean
max	Maximum
min	Minimum
n	number
O	Reference state; outside *roughness*
o	Outer; overall
out	Output
P	Constant pressure or pump

s	Surface
sat	Saturated
shell	Shell variable
shaft	Shaft
tube	Tube variable
V	Constant volume
w	Wall
∞	Ambient

CHAPTER 1: INTRODUCTION

1.1 Importance of energy

From the time we wake up to the time we go to sleep at night, energy affects our lives. Energy is essential to everyone's life, whether we notice it or not; without energy and power our lifestyle would be different and more difficult than what we experience day to day. Energy is the essential element in all aspects of life from human movement to social redevelopment. People are constantly using energy from the beginning of the journey of human life on earth and within every human society, region and country. Human beings use energy in different forms for different utilities, like heat, electricity, etc. The more developed country, the more energy its' population is consuming. Also, it must be mentioned that demand of energy use is increasing every year. Important considerations include: How much energy we are using in this world per year; how efficiently we are using energy; how much energy we are wasting every year. Waste energy has the adverse influence on the environment of effectively increasing environmental entropy. Demand for energy is increasing every year in all parts of the world. As per the United States Energy Information Administration (US EIA) the total energy consumption trend from 2007 to 2035 is projected as shown in Figure 1.1. In 2008 and 2009, World energy consumption was contracted. But it is expected to increase again soon.

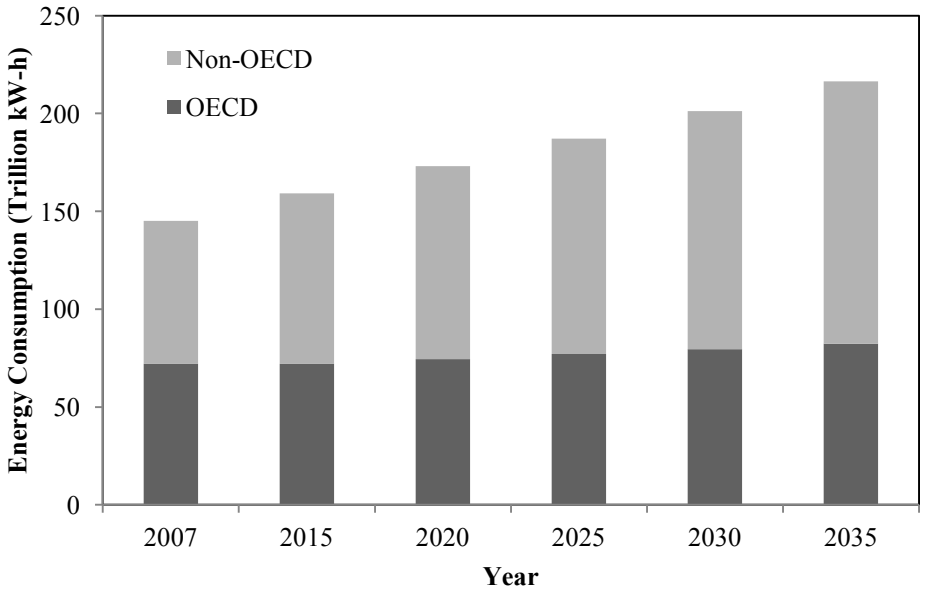

Figure 1.1 World energy consumption [data from (US-EIA, 2010)].

There are many types of energy sources available in this World: Fossil fuel: oil, coal and natural gas; green energy; nuclear, solar, wind power, wave energy, geothermal, hydro-electric, and biomass. With every type of energy used, there is some portion of it lost as waste energy every day, especially from industrial applications. The industry generates low grade waste heat in the form of heat (emission), hot water, flue gas, steam, etc.

In the analysis of energy supply and demand criteria it may be mentioned that energy demand has an inherent trend to increase due to population growth and economic development. On the other hand, energy supply has finite reserve in non-renewable sources and an infinite availability in renewable sources; though the vast majority of the world's energy consumption is still dependent on non-renewable sources, specifically oil, coal and gas. Renewable energy sources may be considered as a cleaner alternative in many applications currently using non-renewable sources. This has the potential to slow the rate of depletion of limited resources; thus, the development of technology for the application of renewable energy sources has become important in the field of research.

1.2 Motivation and Objectives

Low grade heat is abundantly available in renewable energy sources, and in industrial waste. Harnessing this type of sustainable energy could substitute the use of non-renewable energy and eventually mitigate the environmental impacts of non-renewable sources. Development of efficient technologies is required to generate useful work out of these sources. An organic Rankine cycle is a suitable candidate for this purpose.

The organic Rankine cycle (ORC) works with organic, high molecular mass working fluid(s), which have the characteristic of having the liquid-vapor phase change, or boiling point, occur at a lower temperature than the water-steam phase change. The organic fluid allows Rankine cycle heat recovery from lower temperature sources such as biomass combustion, industrial waste heat, geothermal heat, solar collectors, etc. The low-temperature heat is converted into useful work that can itself be converted into electricity. The working principle of the organic Rankine cycle is the similar to the Rankine cycle where the working

fluid is pumped to a boiler for evaporation, passes through a turbine and is finally re-condensed.

Through consideration of the parameters and characteristics of ORCs and various working fluids, the conclusion is made to employ a Scroll compressor operated in reverse as the expander, with R134a as the working fluid for analysis in this project.

The goal of this work is to contribute to the development of a low capacity heat engine for heat recovery and sustainable power production and/or cogeneration applications. Thus, the specific objectives of this thesis are given as following:

- To design a heat exchanger to collect heat from hot air (biomass or other sources) to refrigerant as working fluids (R134a).
- To modify the scroll compressor to become an expander for ORCs.
- To design and construct double pipe heat exchangers to sub-cool working fluids.
- To design and construct the electrical heating wire load to consume generated electrical power.
- To select the proper measuring equipment to measure data from the system.
- To conduct analytical and thermodynamic modeling of the heat transfer process of the boiler and system.
- To design and set-up the heat engine test bench for experiments with different parameters.
- To perform an analysis of the experimental results from the scroll expander and heat exchanger in an ORC test unit.
- To validate the thermodynamic model with experimental results.
- To study both energy and exergy efficiencies for the system and its components.
- To analyze the case studies for system improvement.

CHAPTER 2: LITERATURE REVIEW

The interest in low grade heat recovery has grown dramatically in the past decades. Several possible solutions have been developed to generate electricity from low temperature heat sources available in solar energy, biomass, engine exhaust gases, domestic boilers, and so on. Among those, the Organic Rankine Cycle (ORC) is considered the most suitable due to its simplicity and the availability of its components. In these systems, the working fluid is an organic component and better adapted than water in the context of using lower heat source temperatures. Unlike traditional power cycles, local and small scale power generation is an attractive criterion of using this technology.

Several researchers from different parts of the world have worked and are working on ORC classification, ORC industrial application, ORC design aspects, external heat exchanger uses for the ORC, ORC prime mover, and ORC working fluid selection, among other things. In this chapter, those researches are briefly discussed.

2.1 ORC classification

The Organic Rankine Cycle does not have any standard classification based on their operating temperature range, size of operation or type of heat sources. However, different researchers have classified the ORC in different ways. Peterson et al. (2008) classified heat sources for ORC in three categories based on their operating temperatures as follows:

1. Low-temperature (Temperature range: 80^{o}C - 150^{o}C),
2. Medium-temperature (Temperature range:150^{o}C - 500^{o}C) and
3. High-temperature (Temperature range: 500^{o}C).

However, Borsukiewicz-Gozdur and Nowak (2007) considered a low-temperature range between 25^{o}C and 150 ^{o}C while Saleh et al. (2007) assumed that the low-temperature range is around 100 ^{o}C, and medium-temperature heat sources are between 100^{o}C - 350^{o}C. Latour et al. (1982) categorized temperature levels of 0^{o}C - 121^{o}C as low, 121^{o}C - 649^{o}C and medium, 649^{o}C - 1093^{o}C as high, respectively.

The overall classification of the temperature band is mainly dependent on the type of the source. Geothermal energy, nuclear energy, ocean thermal, solar radiation, biomass and heat recovery from mechanical units can be heat sources for the ORC. Generally, geothermal heat sources are available at temperatures of 80^{o}C - 150^{o}C. Solar radiation on flat panels generates heat at a temperature of approximately 80^{o}C, while at high concentration the temperature goes up to 200^{o}C. Heat recovery unit temperatures vary with the operating temperature of the system equipment and its efficiency. However, nuclear and combustion energy are in the category of high temperature heat sources.

2.2 ORC industrial applications

With the increase of environmental awareness, changes in government policy on environmental issues, the price hike on fuel, and tougher competition on product cost, a growing number of industries are trying to cut their energy bills by using such small, and middle scale power production. ORC manufacturers have been present in the market since the 1980's. They provide wide range of solutions based on the temperature level and sources. Table 2.1 shows the existing ORC manufacturer and their technology.

From Table 2.1 we can conclude that that small and middle scale power production from renewable sources using the ORC can be applied to:

- Biomass and bio-fuel
- Solar power plants
- Heat recovery from mechanical equipment and combustion engines.
- Geothermal energy and ocean thermal energy.

We can also restrict the scope of our review to the range of source temperature between the standard 25°C and 250°C, and denote this range as "low-temperature". The justification of choosing this range is based on two facts:

1. The vast majority of renewable and sustainable energy sources fall within this temperatures range.

2. The current technology allows the use of positive displacement expanders or expander-generator units operating at temperatures below 250°C.

Table 2.1 Energy sources and application of ORC.

Manufacturer	Applications	Power range	Heat source temperature (°C)	Technology
ORMAT, US	Geothermal, WHR, solar	200 kW –72 MW	150 - 300	Fluid: n-pentane
Turboden, Italy	Geothermal, CHP	200 kW–2 MW	100 - 300	Fluids: OMTS, Solkatherm Axial turbines
Adoratec,Germany	CHP	350 kW–1600 kW	300	Fluids: OMTS
GMK, Germany	Geothermal, CHP, WHR	50 kW –2 MW	120 - 350	3000 rpm Multi-stage axial turbines (KKK) Fluid: GL160 (GMK patented)
Koehler-Ziegler, Germany	CHP	70-200 kW	150 – 270	Fluid: Hydrocarbons Screw expander
UTC, US	Geothermal, WHR,	280 kW	>93	
Cryostar	WHR, Geothermal	n/a	100 - 400	Radial inflow turbine Fluids: R245fa, R134a
Freepower, UK	WHR	6 kW - 120 kW	180 - 225	
Tri-o-gen, Netherlands	WHR	160 kW	>350	Turbo-expander
	WHR	50 kW	>93	Twin screw expander
Infinity Turbine	WHR	250 kW	> 80	Fluid: R134a Radial Turbo expander

Sources: Sylvain el (2009), Citrin, (2005, Gaia, (2006), Lorenz, (2006), Holdmann, (2007), Schuster, (2009).

2.2 ORC design aspects

To develop heat engines with externally supplied heat sources, the designer has to give emphasis on two main thermodynamic constraints: the heat source, and the heat sink. These two cycle components determine the magnitudes of the heat transfer between the heat source and the heat sink via the working fluid. The Organic Rankine Cycle, and its variations, is identified as an excellent choice for using the low grade heat sources as mentioned by

Zamfirescu and Dincer (2008). They point out that its flexible nature, and the possibility to adapt precisely to the temperature difference between the heat source and heat sink represents it as an appropriate cycle. Proper selection of working fluid is also an important factor in this respect. Zamfirescu and Dincer (2008) propose a trilateral flash Rankine cycle with a zeotropic ammonia-water as the working fluid. In this cycle, liquid ammonia-water at a high pressure is heated to its saturation temperature and then flashed into the two phase region to generate work with the help of a positive displacement expander. The cycle shows an exergy efficiency of 30% when supplied with a 150^{o}C geothermal heat source. This value is well above the 13% exergy efficiency achieved with a Kalina cycle operating under the same conditions.

The Kalina cycle varies from the Rankine cycle in the context that it uses ammonia-water as the working fluid. Also, the Kalina cycle heats the working fluid into a superheated vapour, as opposed to the Tri-lateral flash cycle. During the boiling process, the ammonia-water varies in temperature. Due to this, the Kalina cycle offers the opportunity to better match the temperature profiles in heat exchangers. Pure ammonia has also been investigated for low power applications. The heat recovery process, coupled with this cycle, is an attractive application. (Koji, 2004). In a transcritical Rankine cycle, carbon dioxide can be used as a working fluid; however, its high operating pressure poses a challenge in using it in a transcritical cycle. Shell construction, internal leakage, bearing load and bearing lubrication are the main concern of this drawback. Due to such challenges, the development of commercial transcritical carbon dioxide Rankine cycles for low capacities may be judged inappropriate.

Chen et al. (2006) depicted in his literature that for a 140^{o}C heat source, a transcritical carbon dioxide Rankine showed an efficiency of 9.2%. When compared to a R123 organic Rankine cycle operating at the same conditions, only a minor increase of 1.4% in efficiency was observed. They mentioned further that the R123 ORC operated at a boiling pressure of 5.87 bar and a condensation pressure of 0.85 bar. The pressure ratio was thus 6.9 and the pressure difference was 5.02 bar. This pressure difference is much lower than the typical transcritical carbon dioxide cycle which is normally 80 bar. Therefore, the ORC works with

less technical problems than the transcritical carbon dioxide cycle. This point signifies the advantage of using organic fluids as working fluid in Rankine cycles.

There are many configurations of the organic Rankine cycle driven from the basic one. The basic configuration of the ORC consists of four components: pump, boiler, prime mover (turbine or expander), and condenser. Dai et al. (2009) conducted a comprehensive parametric study of multiple configurations of the ORC. Apart from the basic Rankine cycle, they identified the following configurations:

- ORC with heat recovery within the system via a heat exchanger.
- Supercritical ORC, where the liquid is pressurized to supercritical pressure and then applied heat to raise the temperature above the critical point before commencing expansion process.
- Subcritical ORC, operating with retrograde working fluids with expansion of saturated vapour.

Other Rankine cycle configurations are those with expansion into the two phase region. The benefit of expanding into the two phase region has been pointed out in the work by Wagar et al. (2010). They explained that expanding into the two phase region is a way of adjusting the cycle to the exterior conditions. Smith et al. (1996) in his research proposed an interesting cycle combined flash expansion and saturated vapour expansion working with R134a as the working fluid. Saturated liquid is first flashed into the two phase region and the two phase mixture is then separated gravitationally into saturated liquid and saturated vapour components. An expander is used to flash the liquid while the saturated vapour is expanded into the two phase region. Selection of the expansion device is an important factor in this case due to the pressure sensitivity of two phase flows. The positive displacement expander is found suitable to work as an expansion device. Smith et al. (1994) incorporated a positive displacement screw expander to flash the liquid and a turbine for expanding the two phase mixture. The advantage of selecting the screw expander is its ability to flash the liquid and expand the saturated vapour while retaining an R134a stream of high quality.

2.2.1 Heat exchanger for ORC

Another important factor that affects the performance of the exhaust waste heat recovery using an ORC is designing the evaporator. The evaporator temperature and evaporator effectiveness are the two main factors in the evaporator side of the cycle. This temperature has to be selected in such a way that no condensation occurs in the evaporator. Water condensation has a great influence on the tube corrosion of the evaporator. Another important phenomenon is that the first and second law efficiencies of an ORC increase with the increment of the evaporator temperature, which will also increase the overall performance of the total ORC system. Regarding the evaporator effectiveness, it is clear that with the increase of evaporator effectiveness, the PPTD [Pinch Point Temperature Difference] decreases. This trend also indicates that higher exergy efficiencies are possible by choosing higher value of evaporator effectiveness. However, as discussed above, this entails a higher cost as a result of the fact that larger evaporators are needed to facilitate heat transfers across smaller temperature differences. On the other hand, favouring the lower evaporator effectiveness presents a practical problem of water condensation in the evaporator tubing. Therefore, a compromise has to be made between these two factors by selecting a temperature which is above the condensation temperature.

Several researchers worked in designing the evaporator based on detailed thermodynamic analysises of an ORC. Evaporators being a heat exchanger, established heat exchanger design principles are used with the determined parameters of an ORC. Probert and Badr (1990) were the first to study the thermal design data of evaporators for ORCs. They considered several factors for designing, particularly:

- the velocity of the heating fluid in the heat exchanger tubes
- the pinch-temperature difference
- the outlet temperature
- the inlet temperature
- the load of the evaporator
- the net power output from the Rankine engine

Dai et al. (2009) applied the second-law analysis of the evaporator for ORC. They concluded that the evaporating pressure plays a key role in evaporator design for ORC system. They also pointed out that designing the evaporator and selecting the fluid should be in such a way as to minimize the second-law losses.

Several researchers have used several types of evaporators for heat recovery in their ORC systems. Hung et al. (2009) used waste heat boiler as an evaporator to collect heat from the solar heat source. However, several researchers like Saleh et al. (2008) and El Chammas and Clodic, 2005, have used a conventional fin type heat exchanger as an evaporator. This type of heat exchanger has the capability to extract more heat from the source stream by the higher exposed surface area. For our experiment, we will use a fin type evaporator for heat recovery from hot air.

2.2.2 Working fluid selection

The selection of working fluid in compliance with the operating parameters determined by thermodynamic analysis is an important factor. Many research works have been done regarding the selection of the best working fluid for an organic Rankine cycle. In most of the research literature it has been indicated that the best available options are pure working fluids, or a mixture of working fluids, where the mixtures can be zeotropic or azeotropic. Fluid characteristics also have a great influence in determining the cycle configuration. For example, if a retrograde fluid is used, then the expansion of saturated vapour occurs in the superheated region. This is due to the fact that the slope of the saturation curve on a T-s diagram for retrograde fluids is always positive. On the other hand, if the fluid is regular, then the expansion of saturated vapour occurs in the two phase region. Harada (2010) emphasized the importance of the retrograde or regular behaviour of the working fluid for low-capacity applications using R134a (regular) and R245fa (retrograde). Borsukiewicz-Gozdur and Nowak (2007) studied propylene, propane, R227ea, R236fa and RC 318. Schuster et al. (2009) studied cyclohexane, R245fa, R141b and R365mfc. Larioala (1995) studied R11, R113, R114, toluene, and fluorinol (CF_3CH_2OH). Saleh et al. (2007) studied 21 organic refrigerants and 10 other organic fluids, among which n-hexane had the highest critical temperature (234.67^{o}C) and R41 the lowest (44.25^{o}C). Mago et al. (2008) studied R113,

R123, R245ca and isobutane. Some zeotropic mixtures of organic fluids were identified by Borsukiewicz-Gozdur and Nowak (2007) as propane-ethan, siloxanes, namely MM, MD_4M, D_4 and D_5. A complete literature summary of the working fluids is given in Table 2.2.

Table 2.2 Summary of different working fluid comparisons.

References	Application	Condenser Temperature (°C)	Evaporator Temperature (°C)	Working Fluid
Saleh et al.	Geothermal	30	100	alkanes, fluorinated alkanes, ethers and fluorinated ethers
Maizza and Maizza (2001)	n/a	35 –60	80 – 100	Unconventional working fluids
Liu et al. (2004)	Waste heat recovery	30	150 – 200	R123, iso-pentane, HFE7100, Benzene Toluene, p-xylene
El Chammas and Clodic (2005)	ICE	55 (100 for water)	60 - 150 (150 – 260 for water)	Water, R123, isopentane, R245ca, R245fa, butane, isobutene and R-152a
Drescher and Bruggemann (2007)	Biomass CHP	90°C	250 - 350	ButylBenzene, Propylbenzene, Ethylbenzene, Toluene, OMTS
Lemort et al. (2007)	Waste heat recovery	35	60 – 100	R245fa, R123, R134a,n-pentane
Hettiarachchia et al. (2007)	Geothermal	30°C	70 – 90	Ammonia, n-Pentane, R123, PF5050
Borsukiewicz-Gozdur and Nowak (2007)	Geothermal	25	80 – 115	propylene, R227ea, RC318, R236fa, ibutane, R245fa
Fankam et al. (2009)	Solar	35	60 – 100	Refrigerants

Various researchers, such as Papdopoulos et al. (2010) and Quoilin and Lemort (2005), suggest that the working fluid selection is the key element for designing an ORC. According to them, the most important fluid characteristics/properties are:

1. Thermodynamic and physical properties; density, boiling enthalpy, liquid heat capacity, viscosity, thermal conductivity, melting point temperature, critical temperature, critical pressure, and the zeotropic or azeotropic characteristic.
2. Lower environmental impact and higher safety: The main parameters are ozone depletion potential (ODP), global warming potential (GWP), toxicity, flammability.
3. Commercial availability and low cost.
4. The life time of the working fluid is also important: according to Harada (2010), the lifetime R11 is 45 years while that of R152 is 0.6 years; however, the R11 has a GWP of 6370 and ODP of 11, while R152 has a GWP of 187 and zero ODP.

2.3 Prime movers for ORC

The prime mover is the main component of any power cycle. According to Harada (2010), the prime mover affects the overall efficiency of the heat engine. While operating with organic fluids, the pressure ratio over the prime mover is typically high. To operate in high pressure, special construction is necessary for the expander. So, different researchers have proposed different types of turbo-expanders, such as turbine and axial piston, rolling piston, rotary vane, screw, scroll and other kinds of compressors. Lariola (1995) first developed turbines to be used as a turbo expander in the ORC. Yamamoto (2001) designed a turbine for a small scale ORC and obtained 15-46% isentropic efficiency where the heat input varied from 13 kW to 9 kW. Generally, ORC turbines are high speed turbines. According to Yogoub et al. (2006), turbine RPM reaches 60,000 or more. Though they are quite effective, they are sensitive to operating conditions and are designed for specific condition. Furthermore, due to the tip leakages in turbines, bypass flow at low capacities is not negligible with respect to the main flow. This decreases the efficiency of the low capacity ORC turbines.

As stated earlier, positive displacement expander can be used as a prime mover in ORC. Smith et al. (1996) reported that twin screw expanders were found to be suitable for a capacity range from tens to hundreds of kW. Again, Maurer et al. (1999) performed an investigation on axial piston expanders and showed its volumetric efficiency as about 30% and the isentropic efficiency is about 41%. Screw expanders show good adaptability to the operating conditions as they are able to work in two phase (Infante Ferreira et al., 2004). Wang et al. (2010) used a rolling piston type expander in an ORC with R245fa using low grade solar heat. It achieved a

maximum isentropic efficiency of 45.2%. Mustafah and Yamada (2010) thermodynamically analyzed a rotary vane expander with R245fa for hot side temperatures between 60^{o}C and 120^{o}C, and predicted that achievable isentropic efficiency could be over 80%. Arguably the best choice of positive displacement expanders at low capacity is scroll.

The geometry of scroll machines is simpler than that of a screw machine because the scroll has 2D geometry while the screw has 3D geometry. Thus, scroll units are comparatively more silent and easier to manufacture at low capacities. Yanagisawa et al. (1988) also modified a refrigeration scroll compressor and tested it in an experimental loop operating with compressed air. The maximum isentropic efficiency determined was 75%. Zanelli and Favrat (1994) converted a hermetic scroll compressor to an expander and tested it in a Rankine cycle. The maximum overall isentropic efficiencies were about 63% at a rotating speed of 2400. Nagatomo et al. (1999) investigated the performance characteristics of a scroll expander modified from a refrigeration compressor in an ORC, and obtained a maximum expander efficiency of 74%. Kim et al. (2001) used a scroll expander in a low temperature recovery system, and found its volumetric efficiency to be 42.3%. Husband and Beyene (2008) presented a theoretical model of low grade heat driven Rankine cycle with a scroll expander and showed thermal efficiency of 11% for a10 kW work output. Harada (2010) tested a scroll expander modified from a refrigeration scroll compressor with R134a and R245fa and found the isentropic efficiency was over 70% for 1 kW power. The geometrical modeling of scroll expanders has been investigated by Bush and Beagle (1992) and Chen et al. (2002), based on the involute curve theory. Expressions for fluid pocket volumes, which are very important in thermodynamic modeling, were developed by Wang et al. (2005). Thermodynamic models for the scroll machine were presented by Lemort et al. (2009), Oralli et al. (2010), and Harada (2010). Leakage or by-pass flows in scroll machines were studied by Tojo et al. (1986), Sufueji et al. (1992), and Puff and Mogolis (1992).

2.4 Experimental system

Two kinds of testing loops for scroll expanders are remarked on in the literature. They are:

1. ORC with Expander: This approach has been adopted by a large number of authors, such as Peterson et al. (2008), Lemort et al. (2009) and Mathias et al. (2009). In this case, they integrated an expander with the ORC loop.
2. ORC loop with compressor: In this case, after expansion, the working fluid is delivered back to the compressor suction to close the loop; this approach has been taken by Harada (2010).

2.5 Closing remarks

In summary, the above presented literature review reveals the following:

- An integrated analysis of the four aspects discussed above (ORC applications, design, prime movers and experimental systems) was not performed thoroughly in the past.
- Simulating a low to moderate heat source and their influence on heat transfer in heat exchanger of the test bench was not performed.
- Test bench pressure head losses within the system were not determined to minimize the fluid power losses.
- Provision for the wide flexibility of the operating parameters of the test bench was not adopted by designing a modified Rankine cycle.
- Reported research in the literature was performed with a single scroll machine which declined the scope of comparing the result for better investigation and conclusion.

CHAPTER 3: BACKGROUND

Thermal energy available in sustainable sources can be used for various purposes, directly in the process plant or converted into mechanical work to generate electrical power. Methods of converting sustainable thermal energy into useful mechanical work represent a very important issue regarding the achievement of developing a clean, non-polluting, non-exhaustible energy supply system for future generations. Use of the source of energy compatible to the heat engine for particular application is a decision factor with respect to efficiency, availability of the equipment, and project cost. In this chapter, we will identify and categorize sustainable thermal energy sources and discuss the available heat engines that can be used to convert thermal energy into useful work. The importance and scope of applications of ORC-based heat engines are explained and the main issues regarding their development are discussed. As the main components of this heat engine are the expansion device, expander and evaporator (boiler), the principal categories of evaporators and their required design parameters for optimal operation in the ORC are reviewed. This chapter focuses on the extended finned evaporator in ORC.

3.1 Sustainable energy sources for heat supply

Currently the main fossil fuel sources for thermal energy are coal, petroleum, and natural gas. The combustion of coal, petroleum, and gases are used to generate high pressure steam to run turbines and generators in large scale power plants to produce electricity. Thermal energy sources and heat engine systems supply the energy needed for our society. As a by-product of the combustion process, it also generates a large amount of GHGs (Green House Gases) and other pollutants. This is the major drawback of the use of fossil fuel. Despite their adverse effect on environment, fossil fuels, in addition to generating electricity, also have wide range of applications in space heating, water heating, and many industrial processes.

Society is on a quest for alternative energy sources to mitigate the environmental impact of fossil fuels. There are established potential sources of energy to replace fossil fuels which are abundant in renewable energy; nuclear energy, and waste heat recovery. Developments of appropriate and effective technology to use these sources are the main concern. In Figure 3.1 the available thermal energy sources are categorized. The probable application of these energy

sources are also mentioned in the figure. Heat engines can be used for sustainable power generation with these and other valuable usage such as heating, cooling and so forth. A more efficient use of simultaneous power generation and heating is possible with a modified ORC heat engine.

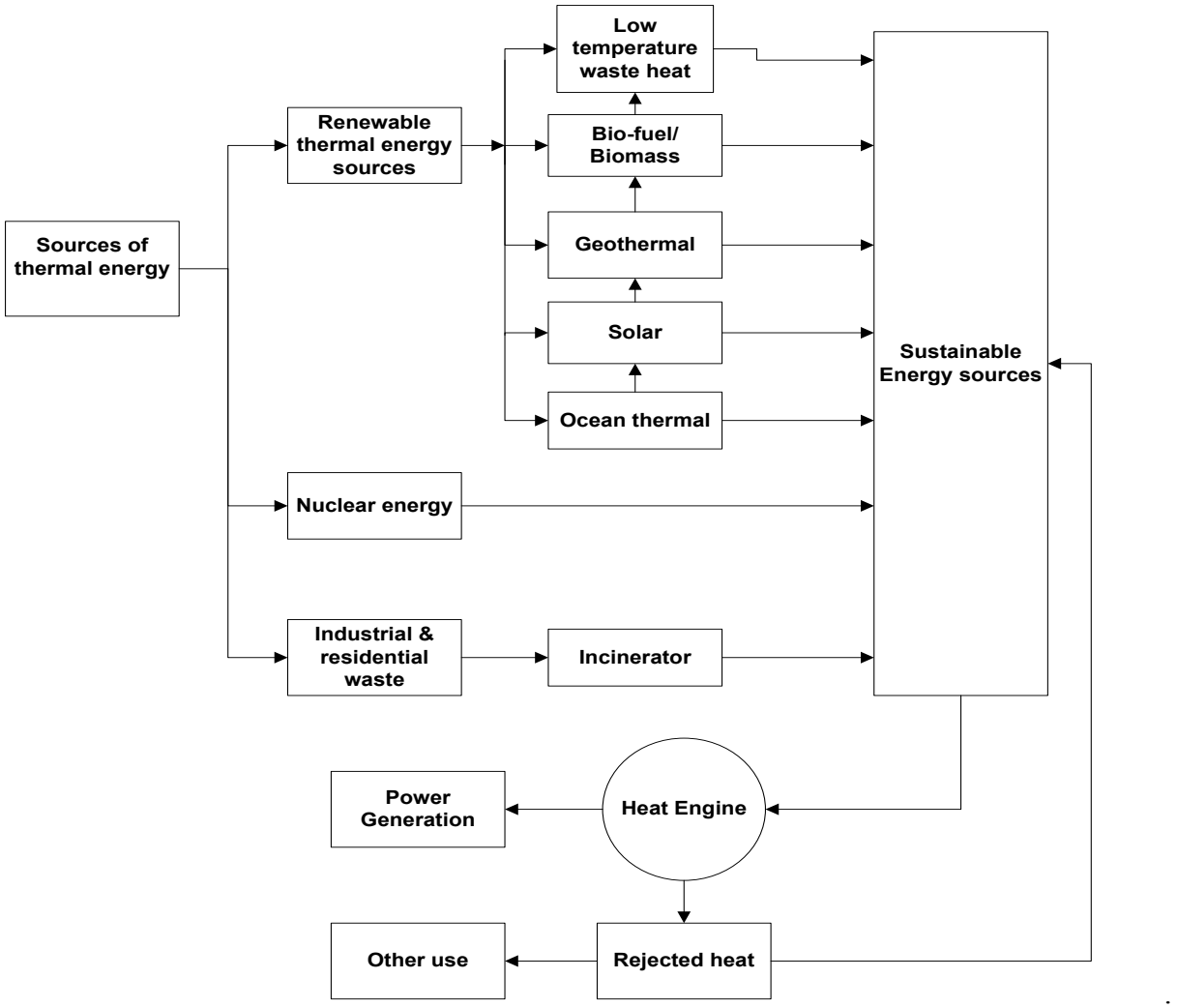

Figure 3.1 Sustainable thermal energy sources and their applications in heat engines.

3.1.1 Thermal energy sources for ORC

Waste heat recovery: Waste heat recovery is one of the most important development fields for the Organic Rankine Cycle (ORC). It may be applied to heat and power plants (for example, a small scale cogeneration plant on a domestic water heater). It also can be used for industrial and farming processes, such as organic product fermentation, hot exhausts from ovens or furnaces, flue gas condensation, exhaust gases from vehicles, inter cooling of a compressor, condenser of a power cycle, and so on (see Quoilin 2007, Delaye 2009).

Biomass power plant: Biomass is available all over the world and can be used for the production of electricity on small to medium size scaled power plants for domestic use. The investment cost is low due to the low working pressures in ORC power plants. The operational life of ORC is long, due to the characteristics of the working fluid, which is non-eroding and non-corroding for valve seats tubing and expander. The ORC process also helps to overcome the relatively small amount of input fuel available in many regions because an efficient ORC power plant is possible for smaller sized plants

Geothermal plants : Geothermic heat sources vary in temperature from 50 to 350°C. The ORC is therefore perfectly adapted for this kind of application. However, it is important to keep in mind that for low-temperature geothermal sources (typically less than 100°C), the efficiency is very low and depends strongly on heat sink temperature (defined by the ambient temperature).

Solar thermal power : The ORC can be used in the solar parabolic trough technology in place of the usual steam Rankine cycle. The ORC allows a lower collector temperature, a better collecting efficiency (reduced ambient losses) and the possibility of reducing the required size of the solar field.

The selection of the working fluid is of key importance in low temperature Rankine cycles. Because of the low temperature, heat transfer inefficiencies are highly prejudicial. These inefficiencies depend very strongly on the thermodynamic characteristics of the fluid and on the operating conditions. In order to recover low-grade heat, the fluid generally has a

lower boiling temperature than water. Refrigerants and hydrocarbons are the two commonly used components.

3.2 Heat exchanger

Heat exchangers are devices that are used to transfer thermal energy between media without mixing the fluid themselves. The media may be fluid to fluid, fluid to solid, solid to solid at different temperatures and in thermal contact directly or through another conductive material. Depending on the process or application, heat exchangers are designed to achieve an efficient transfer of heat.

Common applications are heating or cooling fluid streams and evaporating or condensing single- or multi-component fluid streams. Other applications include the process of heat recovery or heat rejection. Heat exchangers have extensive use in sterilizing, pasteurizing, distilling and controlling of process fluids

Usually, heat transfer between fluids takes place through a wall separating the fluids, or move in and out of walls in a transient style. Many heat exchangers separate fluids using a heat transfer surface, and they do not usually mix or leak. These are referred to as “direct transfer types”, or “recuperators”. Exchangers where there is “intermittent heat exchange” between fluids of different temperatures through thermal energy storage and release through the exchanger surface or “matrix” are referred to as “indirect transfer types” or “regenerators”. Regenerators usually have some leak flow between fluid streams because of pressure differences and ‘matrix’ rotation/valve switching. Some common heat exchangers are: shell-and-tube exchangers; automobile radiators; condensers; evaporators; air pre-heaters; and cooling towers.

Heat exchangers where there are no phase changes in any of the fluids are sometimes referred to as “sensible heat exchangers”. There may be “internal thermal energy sources” in the exchangers (for example, electric heaters, nuclear fuel elements, etc). Different reactions can also take place within the exchangers, such as combustion or chemical reactions, especially in exchangers like boilers and fired heaters. Some exchangers use mechanical devices, such as agitated vessels, scraped surface exchangers and stirred tank reactors.

Heat transfers in recuperators that use separating walls usually occur through conduction, but in heat pipe heat exchangers where the heat pipe is the separating wall, heat transfer occurs through condensation, evaporation and conduction. However, if the fluids are immiscible, the separating wall or heat transfer surface is not needed, as the interface between the fluids can act as them, like in a direct-contact heat exchanger.

A heat exchanger consists of heat transfer elements such as a core or matrix containing the heat transfer surface, and fluid distribution elements such as headers, manifolds, tanks, inlet and outlet nozzles or pipes, or seals. Usually, there are no moving parts in a heat exchanger; however, some exceptions exist, such as a rotary regenerative exchanger (in which the matrix is mechanically driven to rotate at some design speed) or a scraped surface heat exchanger. The core of the heat exchanger transfers heat by conduction through the heat transfer surface to the opposite side of the surface. The heat eventually transfers to the fluid by convection. The portion of the surface that is in direct contact with both the hot and cold fluids and transfers heat between them is referred to as the primary, or direct, surface.

To increase the heat transfer area, appendages may be intimately connected to the primary surface to provide an extended, secondary, or indirect surface. These extended surface elements are known as fins. Thus, heat is conducted through the fins, and convection occurs (and/or is radiated) from the fins (through the fin surface area) to the surrounding fluid, or vice versa, depending on whether the fin is being cooled or heated. As a result, the installation of fins to the primary surface reduces the thermal resistance on that side and thereby increases the total heat transfer from the surface for the same temperature difference.

Fins may form flow passages for the individual fluids but do not separate the two (or more) fluids of the exchanger. These secondary surfaces or fins may also be introduced for structural strength in some cases or to provide thorough mixing of a highly viscous liquid. Heat exchangers are not only used in the process, power, petroleum, transportation, air-conditioning, refrigeration, cryogenics, heat recovery, alternative fuel, and manufacturing industries, but also used as key components of many industrial products available in the market.

Depending on their application, heat exchangers may be of different forms; thus, heat exchangers can be classified in many different ways. Some of their classifications are shown in the Figure 3.2. They are classified according to transfer processes, number of fluids, and heat transfer mechanisms. Conventional heat exchangers are further classified according to construction type and flow arrangement. Another arbitrary classification is made based on the heat transfer surface area/volume ratio, into compact and non-compact heat exchangers. This classification is made because the type of equipment, fields of applications, and design techniques generally differ. All these classifications are summarized in Figure. 3.2 and are discussed in this chapter.

3.2.1 Shell and tube heat exchangers

Shell and tube heat exchangers are very common among the types of heat exchangers and are the most widely used type of heat exchanger in process and power plants. They are used in applications including; solar energy, geothermal, boiler, air preheater, economizer, and waste heat recovery. This type of heat exchanger is shown in Figure. 3.3. Generally, it consists of a bundle of round tubes mounted in a cylindrical shell, with the tubes extended throughout the shell length.

One of the fluids flows through the tubes while the other flows around the tubes. The fluid properties, applicability, and overall equipment design characteristics determine the inner and outer flow pattern. The major components of a typical shell and tube heat exchanger are tubes (or tube bundle), shell, front-end head, rear-end head, baffles, and tube sheets. The components are described briefly later in this chapter.

A variety of internal constructions are used in different shell and tube exchangers, depending on the desired heat transfer, pressure drop performance and the methods employed to reduce thermal stresses, to prevent leakages, to provide for ease of cleaning, to contain operating pressures and temperatures, to control corrosion, to accommodate highly asymmetric flows, and so on.

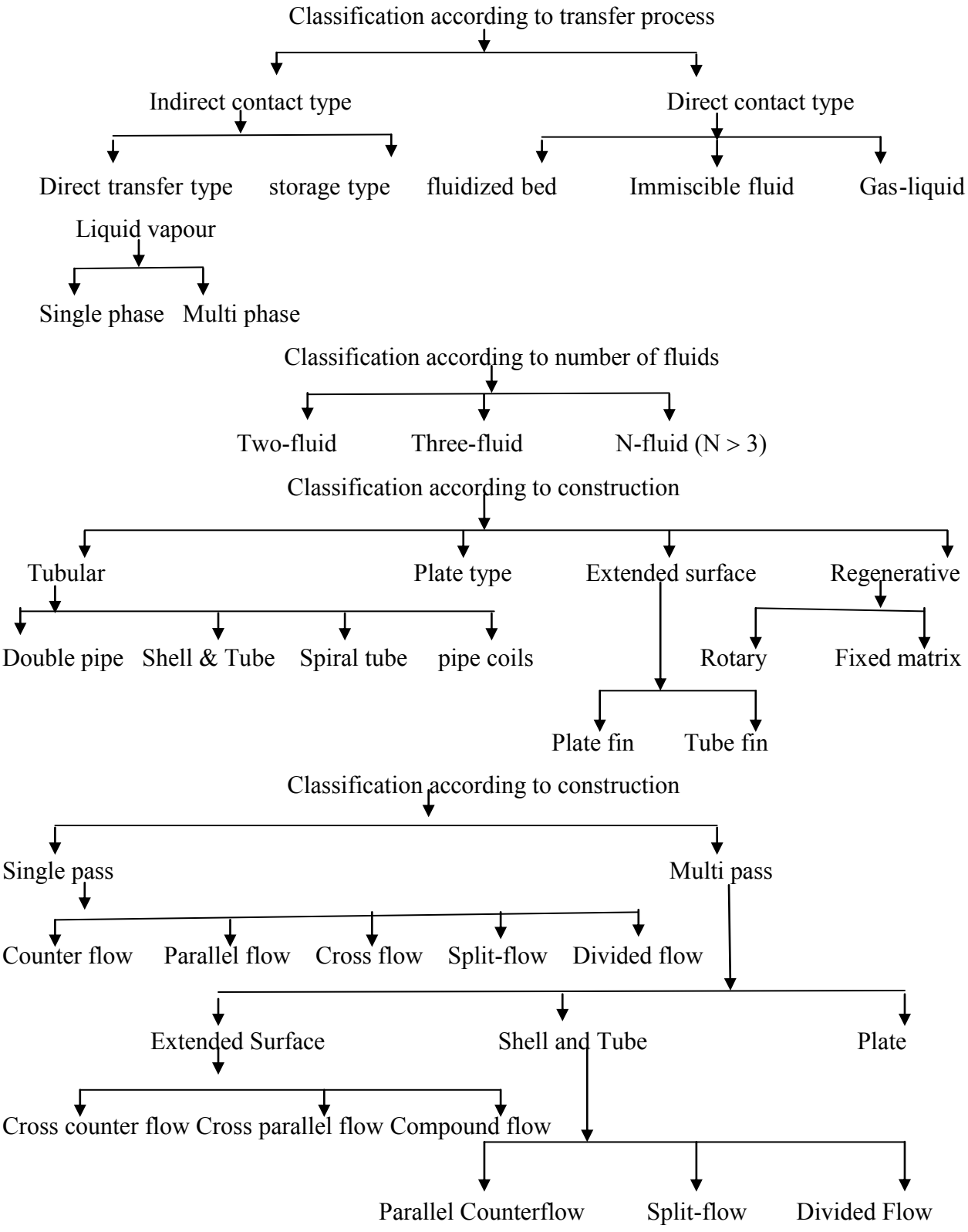

Figure 3.2 Classification of heat exchangers [modified from Shah (1981)].

Shell and tube type exchangers are classified and constructed in accordance with the widely used TEMA (Tubular Exchanger Manufacturers Association) standards (TEMA, 1999), DIN, ASME (American Society of Mechanical Engineers) boiler and pressure vessel codes, and other standards in Europe and elsewhere. TEMA has developed a notation system to designate major types of shell and tube heat exchangers. In this system, each exchanger is designated by a three-letter combination, the first letter indicating the front-end head type, the second the shell type, and the third the rear-end head type. These are presented in Figure. 3.4.

Some common shell and tube exchangers are AES, BEM, AEP, CFU, AKT, and AJW. It should be emphasized that there are other special types of shell and tube exchangers commercially available that have front- and rear-end heads different from those in Figure. 3.4. Those exchangers may not be identifiable by the TEMA letter designation.

The three most common types of shell and tube exchangers are (1) fixed tube sheet design, (2) U-tube design, and (3) floating-head type. In all three types, the front-end head is stationary while the rear-end head can either be stationary or floating (see Figure. 3.4), depending on the thermal stresses in the shell, tube, or tube sheet developed due to temperature differences within the system.

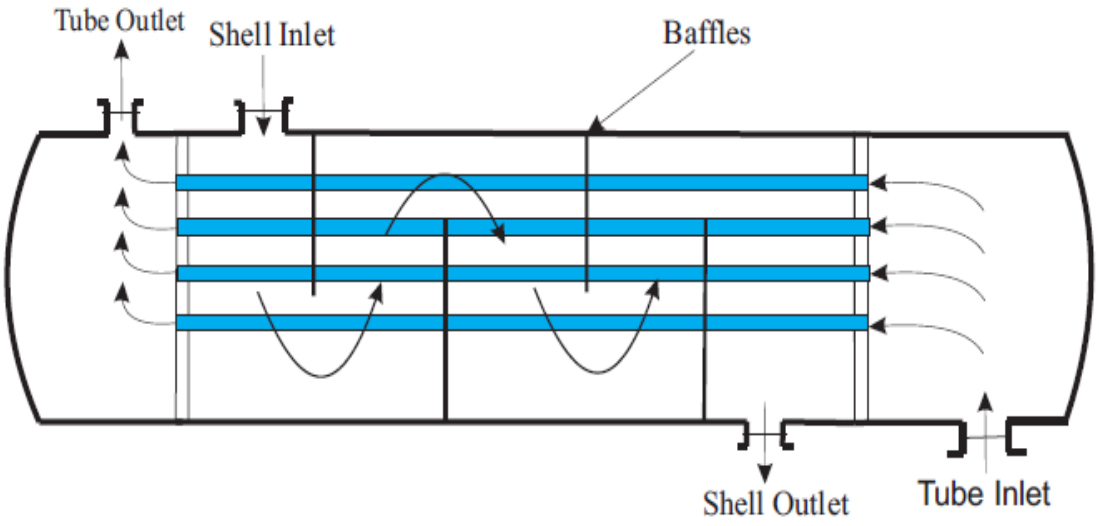

Figure 3.3 Shell and tube heat exchanger [modified from Shah (1981)].

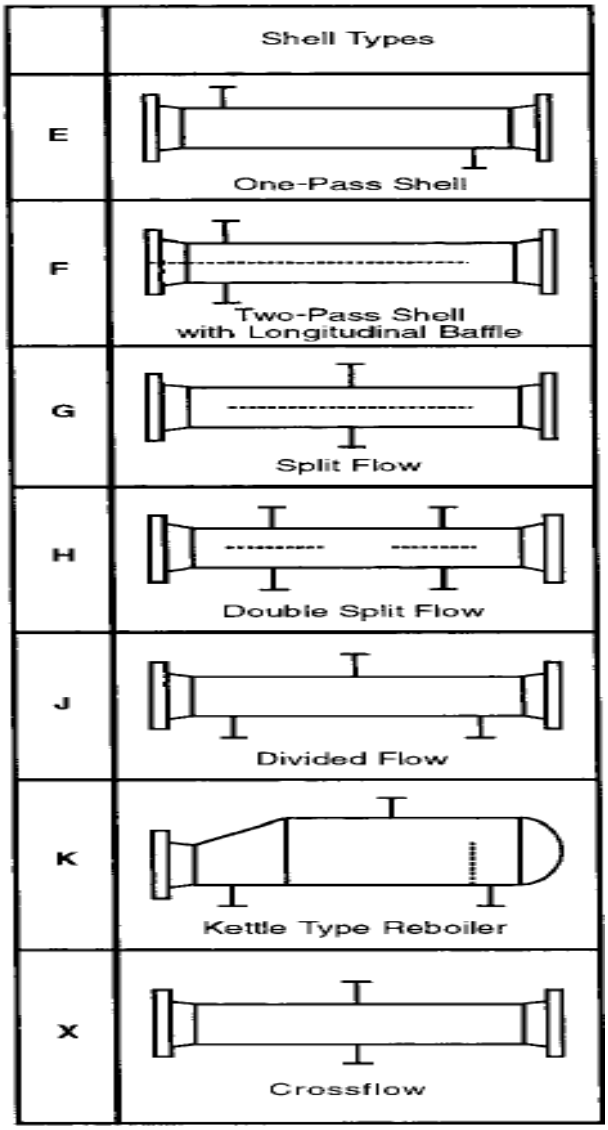

Figure 3.4 Standard shell types and front and rear end head types [modified from Shah (1981)].

The exchangers are normally built in accordance with three mechanical standards that specify design, fabrication, and materials of unfired shell and tube heat exchangers. Class R is for petroleum and related processing applications. Class C is for commercial and general process applications. Class B is for chemical process service. The exchangers are built in accordance to the applicable ASME Boiler and Pressure Vessel Code, Section VIII (1998), and other pertinent codes and/or standards. The TEMA standards supplement and define the ASME code for heat exchanger applications. In addition, state and local codes applicable to the plant location must also be met. The TEMA standards specify the manufacturing tolerances for various mechanical classes, the range of tube sizes and pitches, baffling and

support plates, pressure classification, tube sheet thickness formulas, and so on, and must be consulted for all these details. In this literature, we consider only the TEMA standards where appropriate, but there are other standards, such as DIN (2008).

Tubular exchangers are widely used in industry for the following reasons. They have the flexibility to be built as 'custom designed' for virtually any capacity and operating condition ranges, such as from high vacuum to ultra-high pressure [over 100 MPa (15,000 psig)], from cryogenics to high temperatures [about 1100 ^{o}C (~2000^{o}F)], and any temperature and pressure differences between the fluids, limited only by the materials of construction. They can also be designed for special operating conditions: vibration, heavy fouling, highly viscous fluids, erosion, corrosion, toxicity, radioactivity, multi-component mixtures, and so on. They are the most versatile exchangers, made from a variety of metal and non-metal materials (such as graphite, glass, and Teflon) and range in size from small [0.1m^2 (1 ft^2)] to super-giant [over 105m^2 (106 ft^2)] surface area. They are used extensively as process heat exchangers in the petroleum-refining and chemical industries; as steam generators, condensers, boiler feed-water heaters, and oil coolers in power plants; as condensers and evaporators in some air-conditioning and refrigeration applications; in waste heat recovery applications with heat recovery from liquids and condensing fluids; and in environmental control.

3.2.2 Tubes

Round tubes in various shapes and sizes are used in shell and tube exchangers. Most common are the tube bundles with straight and U-tubes (see Figure. 3.5) used in process and power industry exchangers. However, sine-wave bend, J-shape, L-shape or hockey sticks, and inverted hockey sticks are used in advanced nuclear exchangers to accommodate large thermal expansions of the tubes. Some of the enhanced tube geometries used in shell and tube exchangers are shown in Figure. 3.6. Serpentine, helical, and bayonet are other tube shapes that are used in shell and tube exchangers.

In most applications, tubes have single walls, but when working with radioactive material multiple wall tubing may be used.

Figure 3.5 Different types of tubes with fin inside [modified from Shah (1981)].

A tube bundle is an assembly of tubes, baffles, tube sheets, tie rods, support plates and longitudinal baffles. In case of reactive, toxic fluids or potable water, double-wall tubing is used. In most applications, tubes are bare, but when gas or low heat transfer coefficient liquid is used on the shell side, low-height fins (low fins) are used on the shell side. Also, special high-flux boiling surfaces employ modified low fin tubing. These are usually integral fins made from a thick-walled tube. Tubes are drawn, extruded, or welded, and they are made from metals, plastics, and ceramics, depending on the applications.

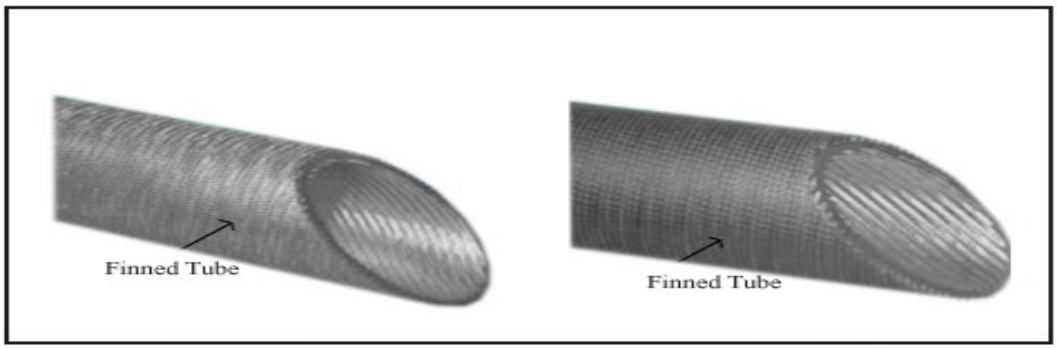

(a) (b)

Figure 3.6 Some enhanced tube geometries used in shell-and-tube exchangers: (a) internally and externally enhanced evaporator tube; (b) internally and externally enhanced condenser tube [modified from Shah (1981)].

3.2.3 Shells

The shell is a container for the fluid flowing around the tubes. Usually it is cylindrical in shape with a circular cross section, although shells of different shapes are used in specific applications and in nuclear heat exchangers to conform to the tube bundle shape. In exchangers where the shell diameter is less than about 0.6m (2 ft), the shell is made from a circular pipe; if greater than 0.6m (2 ft), the shell is made from a metal plate rolled and welded longitudinally. Seven types of shell configurations, standardized by TEMA (1999), are represented by E, F, G, H, J, K, and X, as shown in Figure 3.4. The E shell is the most common, due to its low cost and simplicity, and has the highest log-mean temperature difference correction factor. Although the tubes may have single or multiple passes, there is one pass on the shell side. To increase the mean temperature difference and hence exchanger effectiveness, a pure counter flow arrangement is desirable for a two-tube-pass exchanger. This is achieved by the use of an F type shell having a longitudinal baffle resulting two shell passes. Split and divided flow shells, such as G, H, and J (see Figure 3.4), are used for specific applications, such as in thermo-siphon boilers, condensers, and where shell side pressure drops are low. The K shell is a kettle re-boiler used for pool boiling applications. The X shell is a cross flow exchanger and is used for low pressure drops on the shell side and/or to eliminate the possibility of flow induced vibrations.

Heat transfer analysis of shell and tube heat exchanger is performed with a double pipe type heat exchanger as shown in Figure 3.7. A higher temperature fluid enters through the shell entry while the other fluid passes through the inner tube. The equations may be represented as follows:

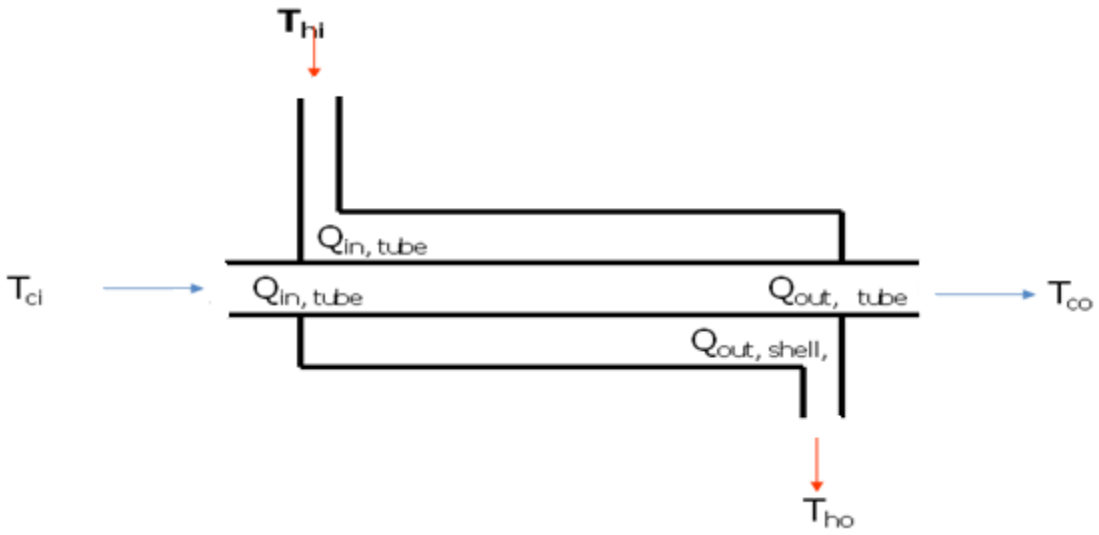

Figure 3.7 Double pipe type shell and tube heat exchanger.

The tube side heat transfer can be calculated by following equation:

$$\dot{Q}_{tube} = \dot{m} C_P \Delta T \tag{3.1}$$

The shell side heat transfer is calculated by

$$\dot{Q}_{shell} = \dot{m} \Delta h + \dot{m} C_P \Delta T \tag{3.2}$$

The overall heat transfer coefficient can be calculated from

$$U_o = \frac{\dot{Q}_{shell}}{A_0 \, \Delta T_{lm}} \tag{3.3}$$

The logarithmic mean temperature difference (LMTD) is calculated as

$$\text{LMTD} = \Delta T_{lm} = \frac{(T_{hi} - T_{co}) - (T_{ho} - T_{ci})}{\ln[(T_{hi} - T_{co}) - (T_{ho} - T_{ci})]} \tag{3.4}$$

3.2.4 Gas-to-fluid heat exchangers

The heat transfer coefficient *h* for gases is generally one or two orders of magnitude lower than that of water, oil, and other liquids. Now, to minimize the size and weight of a gas to-liquid heat exchanger, the thermal conductances (h·A products) on both sides of the exchanger should be approximately the same. Hence, the heat transfer surface on the gas side needs to have a much larger area and be more compact than can be realized practically with the circular tubes commonly used in shell and tube exchangers. Thus, for an approximately balanced design (about the same h·A values), a compact surface is employed on the gas side of gas-to-gas, gas-to-liquid, and gas-to-phase change heat exchangers. The unique

characteristics of compact extended-surface (plate-fin and tube-fin) exchangers, compared to conventional shell and tube exchangers (see Figure 3.6), are as follows:

- Availability of numerous surfaces having different orders of magnitude of surface area density.
- Flexibility in distributing surface area on the hot and cold sides as warranted by design considerations
- Generally, substantial cost, weight, or volume savings.

The important design and operating considerations for compact extended-surface exchangers are as follows:

- Usually, at least one of the fluids is a gas having a low *h* value.
- Fluids must be clean and relatively noncorrosive because of low-Dh [hydraulic diameter] flow passages and no easy techniques for cleaning.
- The fluid pumping power (and hence the pressure drop) is often as important as the heat transfer rate.
- Operating pressures and temperatures are somewhat limited compared to shell and tube exchangers, due to the joining of the fins to plates or tubes by brazing, mechanical expansion, and so on.
- With the use of highly compact surfaces, the resulting shape of the exchanger is one having a large frontal area and a short flow length; the header design of a compact heat exchanger is thus important for achieving uniform flow distribution among very large numbers of small flow passages.
- The market potential must be large enough to warrant the sizable initial manufacturing tooling and equipment costs.

Fouling is a major potential problem in compact heat exchangers (except for plate and frame heat exchangers), particularly those having a variety of fin geometries or very fine circular or non-circular flow passages that cannot be cleaned mechanically. Chemical cleaning may be possible; thermal baking and subsequent rinsing are possible for small units. Hence, extended-surface compact heat exchangers should not be used in heavy fouling applications. Non-fouling fluids are used where permissible, such as clean air or gases, light hydrocarbons,

and refrigerants. In this research, hot air is used to heat R134a through extended surface heat exchanger.

3.3 Heat exchanger (evaporator) for ORC cycle

Most of the researchers used extended surface type heat exchangers for this type of research project. The term extended surface is commonly used to depict an important special case involving heat transfer by conduction within a solid and heat transfer by convection (or radiation) from the boundaries of solid. This extended surface is fins.

Extended surface heat exchanger can be two types: internal finned and external finned. An external finned tube type heat exchanger is suitable for this type of heat engine. Fins of the heat exchanger transfer heat from different types of heating sources to the working fluid (R134a). The working fluid flows into the tubes and hot air, flue gas, waste heat and combustible gas flows through thin fin plates. Only sensible heat or sensible and latent heat exchange can occur simultaneously. Heat transfer rate depends on overall heat transfer coefficient, U area, A, and log mean temperature difference as shown in the equation 3.1.

$$\dot{Q} = UA\Delta T_{lm} \quad (3.5)$$

Improvements in heat transfer rates for a given size of heat exchanger are often possible by increasing one or both the fluid stream velocities.

Use of fins in the heat exchanger increases the cost in terms of pressure drop. More power is required to overcome this pressure drop due to fins. But without fins being used, a large surface area of the heat exchanger is needed to get the same rate of heat transfer, which is also a cost. This is the designer trade off between use of fins or surface area without fin.

The two basic approaches are used to size, analyse, or select heat exchangers are the log mean temperature difference (LMTD) and the effectiveness-number of heat unit transfer (ε-NTU) methods.

With suitable assumptions, it is possible to drive an expression for the mean temperature difference required in equation 3.1 for parallel flow and counter flow. The assumptions are as follows:

The overall heat transfer coefficient U, the mass flow rate $\dot{m}_c$ and $\dot{m}_h$, and the fluid capacity rate C_c and C_h are all constants, where the subscripts c and h refer to the cold and hot streams.

- There is no heat loss or gain external to the heat exchanger, and there is no axial conduction in the heat exchanger.
- A single bulk temperature applies to each stream at a given cross section.

For both counter flow and parallel flow the appropriate mean temperature is the LMTD as given below:

$$\Delta T_{lm} = LMTD = \frac{\Delta T_1 - \Delta T_2}{ln^{(\Delta T_1}/_{\Delta T_2)}} \quad (3.6)$$

In many cases the flow path in the heat exchanger are not simply counter flow or parallel flow, but are quite complex. In this case for LMTD calculation, a correction factor, *F,* is used,

$$\dot{Q} = UAF(\Delta T_{lm}) \quad (3.7)$$

The value of the correction factor depends on the parameters P and R equations as given below:

$$P = \frac{T_{co} - T_{ci}}{T_{hi} - T_{ci}} \quad (3.8a)$$

and

$$R = \frac{T_{hi} - T_{ho}}{T_{co} - T_{ci}} \quad (3.8b)$$

The ε-NTU method has the advantage of eliminating the trial and error procedure of the LMTD method for many practical problems when only the inlet fluid temperature is known.

The heat exchanger effectiveness, ε, is:

$$\varepsilon = \frac{\text{actual heat transfer rate}}{\text{maximum possible heat transfer rate}}$$

The actual heat transfer rate is

$$\dot{Q} = C_h(T_{hi} - T_{ho}) = C_c(T_{co} - T_{ci})$$

and the maximum possible heat transfer rate is expressed by

$$\dot{Q}_{max} = C_{min}\,(t_{hi} - t_{ci})$$

So, the heat exchanger effectiveness is given below:

$$\varepsilon = \frac{\dot{Q}}{\dot{Q}_{max}}$$

The evaporator (finned heat exchanger) has fins on both sides. In this case, the fin efficiency can be calculated by

$$\eta = \frac{\text{actual heat transfer}}{\text{heat transfer with fin all at the base temperature } T_b}$$

Since the base on which the fin is mounted also transfer heat, another way the performance can be described with the overall surface efficiency:

$$\eta_s = \frac{actual\ heat\ transfer\ for\ fin\ and\ base}{heat\ transfer\ for\ fin\ and\ base\ when\ the\ fin\ is\ at\ the\ base\ temperature\ T_b}$$

If we assume the heat transfer coefficient, h is uniform over the fin and base surface, the actual heat transfer rate is written as

$$\dot{Q} = hA\eta_s(T_b - T_\infty)$$

or

$$\eta_s = \frac{\dot{Q}}{hA(T_b - T_\infty)} = \frac{h\,A_b\,(T_b - T_\infty) + hA_f\eta\,(T_b - T_\infty)}{hA\,(T_b - T_\infty)}$$

where A is total surface area of base and fin = $(A_b + A_f)$. So the overall surface efficiency can be written as

$$\eta_s = \frac{A_b + \eta A_f}{A} = 1 - \frac{A_f}{A}\,(1 - \eta)$$

The thermal resistance becomes

$$\acute{R} = \frac{1}{hA\eta_s}$$

The case where the both sides of the heat exchanger have fins, the overall heat transfer coefficient U, without fouling is

$$\frac{1}{UA} = \frac{1}{h_o A_o \eta_{so}} + \frac{\Delta x}{kA_m} + \frac{1}{h_i A_i \eta_{si}}$$

3.4 Optimal characteristics of the working fluid

Isentropic saturation vapour curve : Since the purpose of the ORC focuses on the recovery of low grade heat power, a superheated approach like the traditional Rankine cycle is not appropriate. Therefore, a small superheating at the exhaust of the evaporator is preferred, which gives a disadvantage to "wet" fluids (that are in two-phase state at the end of the expansion). In the case of dry fluids, a regenerator should be used.

Low freezing point, high stability temperature: Unlike water, organic fluids usually suffer chemical deteriorations and decomposition at high temperatures. Thus the maximum hot source temperature is limited by the chemical stability of the working fluid. The freezing point must also be lower than the lowest temperature in the cycle.

High heat of vaporization and high density: A fluid with a high latent heat and density will absorb more energy from the source in the evaporator and thus reduce the required flow rate, the size of the facility, and the pump consumption.

Low environmental impact: The main environmental parameters taken into account are the Ozone depletion potential (ODP) and the global warming potential (GWP).

Safety: The fluid should be non-corrosive, non-flammable, and non-toxic. The ASHRAE safety classification of refrigerants can be used as an indicator of the fluid's dangerousness level.

Availability and low cost: The working fluid is available, easy to purchase and comparatively low cost.

Acceptable pressures: The pressure range should be suitable with design parameters.

CHAPTER 4: EXPERIMENTAL SYSTEM

The evaporator has been selected to use in this research project to extract heat energy from heat source to ORC working fluid. A special air duct is designed and built to conduct the test. A suitable heat exchanger is designed, constructed and installed in the test bench to make sure the ORC working fluid is sub-cooled liquid before entering the liquid flow meter. Refrigeration scroll compressors operating system, geometrical shape, and performance parameters are specified in different manufacturers catalogues. One compressor unit is selected for this research which is purchased and modified for using as an expander. A specialized ORC test bench was designed and built to carry out tests to determine expander and ORC system performance under various operating conditions. In this chapter, illustrations of the experimental systems, the components, the measuring equipment, and the experimental procedures are presented.

4.1 Selection of the scroll machine

For the suitable refrigeration scroll compressors, an extensive search is done through catalogues from various manufacturers and sources. The purpose of this is to identify appropriate units that could operate in reverse as expander for use in the ORC test bench. The power range for the scope of the present work is set to 1-20 kW electric. The range of manufacturers is narrowed down to five choices: Copeland, Bristol, Hitachi, Sanyo, and Bitzer. Several criteria are identified and applied for the selection of the compressor type, some of which are:

- **Source temperature range**

The experimental investigation of ORC is to be restricted to a lower than 300°C temperature range for two reasons: first, the majority of renewable energy sources and waste heat sources are below this temperature; second, at lower temperatures, less mechanical problems concerning thermal expansion are encountered. Finally, one must safeguard against the possibility of oil and refrigerant thermal decomposition.

- **Appropriate pressure ratio**

Precaution must be taken to ensure that the work output from the expander is reasonably sufficient. In expander operation, the pressure ratio must be lower than in compressor operation.

- **Maximum pressure into the system**

Maximum pressure must be less than 4000 kPa for test bench component working conditions, tube safety, and better structural integrity.

- **Built-in volume ratio**

The built-in volume ratio affects the expansion process, so it should be chosen in such a way that the ORC condensation temperature is higher than the sink temperature to ensure heat transfer.

- **Ability to modify**

The compressor should be easily modifiable to an expander.

- **Motor type**

A motor capable of, or easily modified to, working as a generator in reverse operation is preferred.

- **Oil circuit**

Lubrication system and working conditions of this research also working in reverse operation is required.

- **Refrigerant type**

The vapour pressure at standard temperature, normal boiling point, critical pressure and temperature, Ozone Depleting Potential (ODP), Global Warming Potential (GWP), flammability, and toxicity of the working fluid should all be considered for each potential working fluid.

- **Cost criterion**

It should be cost effective and easy for sourcing. The main selection criteria of the selected scroll compressor are indicated on Table 4.1. Based on performance characteristics of the compressor under nominal conditions, the scroll compressor is analyzed for selection. The following parameters are the most important to determine the characteristics of the scroll unit. The temperatures of evaporation, condensation, vapour superheating, liquid sub-cooling, mass flow rate, electric power consumption, angular velocity, and the displaced volume (given in cm^3 of gas pocket at suction per shaft revolution) are the main parameters to consider. The displaced volume has been determined from the displacement (i.e., volumetric flow rate at suction in nominal conditions, see in Table 4.1), the nominal turning speed (NTS) and according to:

$$V_{\mathrm{d}} = 60 \times \frac{\dot{V}_{\mathrm{d}}}{\mathrm{NTS}} \tag{4.1}$$

where $\dot{V}_{\mathrm{d}}$ is the volumetric flow rate (m^3/s)

Table 4.1 Selected scroll compressor units and their main characteristics.

Manu-facturer	Model	Type	Motor		Refri-gerant	Displace-ment, m^3/h	Pressure, kPa		Pressure Ratio
			Power, W	Type			High	Low	
Bristol	H20R483DBE	H	4150	TPI	R22	13.60	2149	626	3.4
Copeland	ZF06K4E-PFV	H	1730	SPI	R404A	7.14	2540	267	9.5
Hitachi	G300DL	H	3750	TPI	R407C	9.87	2461	710	3.5
Sanyo	C-SBN303LBA	H	4450	TPI	R404A	14.02	2313	443	5.2
Bitzer	ECH209Y-02G	SH	1500	TPI	R134a	6.21	1471	377	3.9

SPI = Single-phase induction motor; TPI = Three-phase induction motor; H = Hermetic; SH = Semi-hermetic.

The nominal thermodynamic cycle in *T-s* diagram for each unit is generated with EES software (Klein, 2010). The higher and lower pressure in the system has been calculated based on the condensation and evaporation temperatures, respectively. The flow enthalpy at the compressor discharge is approximated based on the energy balance equation on the "electrical side" and "fluid side", written as follows

$$W_{\mathrm{el}} \cong \dot{m} \times (h_2 - h_1) \tag{4.2}$$

where ṁ is the mass flow rate, h is the enthalpy, state 1 is at suction, and state 2 is at discharge. Based on enthalpy and pressure at discharge, the temperature and the specific entropy are determined with EES, which implements accurate equations of state for each fluid. The volume ratio has been determined for each case as the ratio of specific volumes at suction vs. discharge according to:

$$VR = \frac{v_2}{v_1} \tag{4.3}$$

The volume ratio in nominal conditions is an approximation of the built-in volume ratio which is the geometrical characteristic of positive displacement machines that defines their operation in both ways, as compressor and expander.

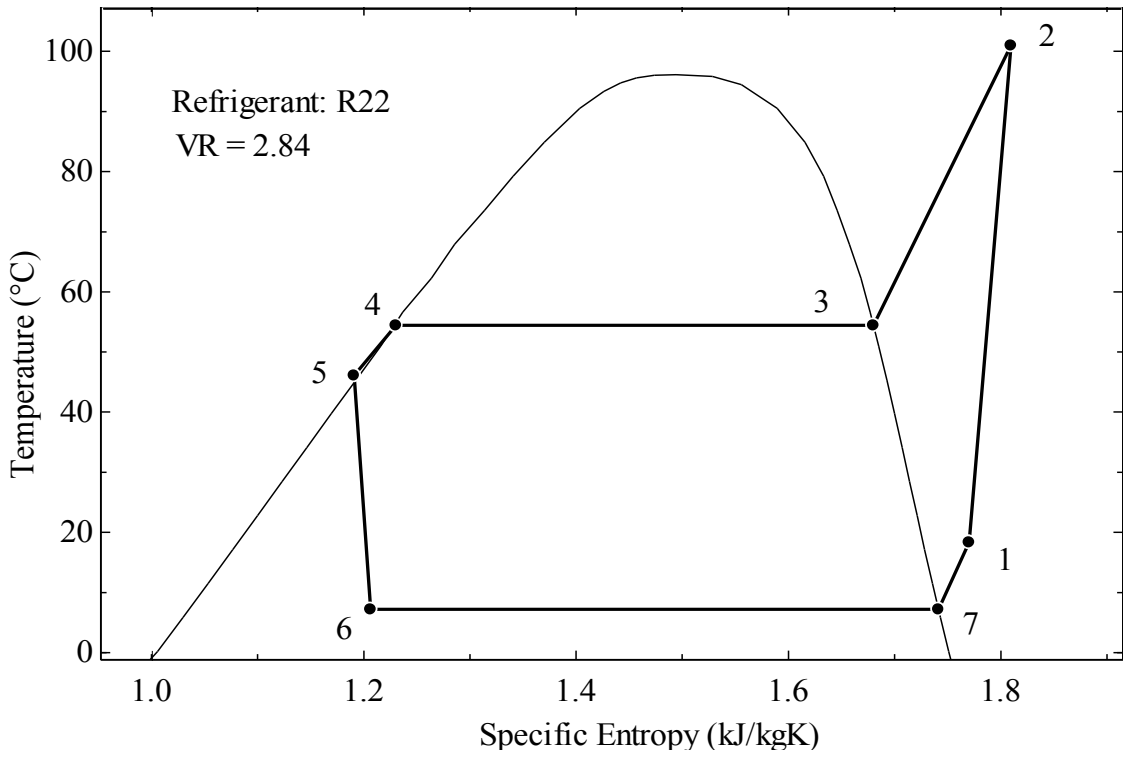

Figure 4.1 Performance parameters and thermodynamic cycle of Bristol H20R483DBE scroll compressor in nominal operation conditions.

Figures 4.1 to 4.5 present the calculated thermodynamic cycles in T-s coordinates for the five selected scroll units; the determined nominal volume ratio is indicated on each diagram. As seen in these figures, the temperature at the compressor discharge varies from 90^{o}C - 120^{o}C; the level of this temperature imposes the maximum temperature in the ORC with no significant modifications of the unit design. The selection should incline toward the units designed for air conditioning applications as those can work with warmer vapours. Another observation is the range of volume ratio, which varied from 2.8 to 5.8. This range is reasonable for the machine to operate in reverse as single stage expander for ORC. This facilitates the design of a compact organic Rankine power generation system.

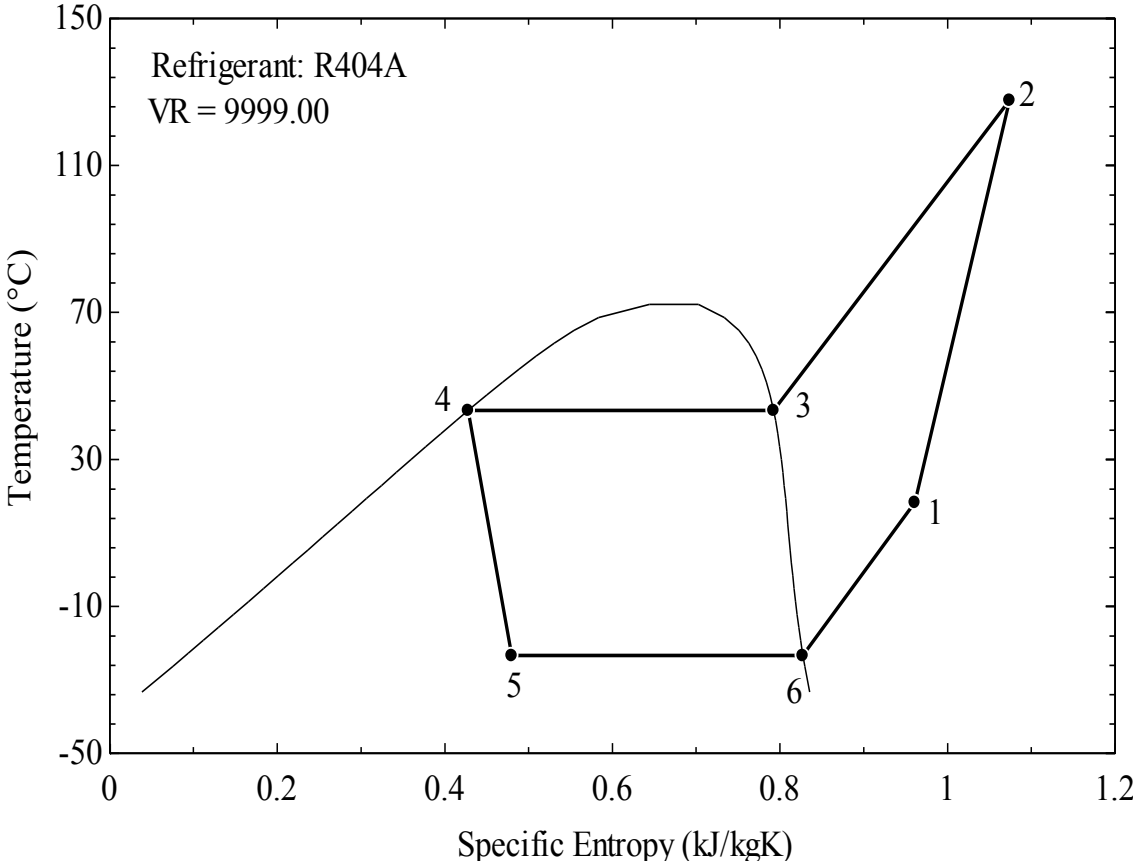

Figure 4.2 Performance parameters and thermodynamic cycle of Copeland ZF06K4E-PFV scroll compressor in nominal operation conditions.

The selected unit is the Bitzer ECH209Y-02G scroll compressor. This unit has about the same range of pressure ratio and volume ratio with the Bristol, but the Bristol has three times more power rating than the Bitzer. The present investigation of power range is set to 1-5 kW. As indicated in Table 4.1, the Bitzer is semi-hermetic. Moreover, the Bitzer unit incorporates a permanent magnet motor which can be reversed to work as generator. This offers an excellent advantage with regards to experimental systems design.

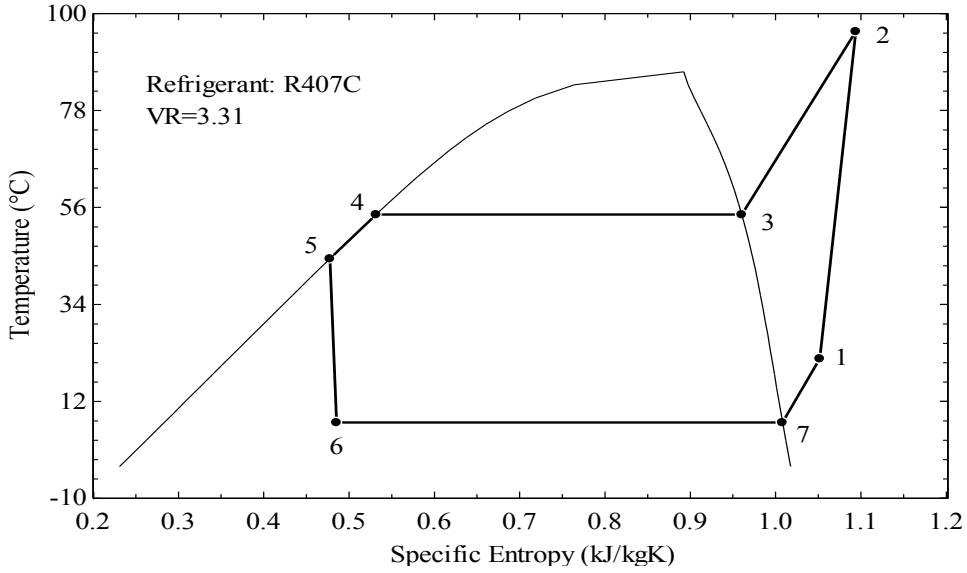

Figure 4.3 Performance parameters and thermodynamic cycle of Hitachi G300DL scroll compressor in nominal operation conditions.

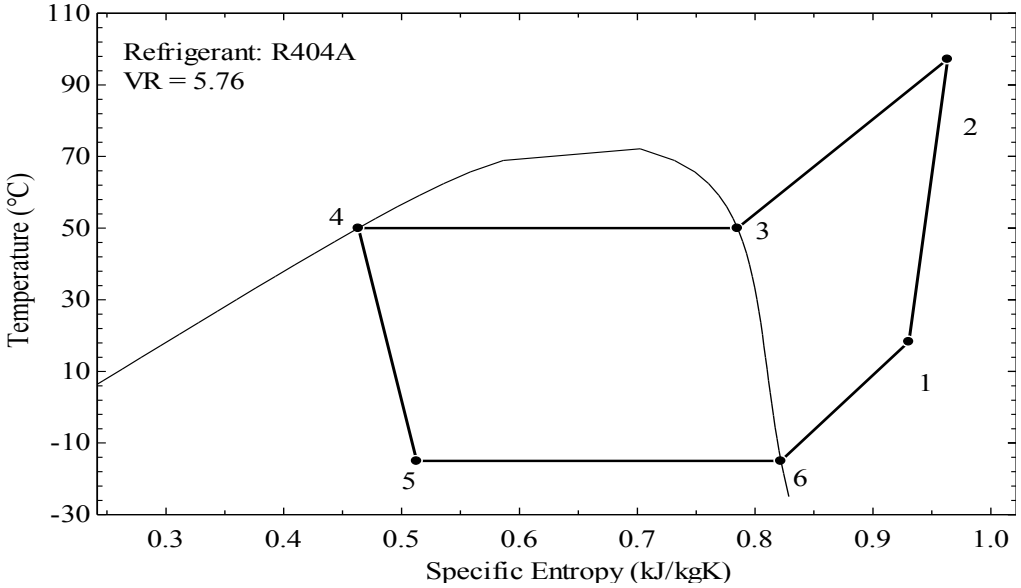

Figure 4.4 Performance parameters and thermodynamic cycle of Sanyo C-SBN303LBA scroll compressor in nominal operation conditions.

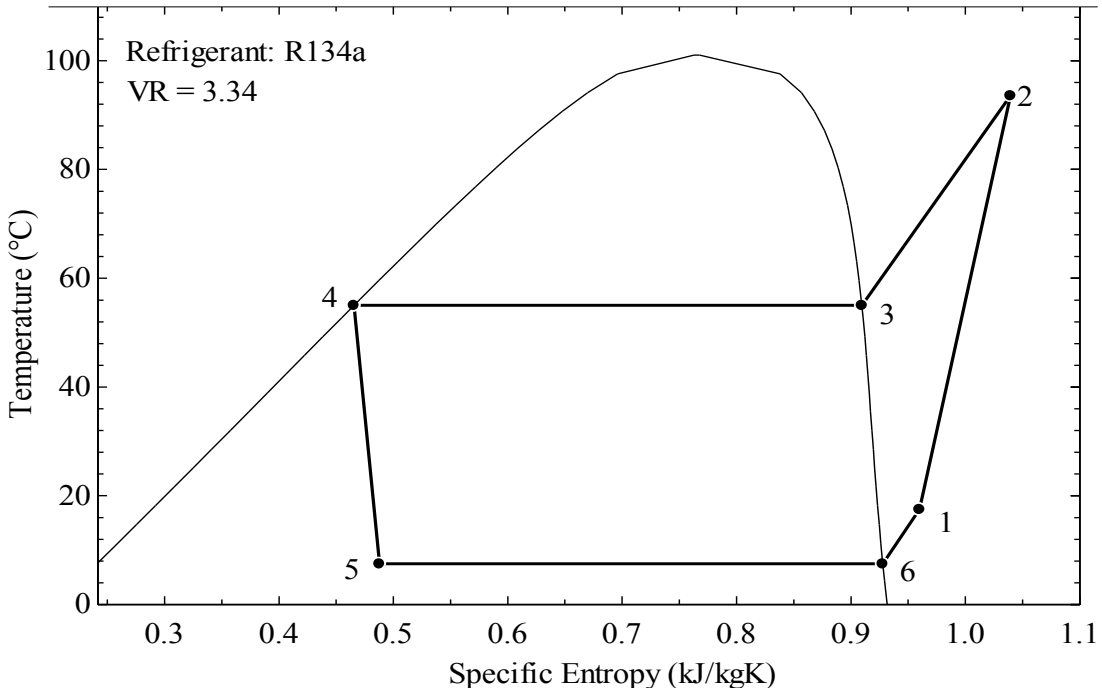

Figure 4.5 Performance parameters and thermodynamic cycle of Bitzer ECH209Y-02G scroll compressor in nominal operation conditions.

4.2 Modifications of the selected scroll unit

The cut-off view of the Bitzer scroll unit is drawn in Figure 4.6. This unit is designed for air conditioning applications of transport vehicles and includes a low voltage motor with 26 V electric DC power supplies. A permanent magnet motor is incorporated in the same housing as the scroll unit, was well as an electronic block which comprises an inverter with the role to convert the DC current to a three-phase AC current that requires driving the unit in compressor mode. In expander-mode operation, a three-phase AC current generates as the shaft rotates, and the inverter plays the role of a rectifier to transform the AC current to DC current.

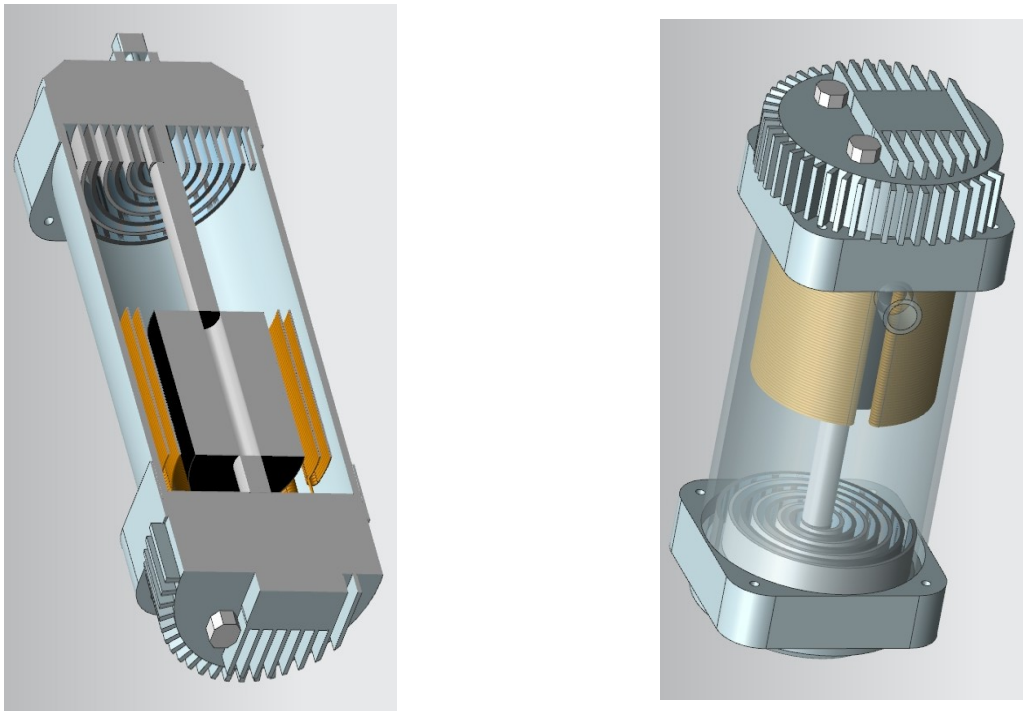

Figure 4.6 Cut-out view Bitzer ECH209Y-02G of the semi-hermetic compressor.

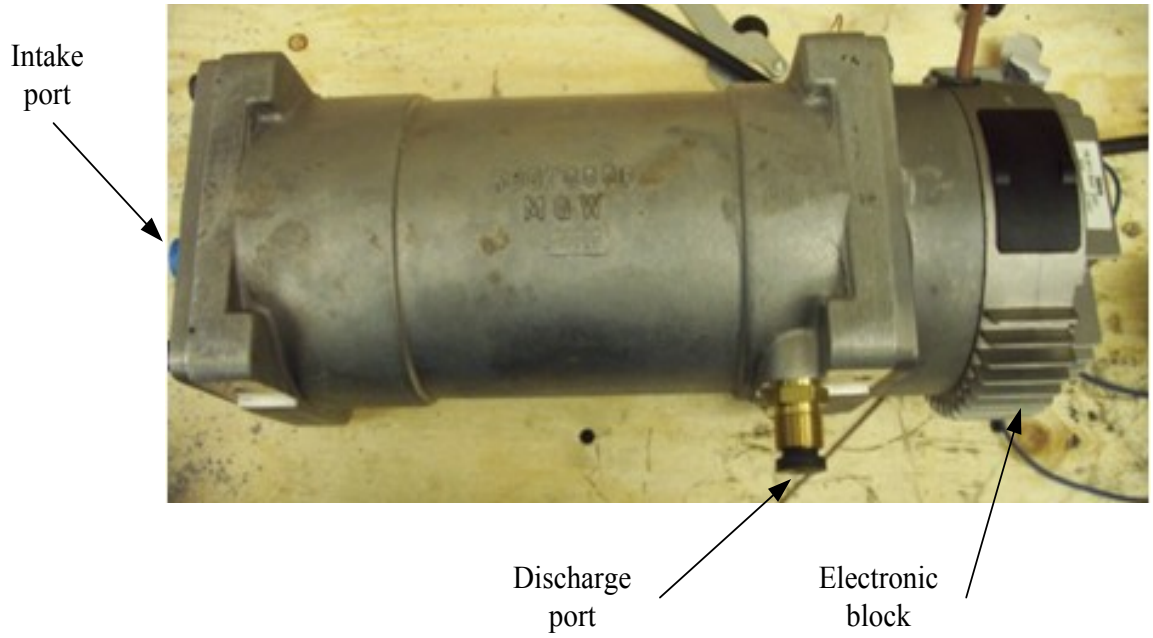

Figure 4.7 Side view of Bitzer ECH209Y-02G scroll unit.

The picture of the Bitzer scroll unit is shown in Figure 4.7. The check valve of the Bitzer unit is turned aside as indicated in Figure 4.8 in order to deactivate its function and let the unit operate in reverse.

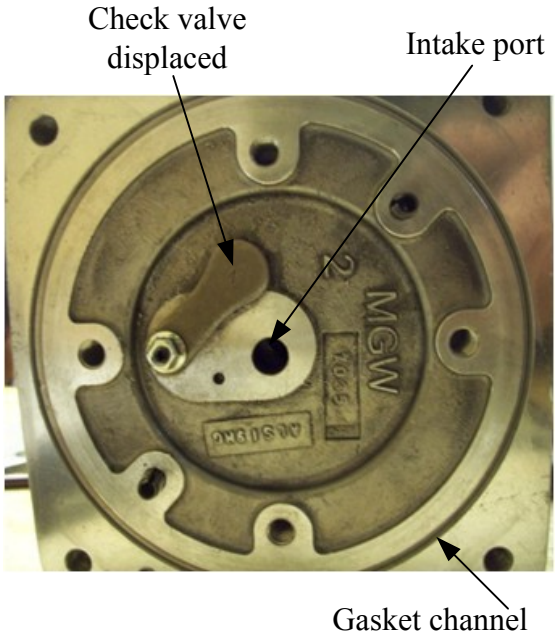

Figure 4.8 End view of the Bitzer unit showing the displacement of the check valve.

4.3 ORC Test bench experimental system

The optimized experimental system is the ORC test bench introduced in Figure 4.9. The test bench is a closed loop configuration comprising of an expander, an air cooled condenser, a compressor, an evaporator, shell and tube heat exchanger, and auxiliary components. The compressor is a reciprocating type for refrigeration application, capable of operating with high pressure ratio and high discharge pressure. Such provisions are taken to have wide flexibility in adjusting the operating parameters during experiments.

The heater is a radiant electric heater composed of six heating elements connected in parallel to operate individually through switches. The heater is designed to operate manually to adjust the fluid temperature within the limit up to 300 ℃. The logic behind this is to simulate the low temperature heat sources that can be obtained from renewable or waste heat sources. The optimized closed-loop air duct is designed and constructed to fit the blower, used

to circulate the heated air within the duct; the heater is designed to provide heat energy in the ORC cycle; and the evaporator to transfer heat into the ORC working fluid. The evaporated gas from the evaporator goes to the expander to rotate the expander and generate electric power.

There is one by-pass line in the liquid side. The liquid side throttle valve is installed to manipulate flow rate through heater and expander. A number of thermocouples and thermo-resistance probes, five pressure gauges and a liquid flow meter are installed within the system as shown in the process and instrumentation diagram (Figure 4.9). A fluid filter dryer is also placed within the system to arrest any solid material incidentally present during the test bench construction. A heat exchanger is also installed in the test bench to sub-cool the working fluid before the liquid flow meter. A data acquisition system is used to record the temperature and flow meter reading during operation.

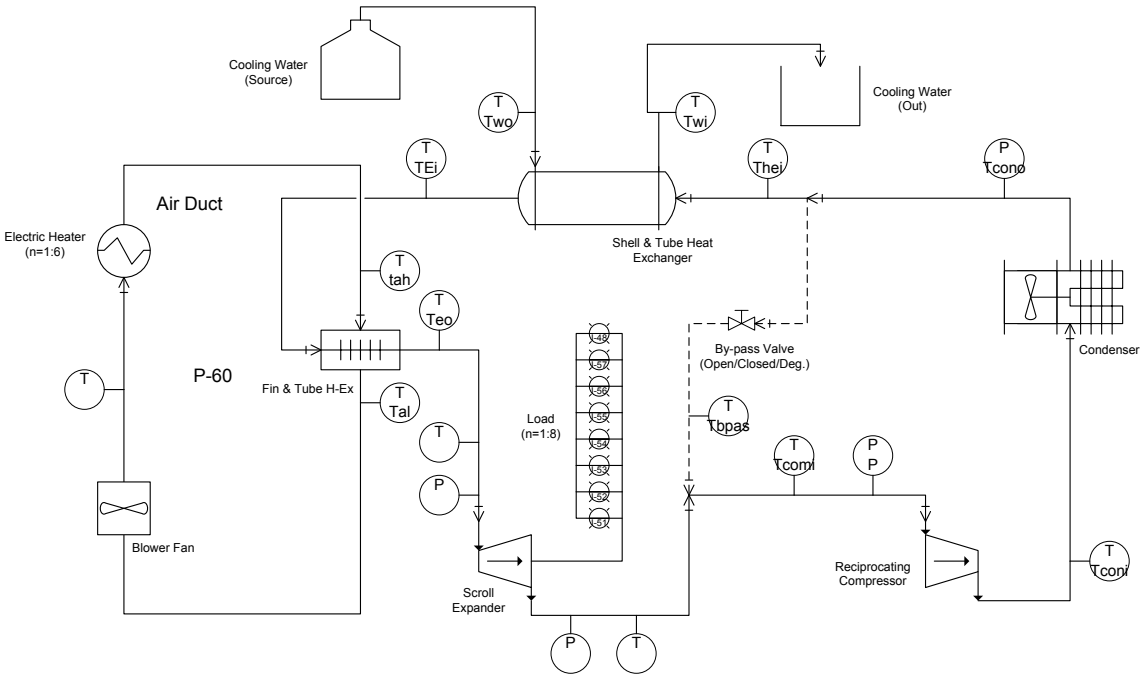

Figure 4.9 ORC test bench.

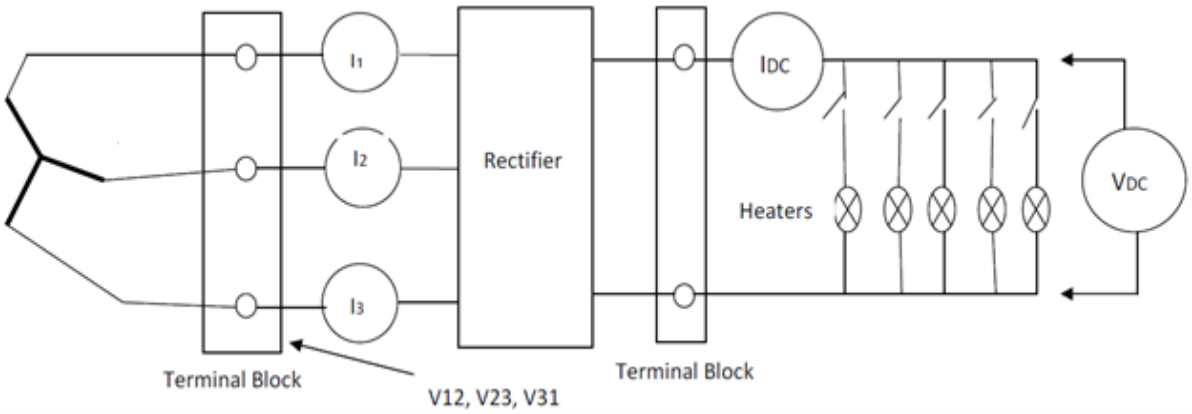

Figure 4.10 Electrical measurement circuits for the ORC test bench.

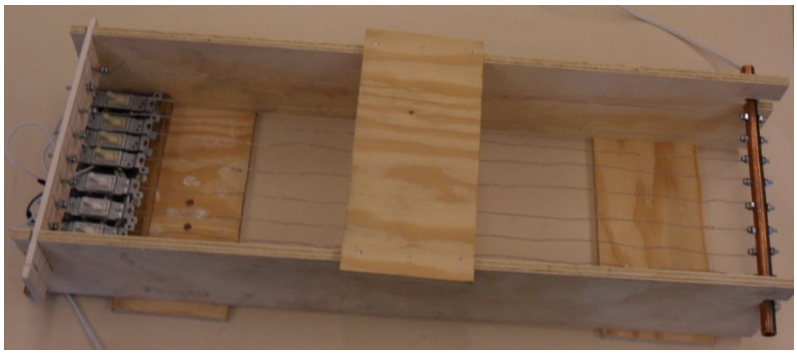

Figure 4.11 Electrical variable loads (heating wire) for the ORC test bench (Total 8 heating wires, 2.5 feet long and 0.4146 ohms/ft).

The expander of the ORC system is coupled to an electric generator. The measurement of the electric generator parameters is extremely important for the experimental investigation since the electric power is the absolute output of the heat engine. The electrical diagram and electrical measurements are indicated in Figure 4.10. The three phase current is rectified, and a resistive load is connected to the DC circuit. The electric potential and current are measured to determine the power. Optionally, the current can be measured for each phase in AC. circuit (I1, I2, I3 in Figure 4.10) and the voltage can be measured between every two phases (V12, V23, V31). Though the focus of the experiments with the ORC test bench is on the expander performance, valuable information can be drawn with regards to the overall ORC operation.

(a)

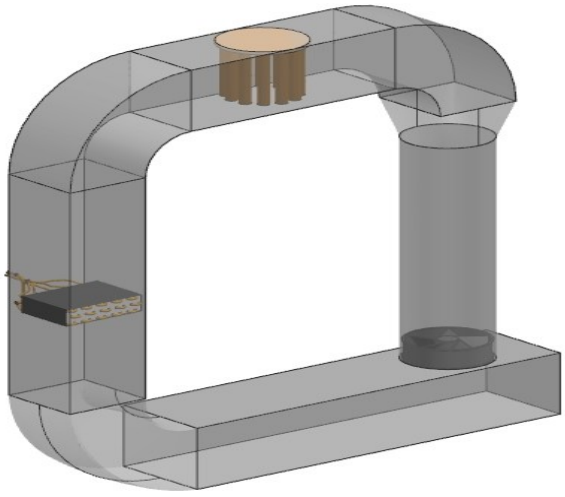

(b)

Figure 4.12 The closed loop air duct of ORC (a) a photo and (b) isometric view in Unigraphics.

The air blower is installed at the bottom of the 10” circular duct (Figure 4.12a) to blow the air inside the closed loop. The bottom part of the duct is 10” x 12” (air plenum) to provide sufficient air at the inlet of the blower. Twelve radiant electric heaters are installed in the top 10” x 10” air duct and the evaporator is installed in the left side 10” x 10” duct of the Figure 4.12. The total air duct, with equipment installed in the air duct, is shown in the Figure 4.12b. The custom made evaporator selected for this project as shown with dimensions in Figure 4.13a consists of a copper coil through which the working fluid flows.

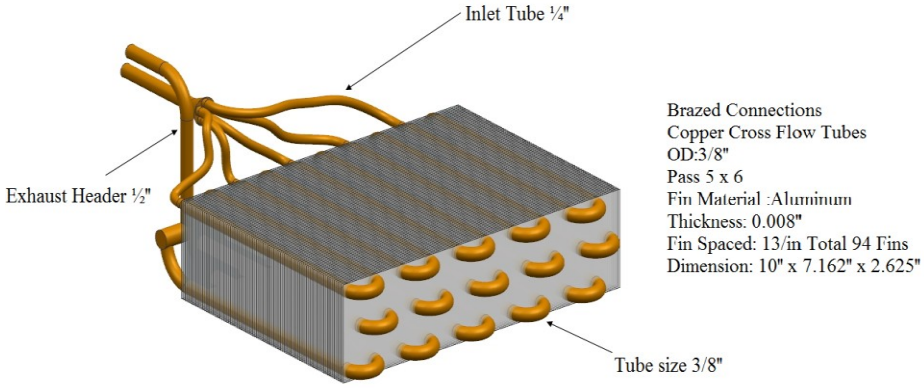

(a)

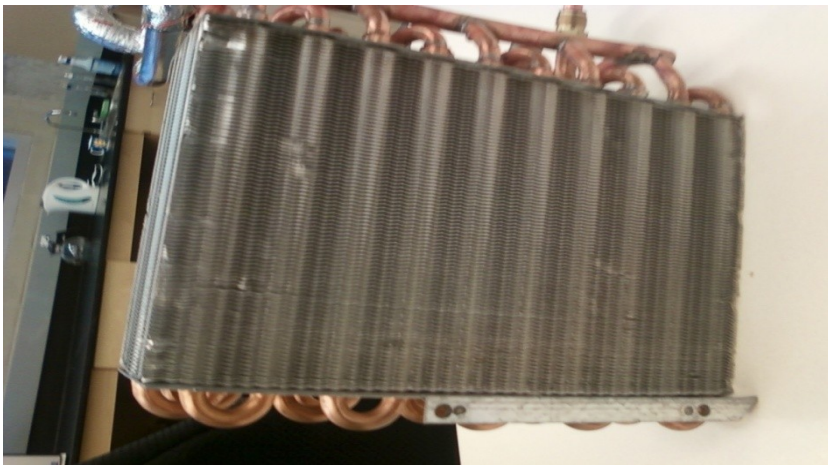

(b)

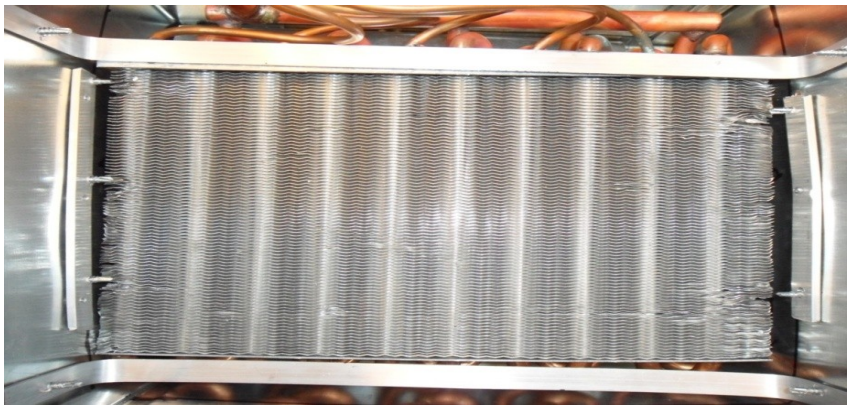

(c)

Figure 4.13 The evaporator for the test bench (a) isometric view in Unigraphics, (b) a photo from the top, and (c) a photo of evaporator inside duct.

The evaporator was procured from Mobile Climate Control (MCC) Ltd. Usually this type of evaporator is used for Trailer air conditioning systems. The size, working performance, and capacity is suitable for this experiment. The pressure difference is nearly 10 psi.

The electric circuit for the heater elements is indicated in Figures 4.14 and 4.15. As shown in the circuit diagram, the pair of heaters is connected to a live line via a manual switch. Additionally, an auto transformer is positioned in sixth pair to control part of the full load.

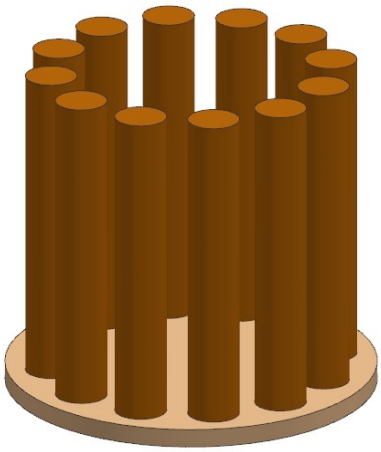

Figure 4.14 Isometric view of electrical heater.

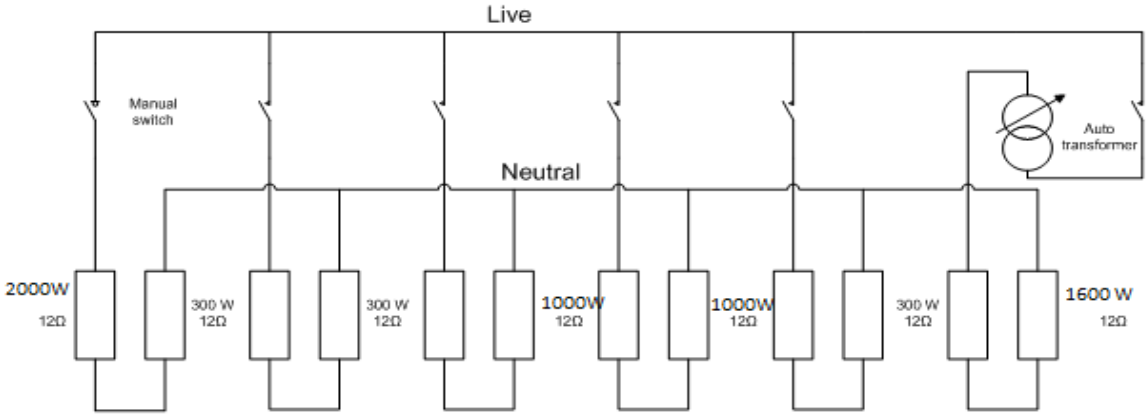

Figure 4.15 Electrical circuit of the boiler heater.

An air blower was selected for this project by considering scfm capacity, blower size, motor capacity, power source type, and the configuration suitability of the project. The motor power consumption is 25 W, two phase, with a 10” diameter blade size. The volumetric flow rate capacity of the fan is 0.0802. The experiment has been done several times with this fan,

and some data have been collected. Analysing the data, the conclusion has come that the fan is not powerful enough to maintain smooth flow through evaporator fins. As a result, another fan is procured (Figure 4.16b) to improve the experimental performance. The fan (b), Figure 4.16 has 0.5 hp power with variable speed (RPM). The highest rpm is 750 and it can create air velocity in the air duct up to 14.2 m/s.

(a)

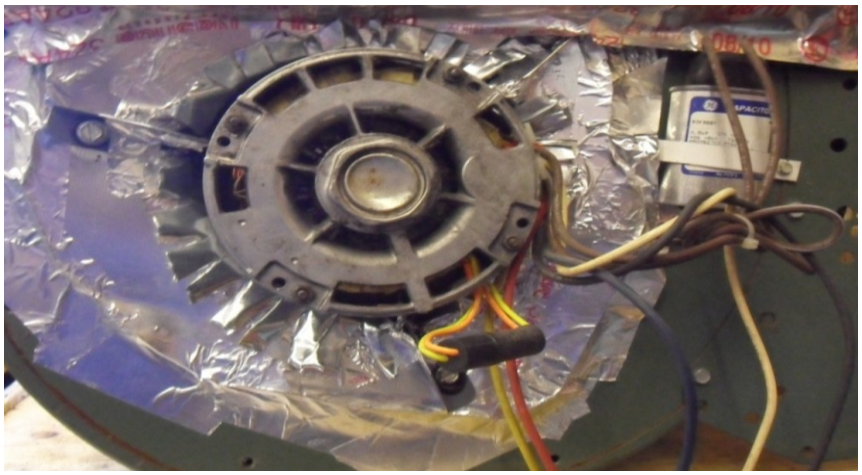

(b)

Figure 4.16 Photos of the air blowers (a) a photo of small flower and (b) a photo of larger blower.

A counter-flow, concentric tube heat exchanger is designed using copper tubing for cooling of the working fluid (R134a) between compression and heating stages. The working fluid exits the compression stage as a saturated liquid, and requires sub-cooling to prevent any bubbles in the fluid in order to obtain a valid volumetric flow reading prior to entering the evaporator (boiler) stage of the cycle. Cooling is accomplished using tap water as the shell fluid.

Table 4.2 Heat exchanger dimensions and material properties.

	Inner tube	Outer shell
Nominal Diameter	0.00953 m (0.375”)	0.0254 m (1”)
Outside diameter (nominal)	0.0127 m (0.5”)	0.0286 m (1.125”)
Wall thickness	0.000635 m (0.025”)	0.000889 m (0.035”)
Inside diameter (nominal)	0.01143 m	0.0268 m
Material	Copper	Copper
Roughness	0.0015 mm	0.0015 mm
Fluid Properties		
	Working Fluid	Cooling Fluid
Fluid	R134a	Water
Flow rate	(mass) 0.01333 kg/s	(volumetric) 0.0000167 m^3/s
Inlet Temperature	50°C	7°C
Designed properties of the heat exchanger.		
Max. Temperature difference	5°C	N/A
Pressure	$P_{sat}(T_i, x = 0)$ = 1314 kPa	170 kPa
Specific Heat	1.545 kJ/kg·K	4.183 kJ/kg·K
Density	1115 kg/m^3	997.1 kg/m^3
Conductivity	0.07195 W/m·K	0.5641 W/m K
Dynamic Viscosity	0.000147 kg/m·s	0.001374 kg/m·s
Prandtl Number	3.154	10.2

Result of EES		
	Working fluid flow [L/m]	Calculated length of heat exchanger ft [m]
	1.0002	3.665’ [1.117]
	10.002	3.562’ [1.086]

The improved length of the heat exchanger is determined based on the EES calculation with certain assumptions of mass flow rate and inlet temperature of the working fluid and the flow rate and inlet temperature of the cooling water.

Figure 4.17 Photo of the counter flow shell & tube heat exchanger (Length is 4', Shell diameter 1" and tube diameter 3/8").

Figure 4.18 Photos of the Tecumseh AWA2460ZXD condensing unit.

Figure 4.18 illustrates a Tecumseh condensing unit, model AWA2460ZXD. This unit is installed in the ORC experimental system. The compressor of this unit has characteristics that fit its use together with the Bitzer expander-generator within the same loop. That is, the Tecumseh unit can satisfy the requirement of the circulated volumetric flow rate and pressure ratio of the Bitzer expander. The volumetric flow rate of the Tecumseh unit is 12.3 m^3/h at a pressure ratio of 8.0, while the Bitzer unit necessitates 6.21 m3/h at a pressure ratio of 3.7. Thus, the Tecumseh unit can sustain the operation of the tested ORC expander with a higher flexibility. The condensing unit comprises several elements, namely: compressor, air cooled condenser, liquid receiver, and an accumulator. The condensing unit is originally designed for R404a; however, it is compatible with R134a, the working fluid used in the experiments.

The ORC plant is constructed on copper piping and insulated thoroughly. It is leak-tested with pressurized nitrogen, and then deep vacuumed with a double stage vacuum pump. The quantity of required working fluid is calculated based on the volume of the ORC plant; only the pipe segments and equipment filled with liquid are considered. The working fluid R134a is purchased and scaled to meter the quantity of the charged fluid. The charged fluid quantity is 3.5 kg.

The ORC system running and experimentation procedures are as follows:

- The two expander isolation valves are fully closed initially.
- The by-pass valve TV_2 is opened.
- The compressor is then started.
- Three heaters out of six are turned on.
- When the temperature of the heater reaches approximately 120℃ the expander is started by slowly opening the isolation valve and simultaneously closing the by-pass valve.
- When the temperatures and pressures are stabilized, the generator power is connected to the load by switching on the electric lamps.
- During the above experiments liquid fluid flow is adjusted by the by-pass valve TV_1 to manipulate the operating parameters.
- Heater/ Boiler outlet temperature, expander inlet temperature are adjusted by manually turning on/off the heating element while controlling liquid flow by the by-pass valve.

The overall picture of the realized ORC test bench experimental system is presented in Figures 4.19 and 4.20. It incorporates the Bitzer ECH209Y-02G expander-generator unit. Other components are the boiler and the condensing unit, Tecumseh AWA2460ZXD which are discussed in the earlier paragraphs.

(a) (b)

Figure 4.19 ORC test bench front view (a) a photo of air duct without insulation and (b) a photo of air duct with insulation.

Figure 4.20 ORC test bench side view.

4.4 Measuring instruments

The experimental activities in this project are sequentially conducted; starting with the expander dynamometer system, expander-generator system, and the ORC system respectively. This strategy permits the use of the same set of measuring instruments for all the experiments. In this section all the measuring instruments used in the experimental activity are described.

The selected flow meter (Figure 4.21) for measurement of the working fluid flow rate (R134a) is the Omega FLR1010ST, having 1% accuracy from full scale and up to 0.2% repeatability. The measurement range is 0.1-1 litres per minute, thus the reading accuracy is ± 10 mL. The flow meter is read through a signal of 0-5 V with a data acquisition system. The pressure drop across the flowmeter is 0.41 bar at maximum flow rate. The flow meter is supplied by an external source of 12.5 Vdc. It is installed in the liquid line of the ORC system.

Figure 4.21 Liquid flow meter for working fluid flow rate measurement, Omega FLR101ST.

The above mentioned flow meter has been disassembled from the test bench after running a couple of tests. The flow capacity of this flow meter is not enough. As a result, we found a huge pressure drop in the working fluid line. The flow rate of the working fluid was calculated analytically, as mentioned in Chapter 5.

For electrical measurement, a regular clamp-on ammeter is used to measure the DC or AC electric current. Note that this instrument, when used for AC current, is calibrated for 60 Hz; thus it must be used with care when measuring the generator; if the generator does not turn at nominal speed, the current frequency is different than 60 Hz. The electrical voltage has

been measured with a regular multi-meter. The used ammeter and multi-meter are shown in Figure 4.22.

Ammeter

(a)

Multi-meter

(b)

Figure 4.22 (a) photo of clamp on ammeter and (b) photo of multi-meter.

For temperature measurement, a RDT Thermo-resistor is used. The flexible molded RTD surface sensors with flexible sensors can be mounted to any shape. The operating temperature range is -50 to 200°C and precision 100 Ω, with class "B" DIN platinum element. These sensors have adhesive backing for easy mounting on a curved shape surface-like tube. It has 4-Wire 26 AWG stranded nickel plated copper and PFA insulated and jacketed cable, 1 m (40") long.

In total, 12 thermo-resistors as indicated in Figure 4.23a are used. The thermo-resistors are connected to a data acquisition system for recording the temperature data. Omega DAQ PRO 5300 data acquisition system is used as shown in Figure 4.23b. The data acquisition system has 8 programmable input channels. The thermo-resistor reading is done with ±0.5% accuracy. The data acquisition is also used to measure the flowmeter signal in the input range of 0-10 V with an accuracy of ±0.5%.

RTD Thermal Resistor Omega DAQ-Pro

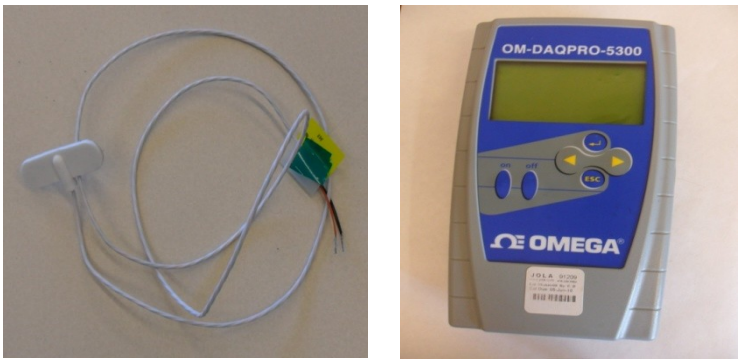

(a) (b)

Figure 4.23 (a) photo of the RTD Thermal Resistor and (b) photo of the Omega DAQ PRO 5300 data acquisition system.

The pressures are measured with bourdon tube manometers typically used for refrigeration installations. Two manifolds of this kind have been purchased, each of them comprising of two manometers with different scales; low scale (blue dial) and high scale (red dial) as shown in Figure 4.24. The blue dial has two scales, of which one measures vacuum gauge pressure from 0 to 30 mm Hg, while the other one measures atmospheric gauge pressure from 0 to 500 psi. The red dial measures in the range of 0 to 800 psi gauge pressure. The manifolds are used also for various procedure like charging the refrigerant, drawing vacuum, pressurization with nitrogen for leak test and so on.

Figure 4.24 Manifolds type pressure gauge for measurements.

Throughout the experimental procedures, extra precautions are taken not to damage or change the calibration of the equipment.

4.5 Uncertainty analysis

Each and every experiment has uncertainty due to measurement and data processing errors. An uncertainty analysis is very important to determine the uncertainty of the measured parameters and the percentage of relative uncertainty of the parameters obtained from measured data. In this experimental process, temperature, pressure, voltage, current and water flow rate are the measured parameters. The accuracy of the measured parameters is determined based on the catalogue data of the measurement equipment. The measurement accuracy data is further used in uncertainty analysis. The value of the measured parameters and the estimated value of the uncertainties are as follows:

$I_{\max} = 10\ A$, $V_{\max} = 15\ V$, $e_I = 0.05\ A$, $e_V = 0.1\ V$, $e_\rho = 1\ kg/m^3$, $e_{\dot{V}} = 18\ ml/\min$,

$e_T = 1\ K$ $e_p = 10\ kPa$, $C_p = 1.5\ kJ/kgK$, $\left(\frac{\partial h}{\partial P}\right)_T = 0.01\ kJ/kg\ kPa$, $T = 150^\circ C$,

$P = P_{sat}\left(50^\circ C\right)$

The temperature measurement equipment RTD has connected with data acquisition equipment to measure temperature with an accuracy of $\pm 0.5\%$. Also, the efficiencies of the air duct fan and electric heater are unknown and estimated. The measurement of the pressure of the working fluid was taken at different points which have some time differences. This time differences could be the reason of uncertainty of correct data. Also in this research, collected temperature data has some correction value as mentioned in the results section.

- The electric power: $\dot{W} = V \times I$, $d\dot{W} = I\ dV + V\ dI$,

  $e_{\dot{W}} = I_{\max} \times e_V + V_{\max} \times e_I$, $\frac{e_{\dot{W}}}{\dot{W}} = 1.25\%$
- The mass flow rate:

  $\dot{m} = \dot{V} \times \rho$, $\rho = \rho_{liq}\left(T_{sat}\right)$, $d\dot{m} = \dot{V}\ d\rho + \rho\ d\dot{V}$, $\dot{V} = 100 + 180\ V\ \left[ml/\min\right]$

  $e_{\dot{m}} = \dot{V} e_\rho + \rho_{\max} \times e_{\dot{V}}$, $e_{\dot{V}} = 180 e_v$, $\frac{e_{\dot{m}}}{\dot{m}} = 3.15\ \%$
- The specific enthalpy of working fluid:

$$h = h\left(T,\ P\right),\ dh = C_p\ dT + \left(\frac{\partial h}{\partial P}\right)_T \times dP$$

$$e_h = C_p\ e_T + \left(\frac{\partial h}{\partial P}\right)_{T,\max} \times e_P \quad \frac{e_h}{h} = 1.6\ \%$$

Therefore, the working fluid temperature data acquisition equipment error is 0.5 %.

The results of the uncertainty analysis for electric power, mass flow rate and specific enthalpy of the working fluid are each shown to be within 94% of confidence level. The highest relative uncertainty is at the determination of the mass flow rate, at approximately 3.5%, while the lowest relative uncertainty is for electric power, at approximately 1.25%.

CHAPTER 5: SYSTEM ANALYSIS

The research project is designed with an aim to develop an ORC heat engine based on the criteria of higher thermodynamic efficiency, potential for practical applicability, and high economic feasibility. The main components of the experimental set up are selected carefully to match the available system components for future build up of the practical heat engine. The test bench consists of air duct, boiler (evaporator), heat exchanger, expander, and condenser as the main components of the ORC. In addition, auxiliary and measuring equipments are incorporated for controlling the operating parameters during the experimental procedures. Each component, and the overall system, is analyzed in the following sections.

5.1 Air duct

The air duct is a closed loop insulated arrangement in which a set of electrical resistance heaters are positioned the maximum output being 7800 W (initially 3600 W). A 25W blower fan circulates the air within the duct carrying the heat from the heaters. A finned-tube heat exchanger (evaporator) placed downstream of the heaters and blower transfers heat from the hot air to the working fluid passing through the tubes by convection. The air-duct set-up represents a practical heat source such as waste heat, flue gas or exhaust gas. Also, it can simulate the heat transfer mechanism of other renewable energy heat sources.

Analysis of heat transfer within this system is performed with measured and assumed parameters described in the following subsections.

5.1.1 Thermodynamic model

An energy balance approach is used to determine the theoretical flow rate of the air through the duct, as well as the calculated heat transfer rate to the evaporator. There is some uncertainty in the calculation due to the unknown fan-efficiency (η_{fan}) and unknown heater efficiency (η_{heater}). The temperatures considered as 'input' and 'output' temperatures of the air are those taken before and after the evaporator. Properties of air are taken at the average air temperature.

$$\dot{Q} = \dot{m}_{air}\, c_{p,air} \left(T_{air,1} - T_{air,2}\right) = \dot{m}_{air} \left(h_{air,1} - h_{air,2}\right) \quad (5.1)$$

Again, we have the total heat from heaters,

$$\dot{Q} = \eta_{heater} N_{heater}\ 600 \quad (5.2)$$

where N_{heater} is the number of heaters.

Using the continuity equation we have equation (5.3) from which the air velocity can be calculated:

$$\dot{m}_{air} = \rho_{air}\, A_{duct}\, v_{air} \quad (5.3)$$

5.1.2 Theoretical analysis

For the purpose of a preliminary air flow model, a temperature distribution is assumed through the duct and a mass flow rate of air at atmospheric pressure is determined from the known heat input of 3600 W.

Table 5.1 Some duct analytical results.

Heat supply to air from heater		$\dot{Q}_{air}$ = 3.6 kW		
Heat input to Evap.		$\dot{Q}_{evap}$ = 3.24 kW		
Air Velocity		v_{air} = 1.333 m/s		
Volumetric Flow Rate		$\dot{V}_{air}$ = 0.06756 m3/s		
Mass Flow Rate		$\dot{m}_{air}$ = 0.06389 kg/s		
State Point	State	Pressure (kPa)	Temperature (°C)	Enthalpy (kJ/kg)
1	Air into evap	101.3	150	424.8
2	Air out of evap	101.3	100	374.1

5.2 Evaporator

A compact heat exchanger (CHE) is selected forn use as the evaporator in the test bench system, as shown in Figure 4.13. The evaporator (heat exchanger) is a finned-tube cross-flow type, mounted within the air-duct in such that air will flow vertically downward through the CHE, with copper tubes oriented horizontally with respect to the air-flow. Rippled-edge, aluminum fins are used to enhance the heat exchange that are spaced as 13 fins per inch, with a total of 94 fins. A header manifold separates the flow of the working fluid into five tube

circuits which carry the flow in a serpentine pattern through the fins with two passes per row over three rows, for a total of six fluid passes. The working fluid is then re-joined at an exit manifold to be fed into the expander.

For modeling purposes, the fins are considered as plain, flat fins. The fluid properties of R134a and air will be taken at their respective bulk temperatures.

The heat transfer to the air by the electric heaters is modeled under the following design parameter:

- The maximum air temperature is 150°C.
- The air temperature after the evaporator is 100°C.
- The air temperature entering the heater section is known.
- The working fluid temperature is constant, at the saturation temperature for the pressure at the entrance to the evaporator.

Table 5.2 Evaporator specification details.

Frontal height (m)	0.254	Nominal tube dia. (m)	9.525×10^{-3}
Frontal width (m)	0.1824	Transverse tube spacing, dx_t (m)	0.0254
Evaporator volume (m^3)	3.119×10^{-3}	Longitudinal tube spacing, dx_l (m)	0.02699
Face attitude	horizontal	Diagonal tube spacing, dx_d (m)	0.01149
Tube attitude	horizontal	Fin thickness (m)	2.032×10^{-4}
Fin geometry	plain fin	Fin pitch (m)	1.941×10^{-3}
Number of rows	3	Heat transfer area (m^2)	6.785
Number of circuits	5	Fin area (m^2)	1.916
Tubes per row per circuit	2	Frontal area (m^2)	0.04677
Fins/in	13	Free flow area (m^2)	0.01467
		Hydraulic diameter (m)	5.692×10^{-4}

5.2.1 Air-side analysis

The mass flow rate of air is calculated by applying energy balance around the heaters, using the known heat input:

$$\dot{W}_{heater} = \dot{m}_{air} \Delta h_{air,3-1}$$

where state 1 is follows the heater section and state 3 is that entering the heater section.

Various geometric details of the evaporator are calculated. They are:

- total air-side heat transfer area, A_{ht},
- minimum free-flow area, A_{ff},
- frontal area, A_{fr} and
- evaporator volume V_{evap}

From these geometric details the volume ratio (α), free low to frontal area ratio (σ), hydraulic radius (r_h), and hydraulic diameter (D_h) can be calculated from the following equations:

$\alpha = \frac{A_{ht}}{V_{evap}}$,

The free-flow to frontal area ratio (σ), $\alpha = \frac{A_{ht}}{V_{evap}}$,

The hydraulic radius, $r_h = \frac{\sigma}{\alpha}$

and the hydraulic diameter, $D_h = 4r_h$

The mass velocity and Reynolds number of the air are determined at the bulk temperature across the evaporator:

$G_{air} = \frac{\dot{m}_{air}}{A_{ff}}$ and

$Re_D = \frac{G_{air} D_h}{\mu_{air}}$

The air-side pressure drop analysis is applied using correlations defined by Wang et al. (2000) for cross-flow finned-tube heat exchangers with multiple rows.

$$\Delta P_{evap} = \frac{{G_{air}}^2 v_{air,i}}{2}\left[(1+\sigma^2)\left(\frac{v_{air,o}}{v_{air,i}} - 1\right) + \left(f_{fanning}\left(\frac{A_{ht}}{A_{ff}}\right)\left(\frac{v_{air,m}}{v_{air,i}}\right)\right)\right]$$

where the fanning friction factor is determined based on three factors which are dependent on tube spacing of the heat exchanger.

$$f_{fanning} = 0.0267 Re_D^{F1}\left(\frac{dx_t}{dx_l}\right)^{F2}\left(\frac{F_p}{D_o}\right)^{F3}$$

$$F_1 = -0.764 + 0.739\left(\frac{dx_t}{dx_l}\right) + 0.177\left(\frac{F_p}{D_o}\right) - 0.00758 N_{row}$$

$$F_2 = -15.689 + \frac{64.021}{\ln(Re_D)}$$

$$F_3 = 1.696 - \frac{15.695}{\ln(Re_D)}$$

where F_p is fin pitch and D_o tube outer diameter and N_{row} number of row.

The convective heat transfer coefficient of the air is derived from the Colburn factor using the relation:

$$j_{Colburn} = \frac{h_{air}}{\rho_{air} V_{max} c_{p,air}} Pr_{air}^{2/3}$$

where the Colburn factor is dependent on the number of rows, using factors provided by Wang et al (2000).

$$j_{Colburn} = 0.086\, Re_D^{E3}\, N_{row}^{E4} \left(\frac{F_p}{D_o}\right)^{E5} \left(\frac{F_p}{D_H}\right)^{E6} \left(\frac{F_p}{dx_t}\right)^{-0.93}$$

$$E_3 = -0.361 - \frac{0.042\, N_{row}}{\ln(Re_D)} + 0.158\, ln\left(N_{row} \left(\frac{F_p}{D_o}\right)^{0.41} \right)$$

$$E_4 = -1.224 - \frac{0.076\left(\frac{F_p}{dx_t}\right)^{1.42}}{\ln(Re_D)}$$

$$E_5 = -0.083 + \frac{0.058\, N_{row}}{\ln(Re_D)}$$

$$E_6 = -5.735 + 1.21 ln\left(\frac{Re_D}{N_{row}}\right)$$

The heat transfer coefficient is used to determine the efficiency of the fins and the overall efficiency of the evaporator.

$$\eta_o = 1 - \frac{A_{fin}}{A_{ht}}(1 - \eta_f)$$

$$\eta_f = \frac{\tanh(m\, r_t\, \phi_{hex})}{m\, r_t\, \phi_{hex}}$$

where the factors m, r_t, and ϕ_{hex} are dependent on the hexagonal fin spacing geometry due to the staggered arrangement of the tubes:

$$m = \sqrt{\frac{2\, h_{air}}{k_{\,fin}\, t_f}}$$

$$\zeta_{hex} = \frac{0.5\, dx_t}{r_t}$$

$$\beta_{hex} = \frac{dx_d}{0.5 dx_t}$$

$$r_{e,hex} = 1.27\, \zeta_{hex} \sqrt{\beta_{hex} - 0.3}\, r_t$$

$$\phi_{hex} = \left(\frac{r_{e,hex}}{r_t} - 1\right)\left(1 + 0.35\, ln\left(\frac{r_{e,hex}}{r_t}\right)\right)$$

Based on the calculated efficiency, the heat transfer from the air to the evaporator is determined, and the following equations are applied to determine the overall heat transfer coefficient, U [W/m^2 K].

$\dot{Q}_{air} = \dot{m}_{air}\Delta h_{air,1-2}$

$\dot{Q}_{evap} = \eta_o \dot{Q}_{air}$

$\dot{Q}_{evap} = UA_{ht}\Delta T_{lm}$

The effectiveness of the evaporator is calculated by the ratio of the actual heat transfer rate to the maximum heat transfer rate, based on the inlet (extreme) temperatures of the two fluids.

$\varepsilon = \frac{\dot{Q}_{evap}}{\dot{Q}_{max}} = \frac{U\ A_{ht}\ \Delta T_{lm}}{\dot{m}_{air}\ c_{p,air}(T_{air,in} - T_{R134a,in})}$

5.2.2 Tube-side analysis

Using the calculated overall heat transfer coefficient, the convective heat transfer coefficient of the working fluid is determined using the thermal resistance network of the air, tube, and working fluid.

$UA_{ht} = R_{air} + R_{tube} + R_{R134a}$

$R_{air} = \frac{1}{h_{air}A_{ht}}$

$R_{tube} = \frac{\ln\left(\frac{r_o}{r_i}\right)}{2\pi L_{tube}\, k_{tube}}$

$R_{R134a} = \frac{1}{h_{R134a}A_{s,tube}}$

The convective heat transfer coefficient is used to calculate the Nusselt number for the working fluid, which can then be related by the Dittus-Boelter equation to calculate the Reynolds number.

$Nu_{R134a} = \frac{h_{R134a}D_i}{k_{R134a}} = 0.023\ Re_{R134a}^{0.8}\ Pr_{R134a}^{0.3}$

The heat transfer coefficient, $h_{R134a} = N_{u_{R134a}}\ \frac{k_{R134a}}{D_i}$

The heat transfer to the working fluid, R134a, is considered to be equal to the heat transfer to the evaporator. The mass flow rate is assumed constant at 25 g/s, and the enthalpy at the inlet is assumed to be the enthalpy of R134a as a saturated liquid at the inlet pressure.

$\dot{Q}_{R134a} = \dot{Q}_{evap}$

$$\dot{Q}_{air} = \dot{m}_{R134a}\ (h_{r134a,2} - h_{R134a,liquid})$$

The outlet enthalpy is used to determine the quality of the working fluid at the exit, which will be either be in the two-phase region, saturated vapour, or superheated vapour.

Table 5.3 EES model result details.

Air-side results		Tube-side results	
T_{in} (°C)	150	T_{in} (°C)	45
T_{out} (°C)	100	T_{out} (°C)	45
P_{in} (kPa)	P_{atm} = 101.3	P_{in} (kPa)	P_{sat} = 1319
$f_{fanning}$	0.05865	Quality (x_{in})	0
$P_{loss,Hex}$ (kPa)	298.6×10^{-3}	Quality (x_{out})	0.8287
$j_{Colburn}$	0.02331	h_{conv} (W/m^{2}K)	417.9
h_{conv} (W/m^{2}K)	122.1	Re_l	6783
Re_D	1902	Nu	37.7
Nu	39.95		

5.3 Expander

In this experimental set-up, the scroll expander acts as the power generating component of the ORC heat engine. Load to the generator is applied by connecting a number of electrical resistances (heater) to the circuit. The load may be varied from 1 to 8 resistances to measure the variation in power, in order to determine the ideal loading condition.

The energy balance of the expander is modeled in the same way as a turbine in a typical Rankine cycle.

$$\dot{W}_{expander} = \eta_{exp}\ \dot{V}_{r134a}\ \Delta P_{exp} = \eta_{exp}\ \dot{m}_{r134a}\ (u_1 - u_2)$$

The efficiency of the expander can be calculated based on measured values of temperature and pressure at inlet and outlet, and determining the temperature under isentropic conditions. The equation for expander efficiency is given by

$$\eta_{exp} = \frac{\dot{W}_{exp,actual}}{\dot{W}_{exp,isentropic}} = \frac{(h_1 - h_2)}{(h_1 - h_{2,S})}$$

where, $h_{2,S}$ is the enthalpy associated with the isentropic entropy value at the outlet pressure.

The shaft power is also measured by the measured current and voltage under various loading conditions.

$$\dot{W}_{\text{shaft}} = V \times I = \omega \times \tau$$

$$V = I \times R$$

5.3.1 Theoretical analysis

The expander is modeled with a 70% isentropic efficiency and a pressure ratio of 2.5. Table 5.4 describes the state points of the cycle, including the expander. Note that a quality value of 100 indicates a superheated vapour state and a value of -100 indicates a sub-cooled liquid state.

Table 5.4 State property values of R134a.

Mass Flow Rate (kg/s)		m_{r134a} = 0.02369 kg/s					
#	State	Pressure (kPa)	Temp.(°C)	Saturation Temp. (°C)	Enthalpy (kJ/kg)	Entropy (kJ/kg K)	Quality
1	Compressor outlet	2066	79.66	68.9	295.8	0.9454	100
2	Cond. outlet / Heat ex. Inlet	1997	67.4	67.4	151.7	0.5249	0
3	Heat ex. Outlet / Evap. inlet	1997	62.4	67.4	143.1	0.4995	100
4	Evap. outlet / Exp. inlet	1928	65.85	65.85	279.9	0.9032	1
5	Exp. Outlet (P_r=2.5)	771.4	30.62	30.03	267.3	0.9209	100
6	After mixer	771.4	30.62	30.03	267.3	0.9209	100
7	Compressor inlet	771.4	30.62	30.03	267.3	0.9209	100
8	By-pass (into mixer)	NA	NA	NA	NA	NA	NA

Based on the EES calculated results summary as given in Table 5.4 with the ORC cycle different state point properties we can have total heat addition in the heating source 3600 W

(electric heaters). The condenser and heat exchanger heat rejection was calculated from mass flow rate of working fluid and enthalpy difference between state 1 to 2 and 2 to 3 respectively. Similarly total work of compressor and expander was found out from mass flow rate of working fluid and enthalpy difference between state 1 to 7 and 4 to 5 respectively. Also evaporator and total heat input was calculated from mass flow rate of working fluid and enthalpy difference between sate 3 to 4.

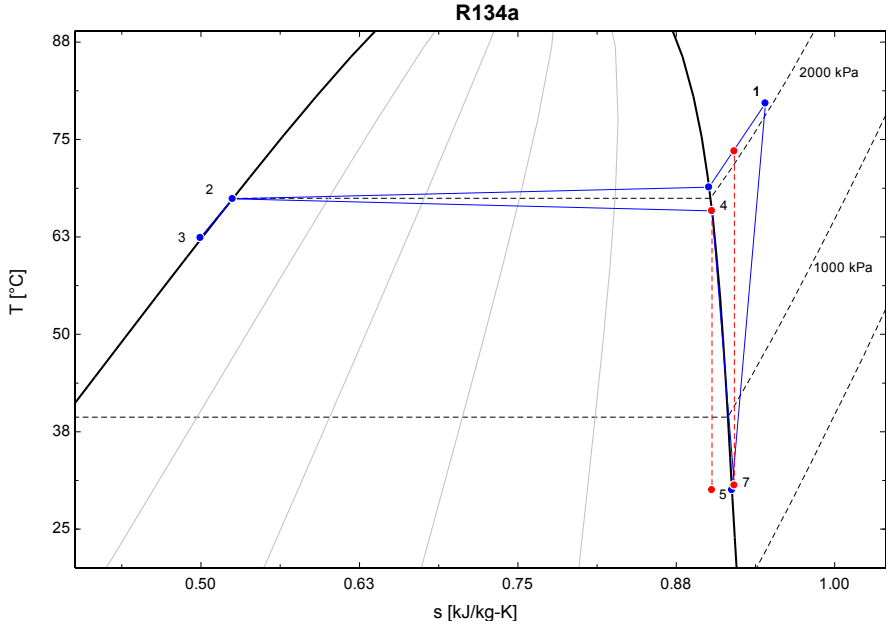

Figure 5.1 T-s diagram of cycle.

Table 5.5 EES calculation results summary.

Inputs		Outputs	
Heater duty to air	$\dot{W}_{air}$ = 3.6 kW	Condenser	$\dot{Q}_{cond}$ = 3.414 kW
Heat input to evap.	$\dot{Q}_{evap}$ = 3.24 kW	Heat exchanger	$\dot{Q}_{h\ ex}$ = 0.2033 kW
Compressor work	$\dot{W}_{comp}$ = 0.6748 kW	Expander work	$\dot{W}_{exp}$ = 0.2971 kW

The thermal efficiency, $\eta_{thermal}$ and exergy efficiency, ψ of the cycle was calculated based on the results summary (Table 5.5). The equations and results are as follows:

$$\eta_{thermal} = 1 - \frac{\dot{Q}_{out}}{\dot{Q}_{in}} = 0.1537$$

where the total heat addition is determined by the equation, $\dot{Q}_{in} = \dot{W}_{air} + \dot{W}_{comp}$ and the total heat rejection by the system is determined by $\dot{Q}_{out} = \dot{Q}_{cond} + \dot{Q}_{h\,ex}$.
The exergy efficiency is the calculated using the following equation

$$\psi = \frac{\dot{W}_{in}}{\dot{E}x_{in}}$$

where the exergy input is calculated from $\dot{E}x_{in} = \dot{m}_{air}\left(h_{a,1} - h_0\right) - T_0\left(s_{a,1} - s_0\right) = 7.508$ kW, and the net work produced is approximated by $\dot{W}_{net} \sim \dot{W}_{exp}$, to better represent the performance with a traditional pump in the ORC, which consumes less work than the compressor utilized in the test bench and is the design intent for the future generation of the heat engine.

5.4 Heat exchanger

A counter-flow, single-pass shell-and-tube heat exchanger is designed and placed within the cycle, after the condenser and prior to the evaporator. The purpose of the shell and tube heat exchanger in this experiment is to slightly sub-cool the working fluid which leaves the condenser in order to obtain a valid volumetric flow rate reading of the working fluid. While the assumption is made that the fluid exiting the condenser is a saturated liquid, they may be a chance that there are small traces of vapour bubbles remaining in the fluid. These bubbles could result in inaccurate readings for flow rate; therefore sub-cooling here by ensures fully liquid flow through the meter.

The temperature difference across the heat exchanger is assumed based on a maximum desired temperature drop of 5°C for the working fluid.

Normal tap water is used to act as cold fluid. The flow rate of the water may be varied based on the degree of sub-cooling required. Water pressure is considered to be 170 kPa with an inlet temperature 13°C. Enthalpy of water for the initial temperature and pressure is 54.66 kJ/kg.

The ε-NTU method is applied in order to determine the minimum required length of the heat exchanger. Basic assumptions were made in order to complete the design; maximum

temperature difference of working fluid (ΔTh_{max} = 5°C), minimum volumetric flow rate of cooling water ($\dot{V}c_{min}$ = 1 Lpm).

The additional assumptions are given as follows:

- The steady operating conditions exist.
- The heat exchanger is insulated; heat loss is negligible (assumes adiabatic shell).
- The surface temperature of tube is considered isothermal at average working fluid temperature.
- The mass flow rate of the working fluid is 25.84 g/s for initial calculations.
- The inlet temperature of working fluid is 50°C (for an assumed range of 40-60°C).
- The pressure of working fluid is assumed as saturated-liquid pressure at T1.
- The inlet temperature of cooling water is 7°C for initial calculations.
- The flow of working and cooling fluids is considered fully developed; no fittings will be considered in pressure loss calculations.

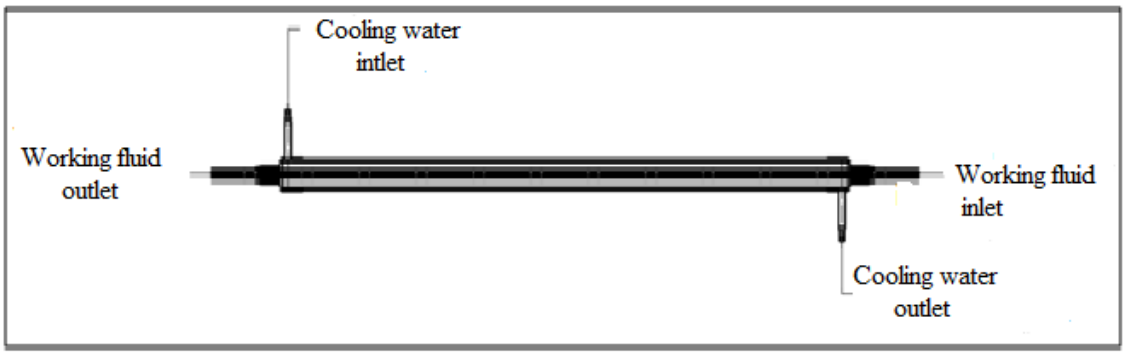

Figure 5.2 Shell and tube heat exchanger.

The energy balance for the shell and tube heat exchanger is given as

$$\dot{Q} = U_o\, A_s\, \Delta T_{lm} = U_o\, A_s\, \frac{(T_{h,1}-T_{c,2})-(T_{h,2}-T_{c,1})}{\ln\left[\frac{(T_{h,1}-T_{c,2})}{(T_{h,2}-T_{c,1})}\right]}$$

The heat transfer rate for each fluid is obtained using energy balance for each based on the inlet and outlet conditions of the fluid. Inlet and outlet temperature readings for each fluid are considered while pressure drop and fouling across the heat exchanger are neglected.

The total heat transfer for cold fluid is being calculated using following equations.

$$\dot{Q} = C_c\,\Delta T_c = \dot{m}_c\,c_{p,c}\left(T_{c,2} - T_{c,1}\right) = \dot{m}_c\left(h_{c,2} - h_{c,1}\right)$$

$$\dot{Q} = C_h\ \Delta T_h = \dot{m}_h\,c_{p,h}\left(T_{h,1} - T_{h,2}\right) = \dot{m}_h\left(h_{h,1} - h_{h,2}\right)$$

$$\dot{m}_h\,c_{p,h}\left(T_{h,1} - T_{h,2}\right) = \dot{m}_c\,c_{p,c}\left(T_{c,2} - T_{c,1}\right)$$

where C_c is thermal capacity of cold fluid and C_h is thermal capacity of hot fluid, respectively.

The effectiveness of the heat exchanger can be calculated as the ratio of the actual heat transfer rate to the maximum possible heat transfer rate;

$$\varepsilon = \frac{\dot{Q}}{\dot{Q}_{max}}$$

The maximum heat transfer rate is given by $\dot{Q}_{max} = C_{min}\left(T_{h,1} - T_{c,1}\right)$, where

$$C_{min} = \begin{cases} C_h\ if\ C_h < C_c \\ C_c\ if\ C_c < C_h \end{cases}$$

The required length, l_{tube} of heat exchanger is determined from the equation for surface area, A_s of a cylinder.

$$A_s = \pi\,D_{i,tube}\,l_{tube}$$

A pressure drop check is performed to ensure that the actual outlet temperature of the working fluid is not higher than the saturation temperature for the outlet pressure of the fluid when losses are considered.

The pressure drop of the working fluid across the heat exchanger is determined in units of kPa by

$$\Delta P = f\,\frac{l_{tube}}{D_{i,tube}}\,\frac{1}{2}\,\rho_h\,\frac{v_{h,avg}^2}{1000},$$

The friction factor for assumed turbulent flow is calculated by the equation

$$\frac{1}{\sqrt{f}} = -1.8 \cdot \log\left[\frac{6.9}{Re_h} + \left(\frac{\text{Relative Roughness}}{3.7}\right)^{1.11}\right]$$

where the relative roughness of the tube is calculated by

$$\text{Relative Roughness} = \frac{\varepsilon_{\text{rougness,copper}}}{1000\ D_{i,tube}}\ (\text{mm}).$$

The power loss due to pressure drop across the heat exchanger is calculated by the following equation:

$$\dot{W}_{\Delta P} = A_{x,tube}\ v_{h,avg}$$

The calculated result and parameter are represented in Table 4.2, considering minimum and maximum working fluid flow rates.

CHAPTER 6: RESULTS AND DISCUSSION

In this chapter the results of this work are presented and discussed. As this work mainly focuses on experiments with the ORC, the core of the results is represented by the measurements with the experimental facility. In addition, a number of models were developed in EES (Engineering Equation Solver) to predict the operation of various components of the ORC and the experimental facility: boiler, expander, condenser, heat exchanger, pump and compressor. These models were used to process the measured data and extract important quantities for the analysis of the investigated the ORC and its performance. The models were validated against the experimental data and further used for analysis of a number of relevant case studies of the ORC applications, when the hot source comes from a hot gas and the heat engine works under co-generation regime such that it always meets the heating demand.

6.1 Experimental results

6.1.1 Measurements and data processing

The experimental system described in Chapter 4 is used to investigate the ORC operation and the behaviour and performance of each of the heat engine components: boiler, expander and heat exchanger. As mentioned earlier, the heat source is hot air at the temperatures of up to 180°C, which simulates any practical situation where heat is recovered from hot gases, like fuel combustion gases. The maximum pressure of the working fluid during operation was 350 psi and the pressure ratio over the expander was varied from 1.5 to 3. The acquired experimental data for all of the runs are centralised in Table 6.1.

This data has been processed based on mass and energy balance equations for each component and for the overall system. Catalogue data of various components, like the compressor, electrical generator, blower, condenser, and condenser fan, have been used for data processing to determine important quantities like flow rate, work input and output. The measured parameters are indicated in Figure 6.1, which illustrates the thermodynamic state points on the operational diagram of the experimental system. The parameters that are directly measured are the temperatures, gauge pressures, voltages and currents; the indirectly measured parameters are the input heat flux and the work rates. The input heat flux is determined from electrical measurements on resistive heaters with $\dot{Q}_{\text{heater}} = VI$. The work

consumed by the compressor as well as by the air blower is determined based on single phase AC measurements.

Table 6.1 Summary of experimentally recorded data.

$\dot{Q}_{\text{heater}}$	Temperature (°C) at:													Pressure (psig) at:					$\dot{W}_{\text{dc}}$		$\dot{V}_{\text{water}}$
(W)	1	3	4	5	6	7	9	10	11	12	13	14	15	2	4	5	6	7	V (V)	I (A)	(l/min)
2400	x	x	46.4	41.3	x	x	x	x	x	x	x	93	51.3	175	x	140	90	65	8.5	6.8	x
2400	x	x	50.3	45.2	x	x	x	x	x	x	x	112.2	56.6	200	x	165	115	77	9	6.7	x
2400	x	x	59.3	53.4	x	x	x	x	x	x	x	99.9	63.2	250	x	200	147	103	9.9	7.3	x
2400	x	x	54.3	58.1	x	x	x	x	x	x	x	98.1	67.1	300	x	240	165	105	11	7.66	x
2400	x	x	60.8	55.7	x	x	x	x	x	x	x	96	66.4	275	x	225	165	150	8.7	6.8	x
2400	x	x	x	x	x	x	x	x	x	x	x	x	x	137	x	108	70	40	7.25	6.1	x
2400	x	x	52.3	46.5	34.3	x	x	x	x	x	x	92	55.4	200	x	175	110	65	11.4	7.8	x
2400	x	x	64	57.8	45.5	x	x	x	x	x	x	103.8	64.7	285	x	140	160	95	13.6	9.8	x
2400	x	x	64	57.8	45.9	x	x	x	x	x	x	108.8	68.5	300	x	140	170	110	11	9	x
2400	x	x	54.3	47.6	x	x	x	x	x	x	x	140	73.3		x	x	x	x	x	x	x
2400	77.4	59.7	57.2	55.6	34.9	22.6	x	x	x	x	87.9	138.8	70.3	245	x	205	110	70	4.9	20.5	x
2400	79.1	61	59.4	58.6	36.9	22.8	x	x	x	x	87.5	132.2	69.9	250	x	215	120	75	5.1	21.4	x
2400	x	x	57.4	56.2	38.6	x	x	x	x	x	x	131.1	68.5		x	212	137		4.25	18.2	x
2400	90.3	59.9	60.1	58.7	41.8	36.9	x	x	x	x	88.7	131	70	288	x	225	150	125	4.3	18.6	x
2400	x	x	64.5	64.7	46.9	x	x	x	x	x	x	133.6	73.7		x	x	x	x	x		x
2400	x	x	63.2	62.3	45.2	x	x	x	x	x	x	143.5	78.7	300	x	250	165	140	3.5	19.6	x
2400	66.1	49.6	49	47.5	26.2	13.8	x	x	x	x	77.3	119	60.1	185	180	160	80	47	3.22	20.1	x
2400	67.8	51.5	51.7	45.6	28.5	14.2	x	x	x	x	77.5	121.1	61.3	200	205	180	90	50	3.75	23.6	x
2400	73.3	50.1	52.8	51.2	29.4	16.2	x	x	x	x	79.9	122.6	62.4	210	210	180	95	55	3.8	24	3.59
2400	x	x	x	x	x	x	x	x	x	x	x	x	x	x	x	x	x	x	5.45	18.5	3.59
2400	x	x	x	x	x	x	x	x	x	x	x	x	x	210	210	175	105	60	8	14	3.59
2400	x	44.4	43.3	x	x	x	14.7	19.4	x	x	x	x	x	160	160	140	65	37	x	x	3.59
2400	x	44.3	43.1	x	x	x	14.7	19.1	x	x	72.5	x	x	160	160	135	65	35	x	x	3.59
2400	67.2	44.2	43	40.1	19.9	69	14.6	19	x	x	x	116.2	54	157	157	x	x	37	3	18.4	3.59
2400	x	x	42.1	40.7	19.8	x	14.5	x	x	x	x	116.1	53.7	155	155	135	65	35	3.5	19.6	3.59
2400	70.8	44.2	42.9	80.2	65	18.1	16.2	21.8	29	44.5	x	130.3	89.7	165	165	150	78	60	3.6	25	2.2
2400	73.1	46.5	44.8	74.1	63.9	27.8	17.2	22.5	29	47.5	x	124.3	81.5	168	168	160	82	65	3.6	24.9	2.2
2400	73.8	46.9	45.4	74.4	61	20.8	17.3	23.1	29	46	x	123.8	81.2	175	175	160	85	65	3.6	23	2.2
6303	75	35.2	24.6	70.5	34	30.6	14.9	15.4	x	x	x	114.4	77.7	120	113	120	40	20	4.8	29	12.2

Table 6.1 Summary of experimentally recorded data (continued).

$\dot{Q}_{\text{heat}}$	Temperature (°C) at:													Pressure (psig) at:					$\dot{W}_{\text{exp}}$		$\dot{V}_{\text{water}}$
(W)	1	3	4	5	6	7	9	10	11	12	13	14	15	2	4	5	6	7	V (V)	I (A)	(l/min)
6303	83.9	37	28.5	60.6	40	36.4	15.4	15.9	x	x	x	106	68.5	150	140	130	60	45	4.2	24	12.2
6303	68.3	41.1	44.2	64.1	52.2	15.2	15.9	21.5	x	x	x	104	69.1	145	145	135	70	55	3.8	24	12.2
6303	69	41.6	41	64.1	50.1	15.8	15.9	21.6	x	x	x	101	66.2	150	150	135	70	50	4.6	22.4	12.2
6303	69.1	41.5	41	61.1	49.2	15.6	15.9	21.5	x	x	x	101	65.7	150	150	130	70	50	4.5	22.6	12.2
6303	69.7	41.8	41.5	57.9	47.6	16.8	16	21.9	x	x	x	99	64.2	150	150	135	72	55	5.8	20	12.2
6303	71.2	43	42.3	59.1	45.2	20.1	16.1	22.5	x	x	x	90.6	60.6	155	155	140	85	65	7.72	14.7	12.2
6303	70.4	41.8	41.5	52	40.8	18.3	16.3	23.1	x	x	x	95.5	59.6	155	150	140	80	65	8.02	13.2	12.2
7800	70.8	44.2	42.9	80.2	65	18.1	16.2	21.8	x	130	89.7	x	x	180	180	165	93	75	3.6	25	2.2
7800	73.1	46.5	44.8	74.1	63.9	27.8	17.2	22.5	x	124	81.5	x	x	183	183	175	97	80	3.6	24.9	2.2
7800	x	x	x	x	x	x	x	x	x	x	x	x	x	x	x	x	x	x			2.2
7800	73.8	46.9	45.4	74.4	61	20.8	17.3	23.1	x	124	81.2	x	x	190	190	175	100	80	3.6	23	2.2
7800	x	x	x	x	x	x	x	x	x	x	x	x	x	x	x	x	x	x			2.2
7800	x	x	x	x	x	x	x	x	x	x	x	x	x	x	x	180	95	x	3.6	25.8	2.2
7800	x	x	x	x	x	x	x	x	x	x	x	x	x	x	x	180	100	x	4.9	22.4	2.2
7800	x	x	x	x	x	x	x	x	x	x	x	x	x	x	x	180	115	x	8.6	14	2.2
7800	x	x	x	x	x	x	x	x	x	x	x	x	x	x	x	190	120	x	8.2	14	2.2

Note: each row represents an experimental run; "x" stands for "measurement not taken".

This is done according to $\dot{W}_{\text{comp}} = [VI\cos\phi]_{\text{comp}}$ and $\dot{W}_{\text{blow}} = [VI\cos\phi]_{\text{blow}}$, where ϕ is the phase shift angle between the current and voltage. ϕ is assumed based on equipment catalogue data as 0.8 for both the compressor and blower motors. The compressor power is around 2.5-3 kW according to manufacturer data, while the blower's maximum power consumption is 0.5 HP. The work produced by the generator connected to the expander is determined with $\dot{W}_{\text{dc}} = V \times I$ based on the current and voltage measurement of the DC after the rectifier. Based on the generated power in the DC, the AC power is determined. The three-phase rectifier coupled to the generator includes 2 diodes per phase which dissipate power according to the voltage in the direct current coupling. The typical voltage for direct polarization of diodes is ~0.6 volts. Therefore, the AC voltage is calculated by

$$\dot{W}_{\text{gen}} = (V + 1.2)I \tag{6.1}$$

where $\dot{W}_{\mathrm{gen}}$ is the three-phase power produced by the generator.

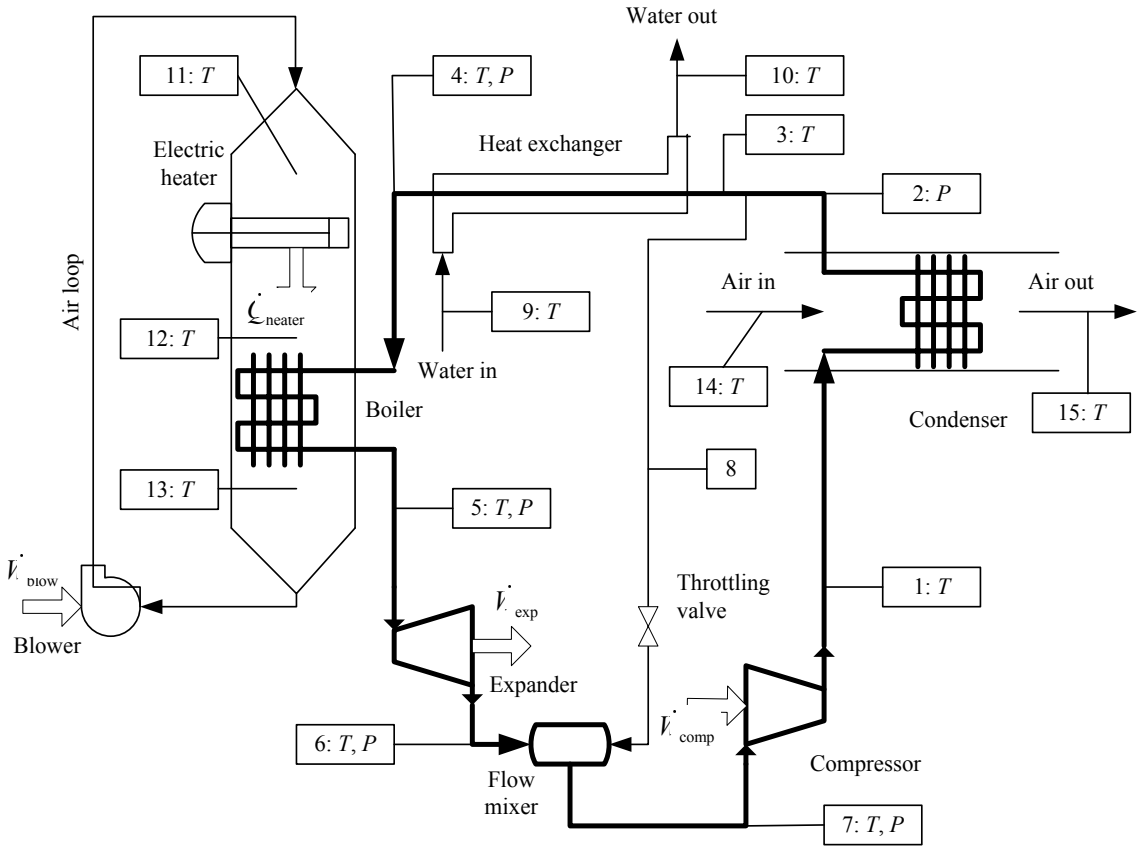

Figure 6.1 Experimental system with indicated state points and measured parameters.

The temperatures at each measurement station were corrected based on the local heat loss analysis. In the actual configuration, the fluid temperature has been estimated based on measurement at the tube wall exterior. Therefore, the following heat transfer equations were used to derive a relationship between the wall temperature and the actual fluid core temperatures:

$$\left.\begin{aligned} T_{\mathrm{f}} - T_{\mathrm{w}} &= \frac{q'}{h_{\mathrm{i}}\,\pi\,D_{\mathrm{i}}} \\ T_{\mathrm{w}} - T_{\mathrm{s}} &= \frac{q'}{k\,\ln\left(1+\frac{2\delta}{D_{\mathrm{i}}}\right)} \\ T_{\mathrm{s}} - T_{\infty} &= \frac{q'}{h_{\mathrm{o}}\,\pi\,(D_{\mathrm{i}}+2\delta)} \end{aligned}\right\} \tag{6.2}$$

where the indices f, w, s, ∞ indicate the fluid, wall, insulation surface, and air temperatures respectively. Indices i and o represent tube wall inner and outer respectively, while q' is the

heat flux per unit of tube length, h is the heat transfer coefficient, k is the thermal conductivity of the pipe insulation, δ is the tube wall thickness and D is the tube diameter.

Table 6.2 Corrected fluid temperatures at each measurement station**.**

Station	Run														
	1	2	3	4	5	6	7	8	9	10	11	12	13	14	15
1	61	65	74.2	94.5	78.2	x	73.2	73.2	116.6	x	78.2	80.9	x	91	x
2	x	x	x	55.4	x	x	x	x	64.6	x	61.1	61.3	x	x	x
3	x	x	x	x	x	x	x	x	x	x	61.1	61.3	x	60.8	x
4	46	51.1	60.7	55.3	61.2	x	57.7	57.7	64.3	x	58.3	61.3	x	62.1	65.9
5	41	46.2	55.6	61.8	56.1	x	56.3	56.3	58	x	56.2	60.2	x	59	65.9
6	27.2	36.1	44.7	48.2	48.2	x	34.1	34.1	52.2	x	33.9	36.7	x	43	47.8
7	19.3	24.6	32.4	39.2	46.8	x	21.2	21.2	49.1	x	20.7	22.6	x	38.0	x
Station	Run														
	16	17	18	19	20	21	22	23	24	25	26	27	28	29	30
1	x	x	68.9	x	x	x	x	x	x	x	x	70.8	74	x	76.1
2	x	x	x	x	x	x	x	x	x	x	x	x	x	x	x
3	x	x	45.8	x	x	x	x	x	x	x	x	46	47.8	x	36.4
4	x	x	45	x	x	x	x	x	x	x	x	43.2	45.1	x	25.1
5	x	48.1	50.7	50.7	x	x	x	x	x	x	x	81.3	75	x	71
6	x	22.6	27.7	29.4	x	x	x	x	x	x	23.6	66.9	65	x	35.3
7	x	x	70.2	x	x	x	x	x	x	x	x	19.3	29	x	31.9
Station	Run														
	31	32	33	34	35	36	37	38	39	40	41	42	43	44	45
1	x	x	x	x	70.2	x	x	x	x	x	x	70	x	x	x
2	x	x	x	x	x	x	x	x	x	x	x	x	x	x	x
3	x	x	x	x	42.1	x	x	x	x	x	x	43	x	x	x
4	x	x	x	x	42	x	x	x	x	x	x	41.5	x	x	x
5	x	x	x	x	58.3	x	x	x	x	x	x	59	x	x	x
6	x	x	x	x	48.4	x	x	x	x	x	x	41	x	x	x
7	x	x	x	x	17.6	x	x	x	x	x	x	19	x	x	x

Note: all temperature values are in ^{o}C and x data not recorded or assessed.

Based on the above relation one can derive the following one, by eliminating T_{s}

$$T_{\mathrm{f}} = T_{\mathrm{w}}(1 + R) - R\,T_{\infty} \tag{6.3}$$

were the dimensionless term R is defined by

$$R = \frac{1}{h_{\mathrm{i}}\pi D_{\mathrm{i}}} \times \left[\frac{1}{k \times \ln(1+2\delta/D_{\mathrm{i}})} + \frac{1}{h_{\mathrm{o}}\pi(D_{\mathrm{i}}+2\delta)}\right] \tag{6.4}$$

Based on actual data, namely the thermal conductivity of the pipe insulation (around 0.5 W/mK), pipe diameter (~10 mm), heat transfer coefficient by natural convection at the insulation surface (~5 W/m^{2}K), and heat transfer coefficient by forced convection inside the tube (around 50 W/m^{2}K for gas flow and 500 W/m^{2}K for liquid flow), an estimate of R in the range 1.015 to 1.15 is concluded. For example, for a measured wall temperature of 50^{o} C,

assuming that the fluid is in gas state, the actual fluid temperature is estimated to 53.5^{o} C, while if the fluid is a liquid, then its temperature is 50.4^{o} C.

Table 6.3 Pressures (absolute) and electrical powers for each run.

Parameter	Run														
	1	2	3	4	5	6	7	8	9	10	11	12	13	14	15
$\dot{Q}_{\text{boil}}$	2.16	2.16	2.16	xx.x	2.16	xx.x	2.16	2.16	2.16	xx.x	2.16	2.16	xx.x	2.16	x
$\dot{W}_{\text{exp}}$	0.07	0.08	0.09	xx	0.07	xx	0.14	0.14	0.12	xx	0.14	0.15		0.11	x
P_2	1301	1480	1825	xx	1997	xx	1791	1791	2170	xx	1791	1825		2087	x
P_4	1203	1329	1655	xx	1715	xx	1574	1791	2170	xx	1791	1825		2087	x
P_5	1067	1239	1480	xx	1653	xx	1515	1515	1273	xx	1515	1584		1653	x
P_6	722	894	1115	xx	1239	xx	860	860	1067	xx	860	929		1136	x
P_7	550	632	812	xx	1136	xx	584	584	860	xx	584	618		963	x
Parameter	Run														
	16	17	18	19	20	21	22	23	24	25	26	27	28	29	30
$\dot{Q}_{\text{boil}}$	x	2.16	2.16	2.16	x	x	x	x	x	x	2.16	2.16	5.67	5.67	5.67
$\dot{W}_{\text{exp}}$	x	0.10	0.13	0.13	x	x	x	x	x	x	0.13	0.13	0.19	0.19	0.14
P_2	x	1377	1515	1549	x	x	x	x	x	x	1239	1260	929	929	1136
P_4	x	1342	1480	1549	x	x	x	x	x	x	1239	1260	929	929	1067
P_5	x	1205	1342	1342	x	x	x	x	x	x	1136	1205	881	881	998
P_6	x	619	722	756	x	x	x	x	x	x	639	667	377	377	515
P_7	x	425	446	481	x	x	x	x	x	x	515	550	239	239	412
Parameter	Run														
	31	32	33	34	35	36	37	38	39	40	41	42	43	44	45
$\dot{Q}_{\text{boil}}$	5.67	5.67	5.67	5.67	5.67	5.67	7.03	7.03	x	7.03	x	x	x	x	x
$\dot{W}_{\text{exp}}$	0.13	0.14	0.14	0.16	0.15	0.15	0.13	0.13	x	0.12	x	x	x	x	x
P_2	1101	1136	1136	1136	1170	1170	1342	1363	x	1411	x	x	x	x	x
P_4	1101	1136	1136	1136	1170	1136	1342	1363	x	1411	x	x	x	x	x
P_5	1032	1032	998	1032	1067	1067	1239	1308	x	1308	x	x	x	x	x
P_6	584	584	584	598	687	653	743	770	x	791	x	x	x	x	x
P_7	467	446	446	481	550	550	619	653	x	653	x	x	x	x	x

Note: all pressures are in kPa absolute and x represents data not recorded or assessed.

Actual experimental observation shows that applying temperature correction is crucial, especially when the measurements are in the vicinity of saturation states. Table 6.2 indicates the corrected temperatures for each run. Note that air temperatures at stations 11-15 are measured with immersed sensor and do not need correction. Regarding the pressures, those are converted from gauge psi (ponds per square inch) to absolute kPa and the results are given in Table 6.3. In the same table the power produced by the generator ($\dot{W}_{\text{gen}}$) as calculated by Equation (6.1) and the heater power ($\dot{Q}_{\text{heater}}$) based on pressure and temperature measurements, the degree of sub-cooling or super-heating of the working fluid is determined, whichever applies. If the state is within the two-phase region, the vapour quality is

approximated based on energy balance on the involved system components and the overall energy balance.

Table 6.4 Degree of sub-cooling or super-heating or the vapour quality at each state.

#	Run														
	1	2	3	4	5	6	7	8	9	10	11	12	13	14	15
1	+10.0	+10.0	+10.0	x	+10.0	x	+10.0	+10.0	+43.0	x	+12.4	+13.3	x	+18.8	x
2	+10.0	+10.0	+10.0	x	+10.0	x	+10.0		-7.1	x	-2.9	-2.5	x	+0.3	x
3	+10.0	+10.0	+10.0	x	+10.0	x	+10.0	-5.4	-7.1	x	-2.9	-2.5	x	+0.3	x
4	-3.1	-4.4	-4.2	x	-6.6	x	-5.4	-5.4	-9.1	x	-5.4	-4.1	x	x	x
5	94%	94%	96%	x	100%	x	91%	91%	x	x	91%	90%	x	92%	x
6	96%	95%	96%	x	100%	x	93%	93%	x	x	92%	91%	x	92%	x
7	0.0	0.0	0.0	x	+2.0	x	0.0	0.0	+14.8	x	+1.9	+0.3	x	-1.1	x
#	Run														
	16	17	18	19	20	21	22	23	24	25	26	27	28	29	30
1	x	+23.5	+9.5	+14.1	x	x	x	x	x	x	+20.2	+21.8	+55.1	+55.1	+39.4
2	x	+2.1	+4.1	+6.4	x	x	x	x	x	x	+3.3	+1.7	+1.4	+1.4	+7.2
3	x	+2.1	+4.1	+6.4	x	x	x	x	x	x	+3.3	+1.7	+1.4	+1.4	+7.2
4	x	+1.7	+3.0	+6.4	x	x	x	x	x	x	+4.6	+3.4	+12.1	+12.1	+13.3
5	x		94%	96%	x	x	x	x	x	x	100%	100%	100%	100%	100%
6	x	100%	96%	96%	x	x	x	x	x	x	100%	100%	100%	100%	100%
7	x	+13.1	+2.0	+1.7	x	x	x	x	x	x	+1.5	+9.1	+25.1	+25.1	+26.6
#	Run														
	31	32	33	34	35	36	37	38	39	40	41	42	43	44	45
1	+12.1	+14.9	+14.8	+12.8	+10.6	+9.4	+9.5	+12.0	x	+9.6	x	x	x	x	x
2	+1.9	+2.6	+2.7	+2.4	+2.3	+3.5	+6.5	+4.8	x	+5.8	x	x	x	x	x
3	+1.9	+2.6	+2.7	+2.4	+2.3	+3.5	+6.5	+4.8	x	+5.8	x	x	x	x	x
4	-1.2	+3.2	+3.2	+2.7	+3.0	+2.7	+7.8	+6.5	x	+7.3	x	x	x	x	x
5	100%	100%	100%	100%	100%	100%	100%	100%	x	100%	x	x	x	x	x
6	100%	100%	100%	100%	100%	100%	100%	100%	x	100%	x	x	x	x	x
7	+1.6	+3.6	+3.4	+2.3	+1.4	+0.2	+0.5	+3.5	x	+0.7	x	x	x	x	x

Note: "+" sign indicates superheating degree, "-" sign indicates sub-cooling degree, "%" suffix indicates vapour quality of the two-phase flow and x data not recorded or assessed.

The specific enthalpy and entropy of the working fluid are calculated at each measurement station based on the recorded pressure and temperature. Several assumptions are made for these determinations:

- The pressure at state 1 is estimated based on pressure at state 2 and assuming a pressure drop on the condenser to a typical value of 1 bar

- The pressure at state 3 is approximated as equal to that measured at state 4 (since the tube-in-tube heat exchanger 3-4 has a short length (1m), there is no significant pressure drop across it).
- The temperature in 2 is approximated as equal to temperature in 3 (because the pipe segment between 2 and 3 is well insulated)
- The specific enthalpy and entropy at states 2 and 3 are assumed equal
- For those experiments where the boiler inlet has been in two phase, the enthalpy in state 4 is estimated based on enthalpy in state 2 and energy balance on the heat exchanger
- For those experiments where the boiler outlet was in two phase, the enthalpy and entropy is determined based on enthalpy at boiler inlet and energy balance on the boiler which involves the analysis of hot air to working fluid heat transfer
- For those experiments where the expander discharge was in two phase, the enthalpy, vapour quality and entropy are calculated based on the energy balance for the expander, which involves the estimation of the work rate developed by the working fluid based on the electrical measurements.

The calculated enthalpies and entropies at each state point are included in Table 6.5; the equation of the state for R134a – incorporated in EES – is used for the calculations (Tilner-Roth and Baehr 1994). Regarding the enthalpy of air, they are calculated in two ways for comparison purpose:

1. Using an equation of state for humid air as implemented in EES, namely the subroutine AirH_2O which assumes the air as an ideal mixture of gases comprising steam and dry air; for steam the equation of state by Hyland and Wexler (1883) is used, while the air is modeled as an ideal gas using a model of specific heat variation with temperature according to Lemmon et al. (2000).
2. Using an equation of state for dry air – also implemented in EES – based on the work by Lemmon et al. (2000).

Table 6.5 Specific enthalpy and entropy values of R134a at each state point o experimental runs.

Run	Thermodynamic state location #						Run	Thermodynamic state location #					
	1	3	4	5	6	7		1	3	4	5	6	7
1	287 (xxx)	123 (xxx)	118 (xx)	263 (xx)	258 (xx)	258 (913)	24	x	x	x	x	x	x
2	289 (xxx)	131 (xx)	124 (xx)	266 (xx)	261 (xx)	261 (913)	25	x	x	x	x	x	x
3	293 (xxx)	145 (xx)	138 (xx)	272 (xx)	266 (xx)	266 (913)	26	299 (982)	115 (414)	113 (408)	313 (1032)	300 (1038)	261 (929)
4	xxx (xxx)	xx	xx	xx	xx	xx	27	301 (987)	118 (425)	116 (417)	305 (1006)	293 (1014)	270 (953)
5	294 (xxx)	152 (xx)	141 (xx)	280 (xx)	275 (xx)	275 (xx)	28	330 (1088)	101 (372)	86 (322)	306 (1032)	299 (1073)	279 (1045)
7	293 (xxx)	144 (xx)	135 (xx)	264 (xx)	256 (xx)	256 (xx)	29	330 (1088)	101 (372)	86 (322)	306 (1032)	299 (1073)	279 (1045)
8	293 (xxx)	143 (xxx)	135 (xxx)	264 (xxx)	256 (902)	256 (902)	30	318 (1042)	104 (380)	91 (340)	294 (987)	289 (1019)	281 (1010)
9	334 (1053)	156 (507)	146 (xx)	286 (946)	283 (950)	284 (967)	31	288 (956)	110 (400)	274 (919)	297 (994)	297 (1034)	260 (930
10	xx	xx	xx	xx	xx	xx	32	292 (965)	111 (402)	110 (399)	297 (994)	292 (1021)	261 (938)
11	297 (953)	139 (487)	135 (475)	264 (868)	256 (875)	262 (922)	33	291 (965)	111 (402)	110 (399)	295 (989)	290 (1013)	261 (937)
12	298 (956)	141 (493)	138 (486)	263 (864)	254 (867)	263 (922)	34	289 (958)	111 (403)	111 (402)	291 (974)	286 (998)	261 (932)
13	x	x	x	x	x	x	35	287 (950)	113 (409)	112 (405)	291 (974)	287 (991)	262 (928)
14	307 (974)	154 (533)	154 (533)	267 (873)	261 (876)	270 (916)	36	286 (946)	111 (403)	111 (402)	284 (951)	279 (972)	261 (924)
15	x	x	x	x	x	x	37	288 (946)	115 (414)	113 (408)	311 (1022)	307 (1047)	263 (923)
16	x	x	x	x	x	x	38	292 (954)	118 (425)	116 (417)	303 (996)	300 (1023)	267 (933)
17	305 (992)	123 (440)	122 (437)	276 (919)	269 (941)	269 (968)	39	x	x	x	x	x	x
18	290 (944)	126 (448)	126 (450)	267 (884)	258 (895)	259 (932)	40	289 (945)	119 (427)	116 (419)	304 (997)	300 (1023)	265 (923)
19	296 (960)	124 (441)	124 (441)	269 (891)	260 (898)	260 (930)	41	x	x	x	x	x	x

Note: run 6 skipped for inconsistency; specific indicated with no parentheses enthalpy in kJ/kg; specific entropy indicated within parentheses in J/kg K

Table 6.6 The mass flow rates determined for each experimental run.

Run	Thermodynamic state location #					Run	Thermodynamic state location #				
	2	4	10	12	14		2	4	10	12	14
1	15	15	x	51	307	24	x	x	x	x	x
2	15	15	x	38	306	25	x	x	x	x	x
3	16	16	x	58	306	26	11	11	37	53	317
4	17	17	x	69	306	27	11	11	37	50	317
5	15	15	x	72	306	28	26	26	203	153	317
7	17	17	x	31	306	29	26	26	203	153	317
8	17	17	x	31	306	30	28	28	203	150	324
9	17	17	x	53	306	31	245	245	203	156	324
10	x	x	x	x	x	32	30	30	203	159	324
11	17	17	x	31	321	33	31	31	203	159	324
12	17	17	x	34	321	34	32	32	203	161	324
13	x	x	x	x	x	35	32	32	203	187	324
14	20	20	x	35	321	36	33	33	203	157	324
15	x	x	x	x	x	37	35	35	37	171	324
16	x	x	x	x	x	38	37	37	37	162	324
17	14	14	x	36	321	39					
18	15	15	x	36	324	40	38	38	37	163	324
19	15	15	x	35	323	41	x	x	x	x	x

Note: all mass flow rates are in g/s; run 6 is skipped for inconsistency.

When humid air subroutine is used, the moisture content of air in the air duct is calculated under the assumption that the duct is sealed during the experiment and the air in the duct prior to the experiment has the properties of the air in the lab room which has been assumed of 60% (this value is typically maintained by the HVAC system of the lab). The comparison between two approaches has been made for several relevant situations; the predictions of the two were close to each other. It is concluded that dry air model can be used as it give correct estimates of densities and enthalpies without affecting the experimental accuracy. In the modeling section, the specific equation and EES code for air-side modeling of the system will be presented.

The thermodynamic properties of water are calculated with EES based on embedded tables originated from Harr et al. (1984). Based on the EES subroutines, the enthalpy, density, specific heat, viscosity and thermal conductivity of water were determined for heat transfer calculations.

The flow rate of the water is determined based on volumetric measurements using a fixed volume container and a stopwatch. The flow rate of the refrigerant is indirectly determined based on the energy balance on the compressor, heat exchanger and boiler. Details regarding

the energy balance calculations are indicated in the subsequent modeling section and in the validation section. When the expander by-pass is used, the mass balance equation is also necessary to determine the mass flow rate of the throttled flow. This writes $\dot{m}_8 = \dot{m}_2 - \dot{m}_4$. The flow rates determined during each of the experimental runs are summarized in Table 6.7.

Figures 6.2 to 6.11 indicate on a temperature-entropy diagram, the evolution of the working fluid for three typical cases that were investigated. There were experiments where the achieved boiling process proceeded from slightly sub-cooled process until a two phase flow not complete saturation (e.g., Figures 6.2 and 6.4); other experiments in which the heating process of the working fluid proceeded first with the heating of the sub-cooled liquid followed by incomplete boiling (e.g., Figure 6.6), or processes where superheated vapour were generated (e.g., Figures 6.8 – 6.11). Slightly superheated vapour was obtained, as an example, from Figure 6.7. For higher degrees of superheating the by-pass valve has been opened, thus a throttled (cold) flow was produced to and mixed with the flow at expander discharge, for cooling prior to pressurization (Figure 6.11).

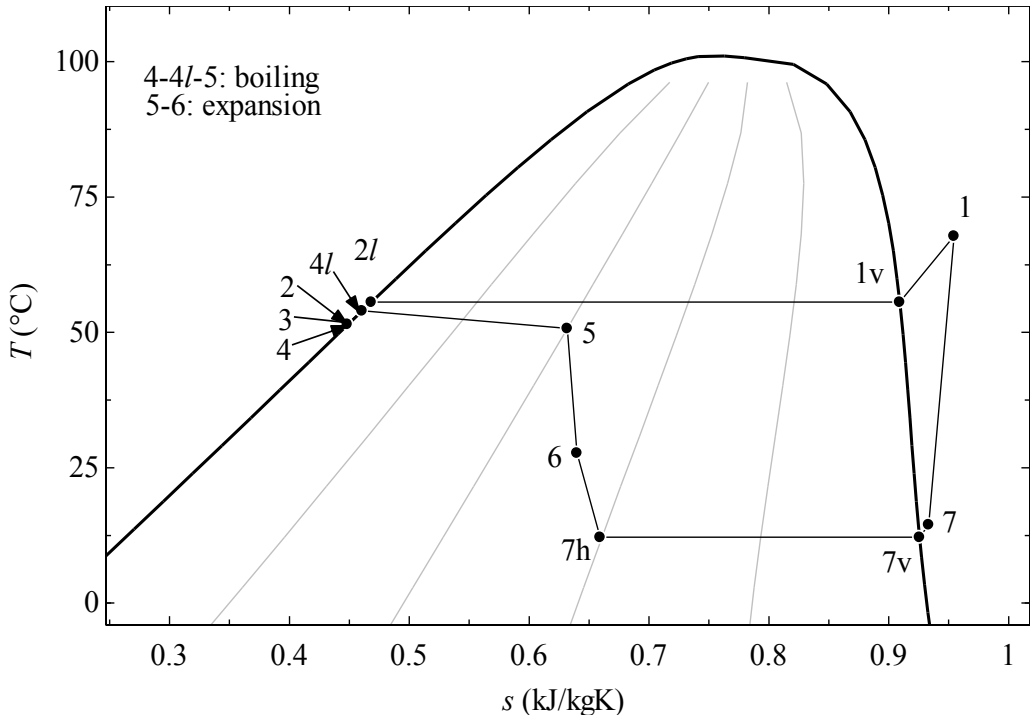

Figure 6.2 Experimental run for two-phase expansion.

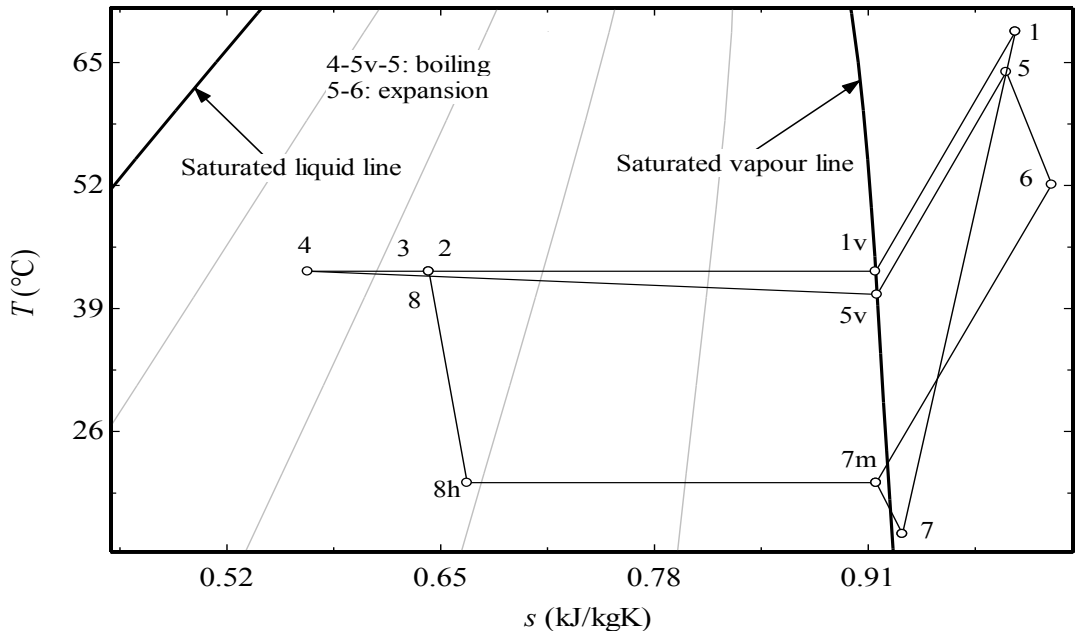

Figure 6.3 Experimental run for superheated expansion and incomplete condensation.

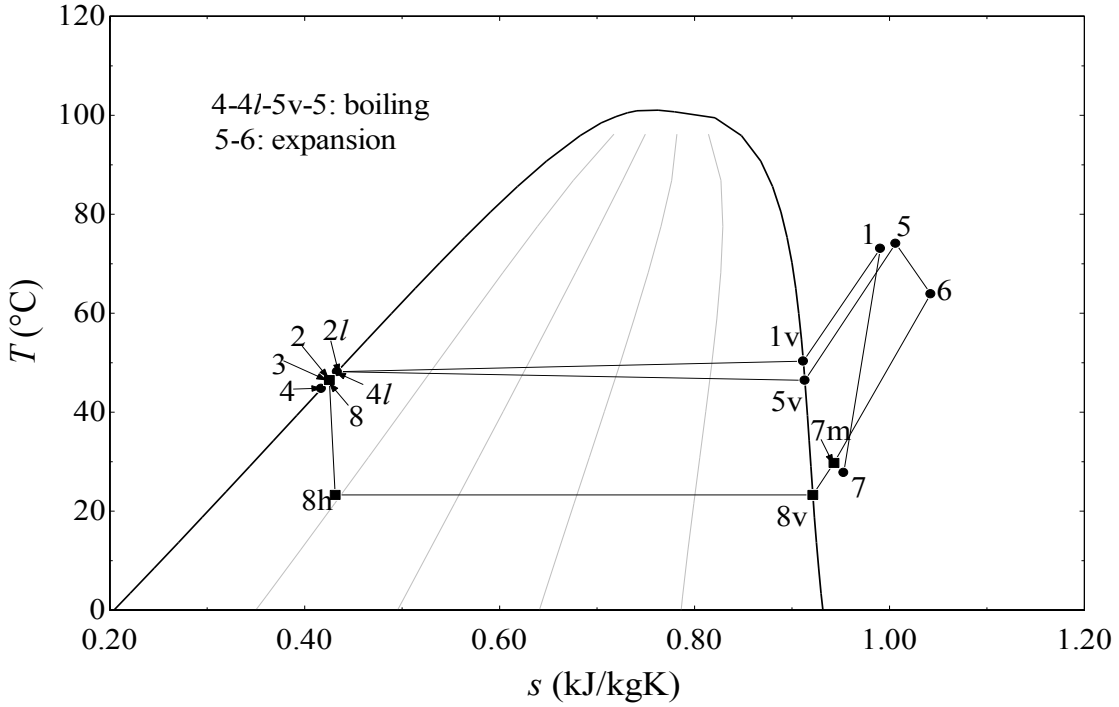

Figure 6.4 Experimental run for superheated expansion, complete condensation, and liquid subcooling.

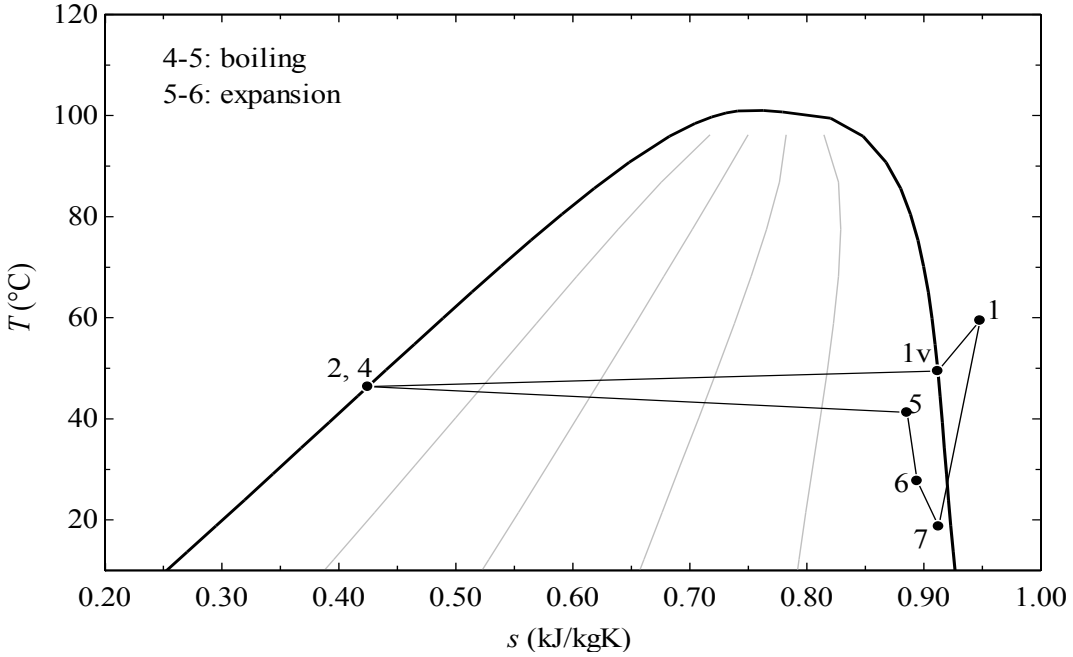

Figure 6.5 Experimental run with boiling and expansion of saturated liquid.

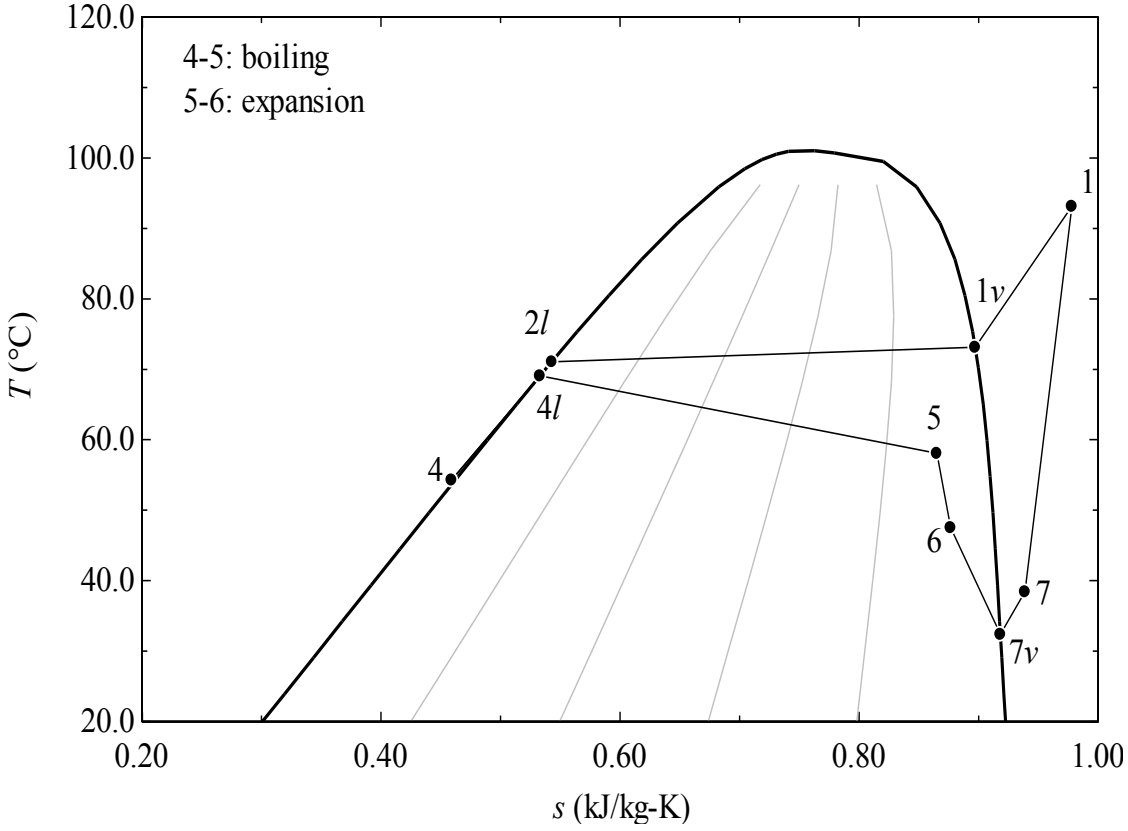

Figure 6.6 Experimental run for preheating, boiling, and expansion of the working fluid.

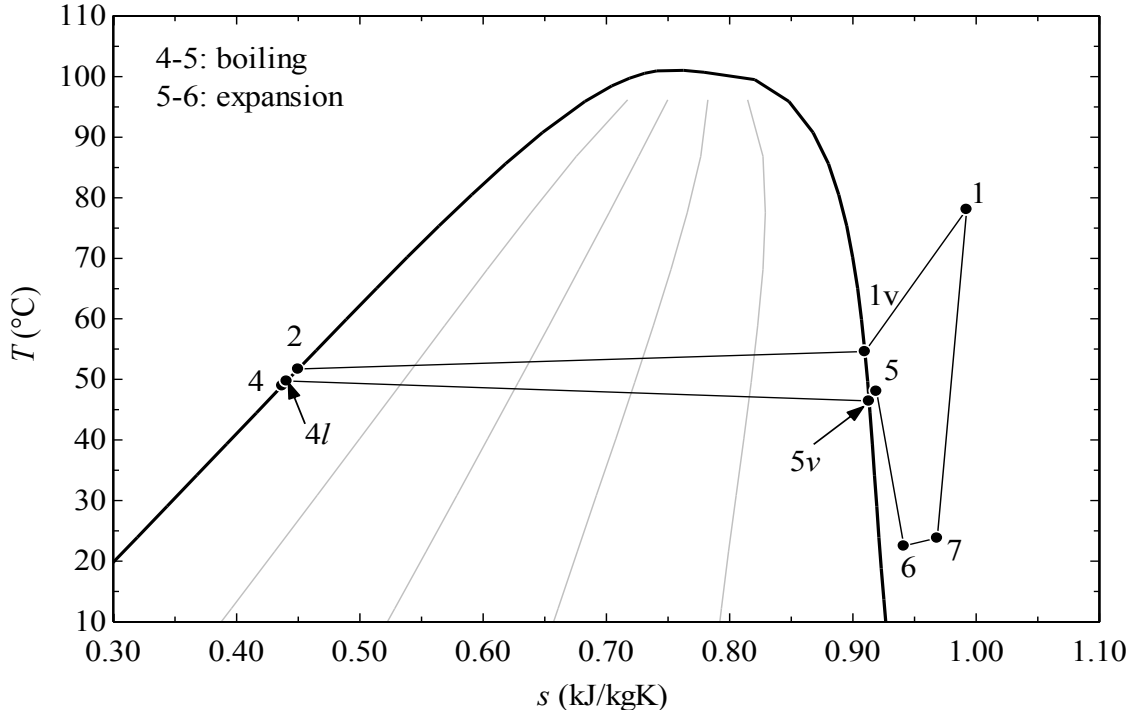

Figure 6.7 Experimental run with expansion of a slightly superheated working fluid.

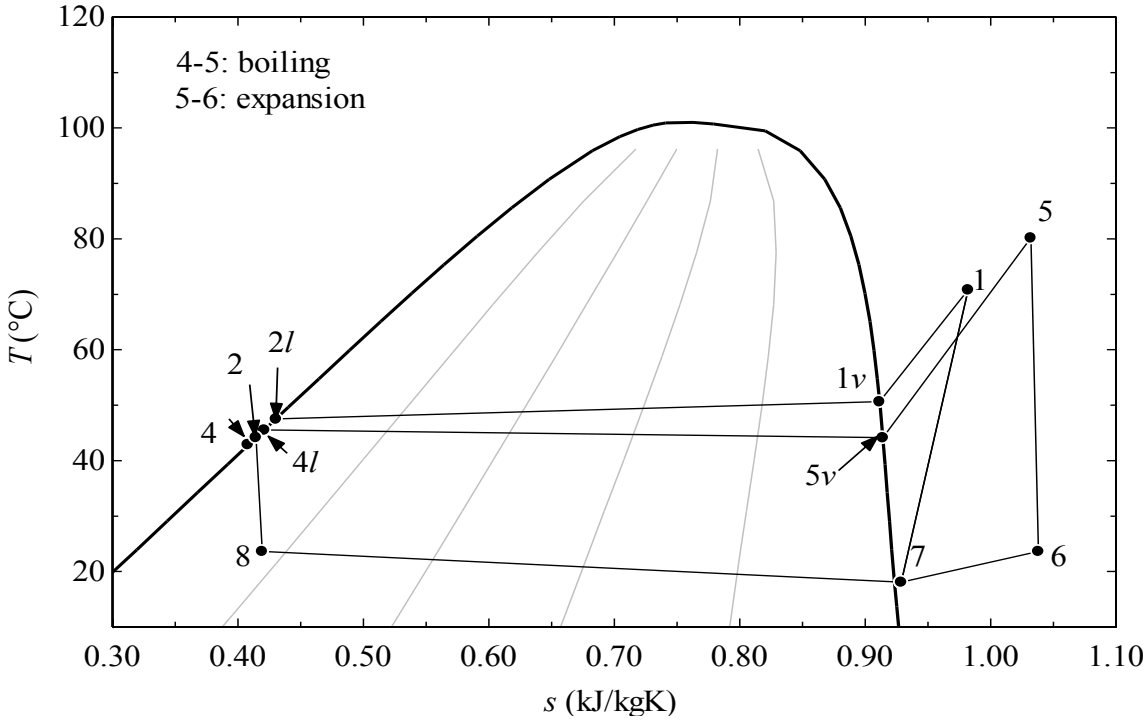

Figure 6.8 Experimental run with expansion of superheated fluid.

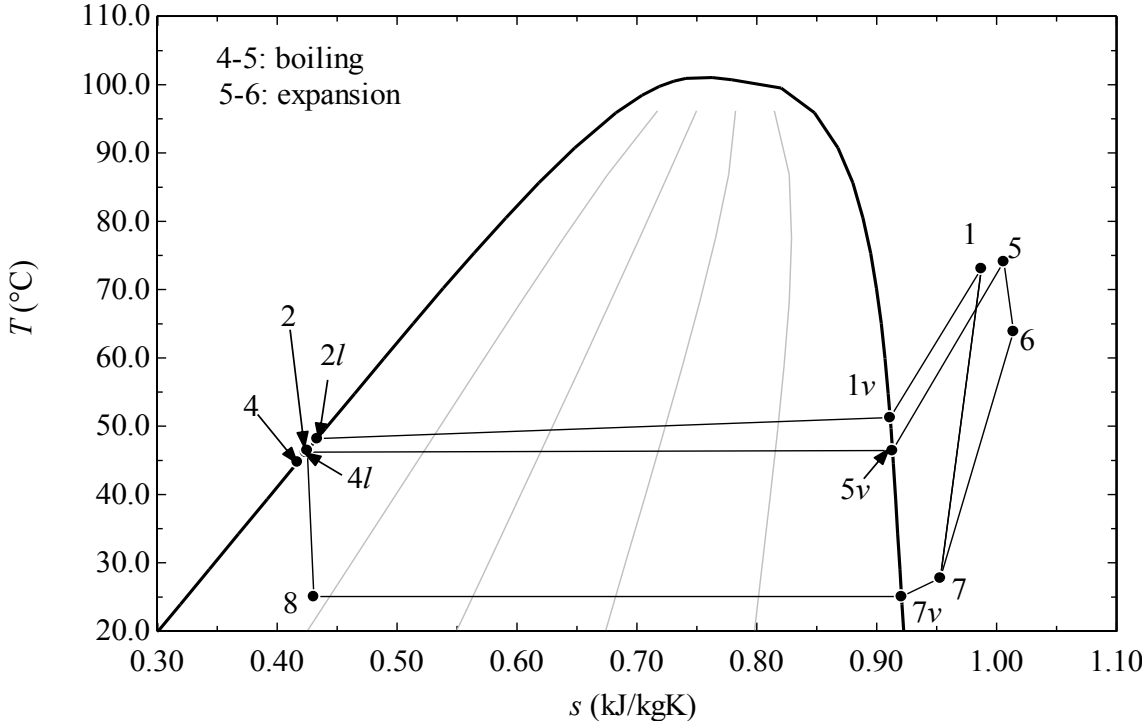

Figure 6.9 Expansion of superheated flow with smaller pressure ratio.

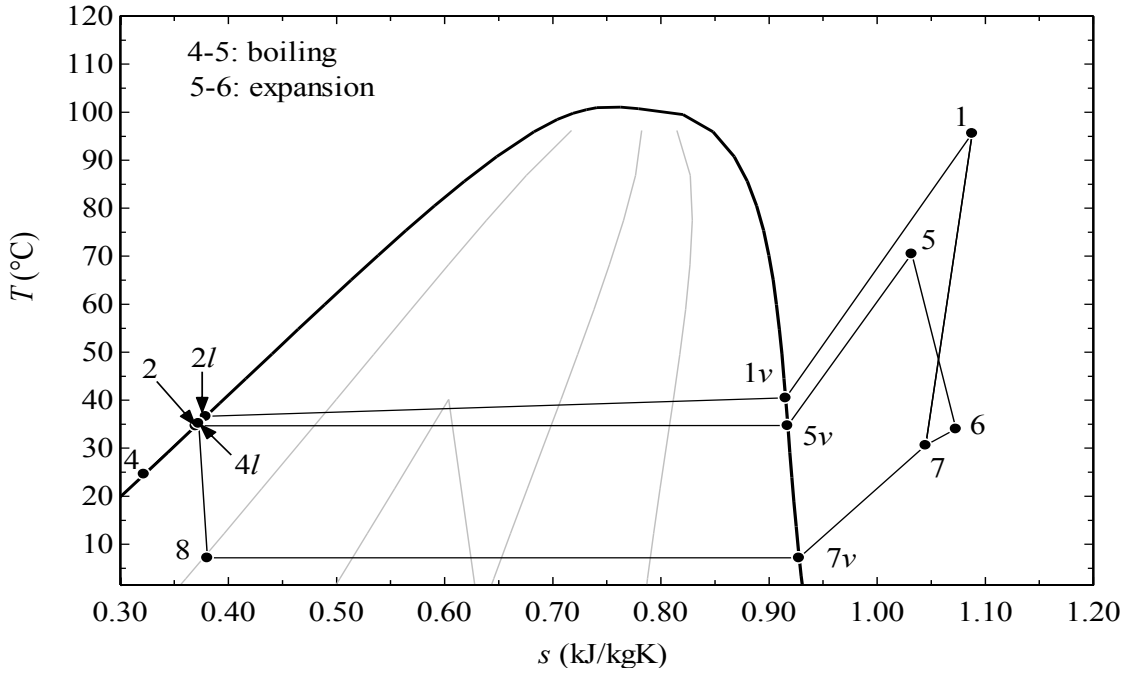

Figure 6.10 Expansion of superheated fluid at an intermediate pressure ratio.

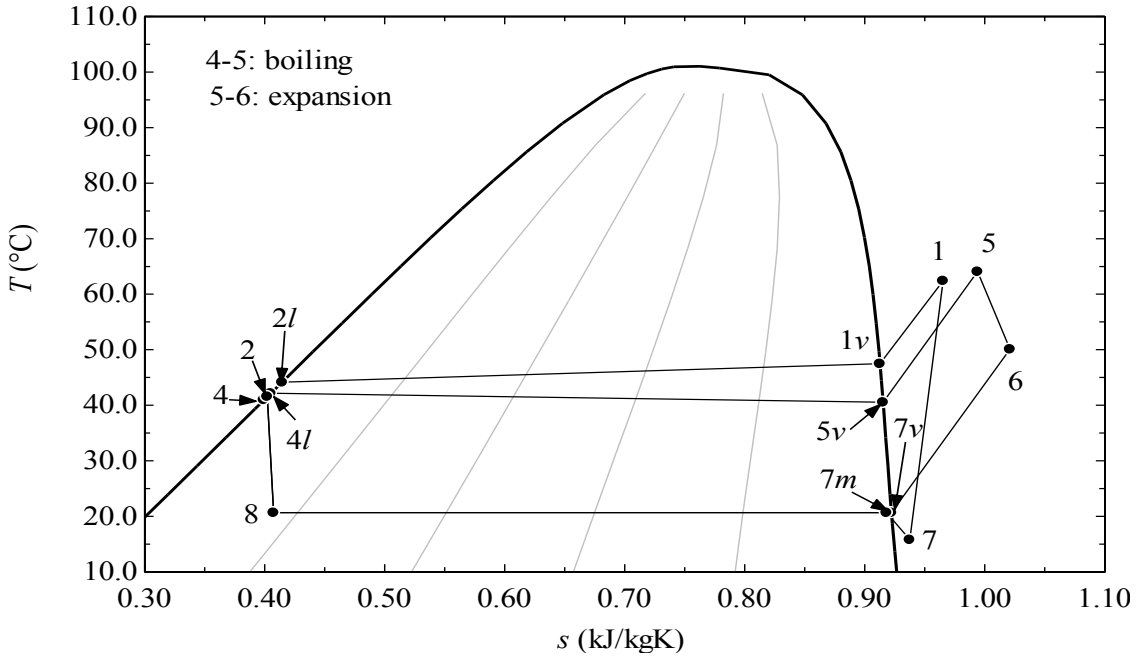

Figure 6.11 Experimental run with superheated expansion and throttling process between the mixed flow (7m) and compressor suction (7).

6.1.2 Boiler measurements

In a first set of experiments, the air has been circulated with a fan of 25 W motor capacity for which – as mentioned above – the developed head was insufficient to allow for a good Reynolds number. For these experiments, the flow regime inside of the air duct is of turbulent natural convection. This regime has been indicated by the distribution of air temperatures at state points (#) 11, 12 and 13: that is, the temperature at 11 is higher than that at 13. Consequently, the heat transfer at the boiler was poor and therefore no vapour superheating could be achieved.

The temperature profiles across the boiler, in the $T - s$ and the $T - \dot{Q}$ diagrams for this set of experiments are indicated in Figure 6.12. There is a measurable pressure drop across the boiler. Therefore, the boiling process does not occur at a constant temperature and a temperature drop has been observed. The temperature at the boiler outlet must correspond to the saturation at the measured pressure. Consequently, the temperature at boiler exit – for the experiments of incomplete boiling – can be double determined, namely, from pressure measurement and from direct measurement. This opportunity is used to calibrate the temperature reading at the boiler outlet via determination of the parameter R from Equation

6.3 based on actual measurements. This parameter is found to be 1.1 for all two-phase experiments.

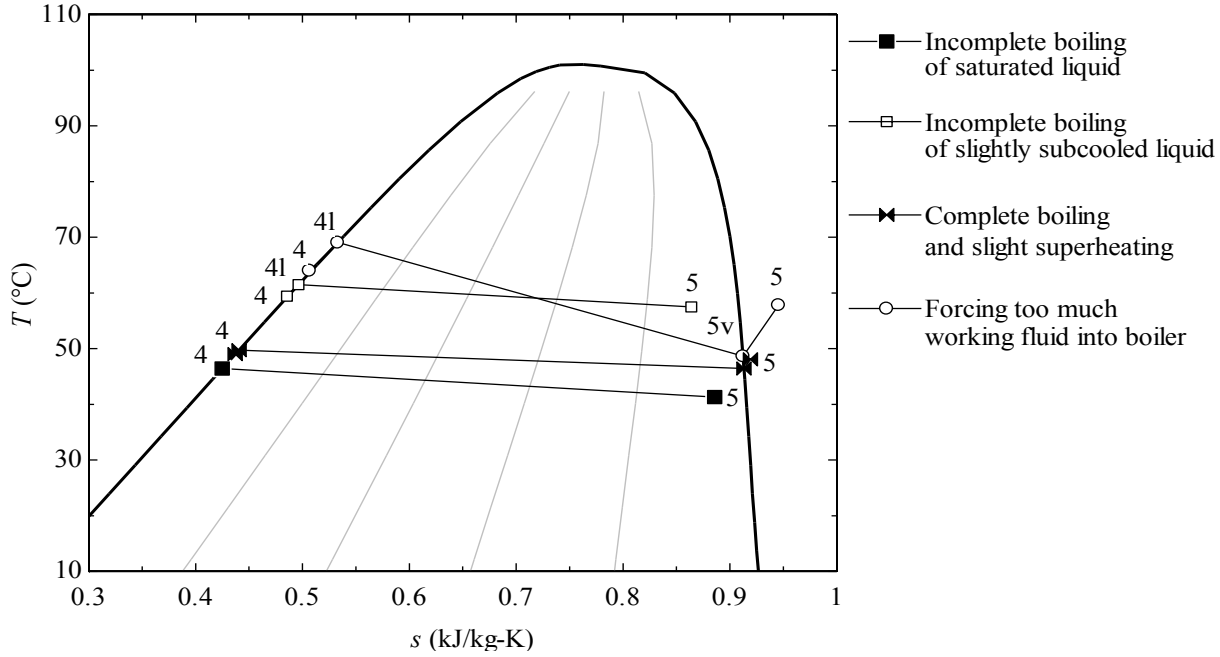

Figure 6.12 Experimental runs for boiling process with small fan used in the air duct.

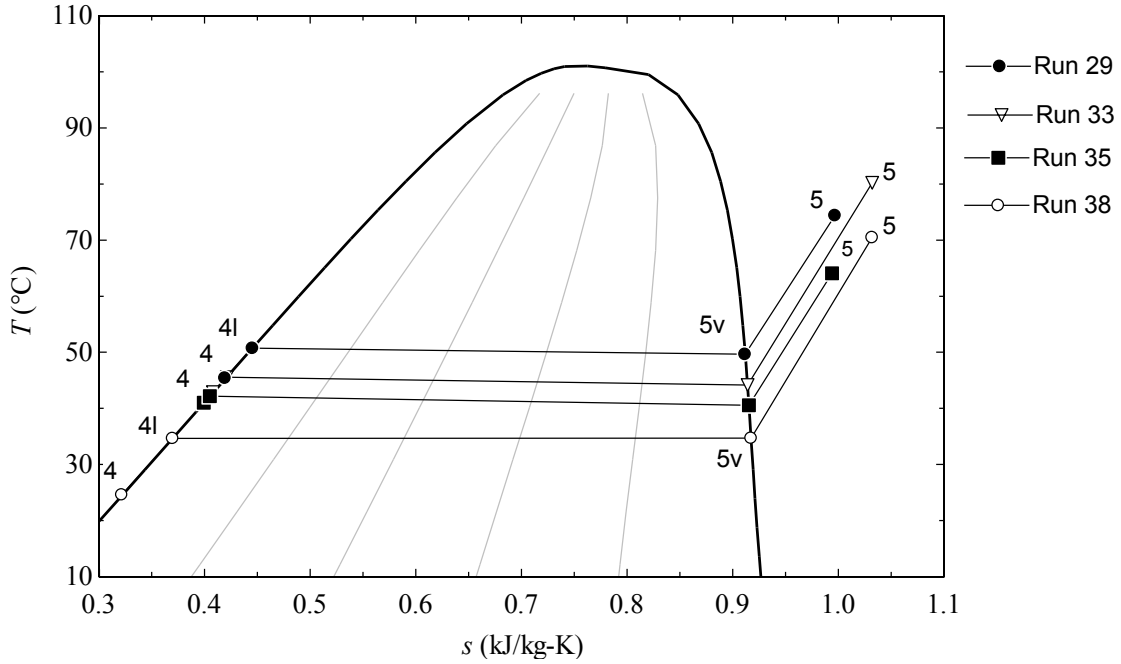

Figure 6.13 Experimental runs for boiling with superheating with larger blower in the air duct.

Further experiments were run with a strong furnace blower in the air duct (see the notes in Chapter 4). With this blower, better heat transfer at the boiler was obtained.

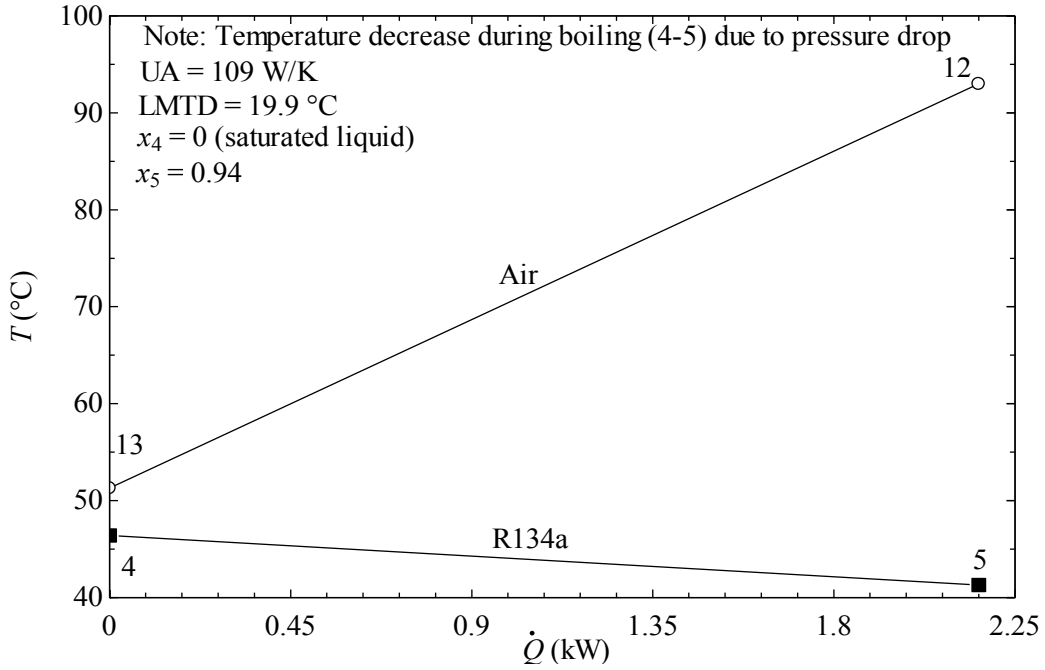

Figure 6.14 Temperature – heat transfer rate diagram at incomplete boiling of saturated liquid.

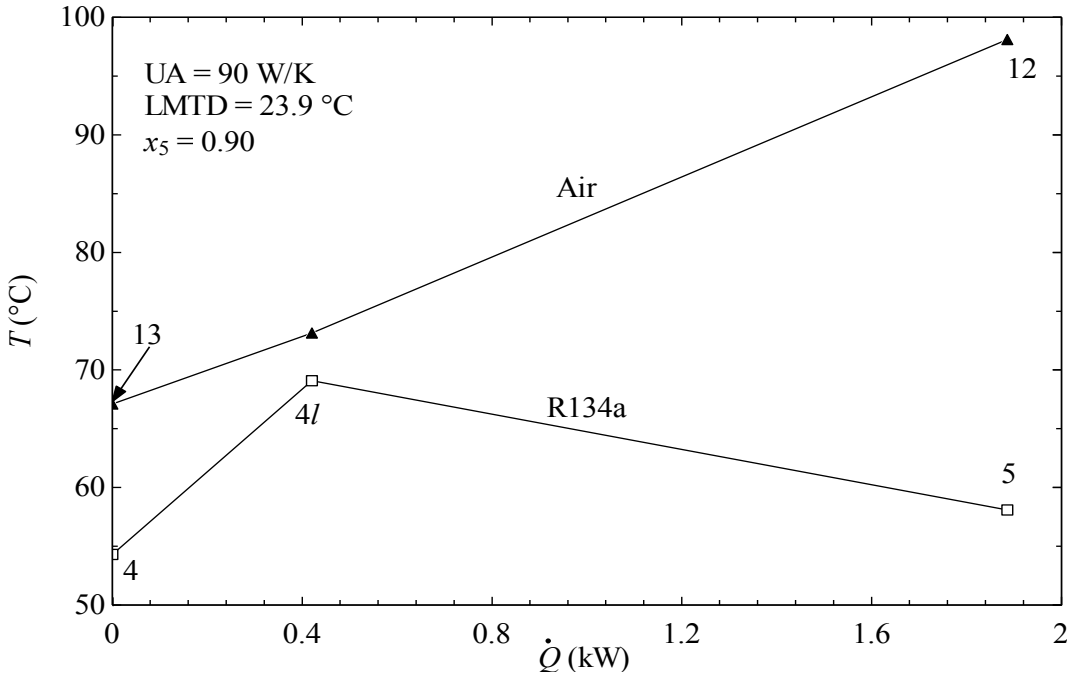

Figure 6.15 Temperature – heat transfer rate diagram at boiling of subcooled liquid.

Thus, it was possible to obtain the complete convective boiling process, starting from subcooled liquid, to saturated liquid, to saturated vapour and eventually to superheated vapour. The relevant experimental runs, showing the achieved boiling process in this case, are exemplified in Figure 6.14-6.20. In Figure 6.14 is shown the case when the fluid at boiler entrance was at saturated liquid state, while at the boiler exit the state was of two-phase flow with vapour quality of 0.94 (as indicated). In the next exemplified case – Figure 6.15 – the fluid at the boiler entrance is subcooled liquid; the result is a two-phase flow with 0.9 vapour quality at the boiler outlet. In Figures 6.16 and 6.17 is represented the experimental case where both the degrees of subcooling and superheating are small. The case from Figure 6.17 illustrates a situation when the overall heat transfer rate (UA) of the heat exchanger degraded very much and consequently the boiler operates at a higher LMTD.

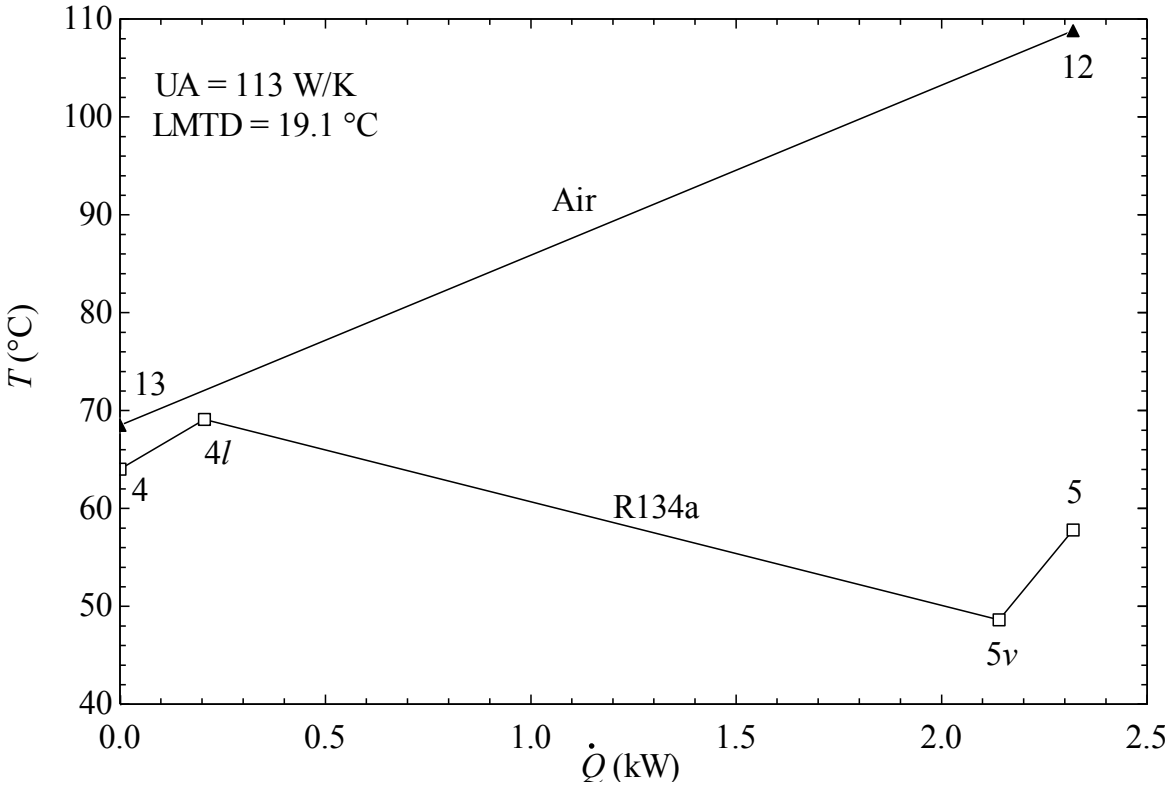

Figure 6.16 Temperature – heat transfer rate diagram for superheated vapour at boiler exit.

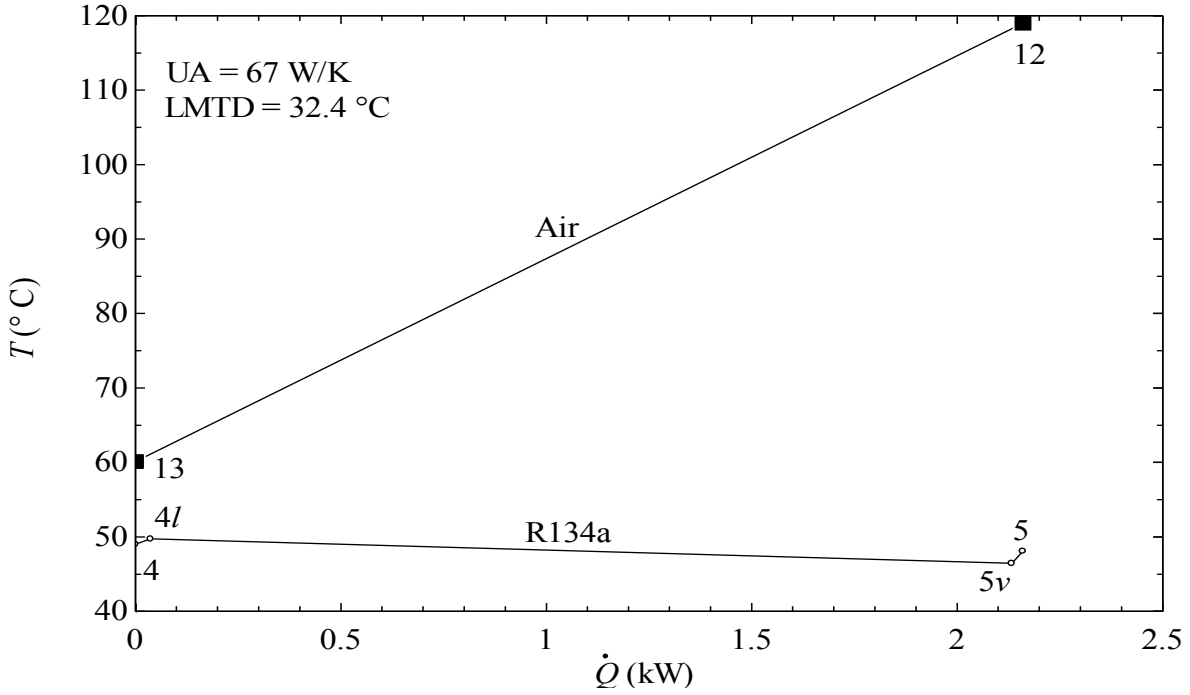

Figure 6.17 Temperature – heat transfer rate diagram for slight superheated vapour at boiler exit.

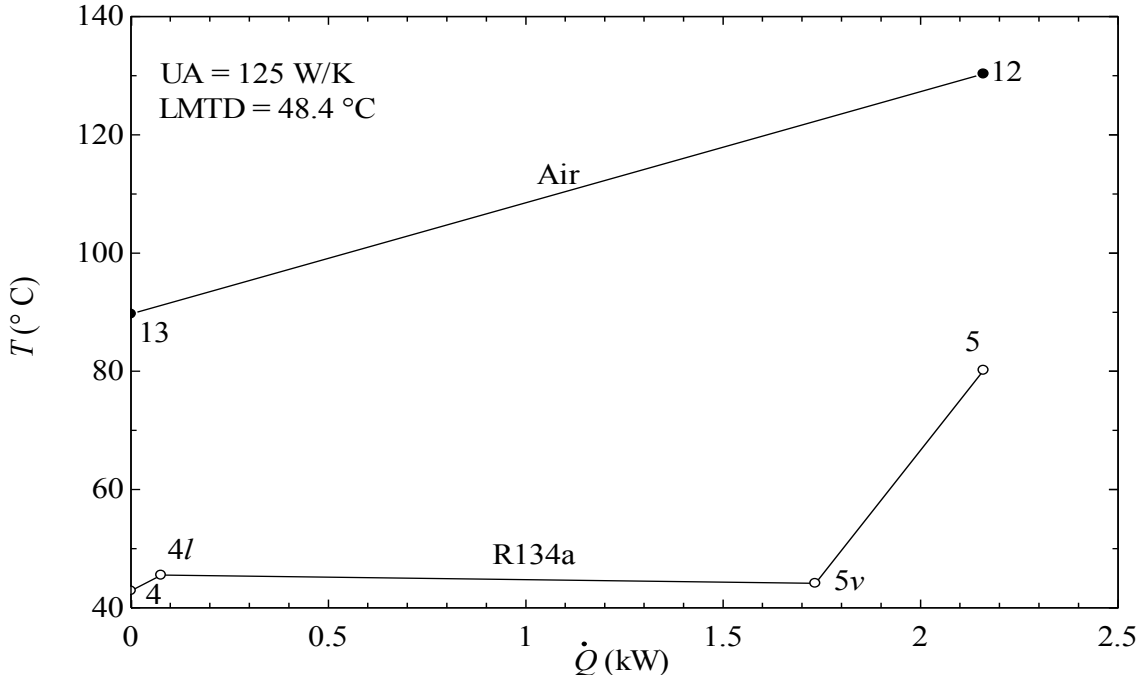

Figure 6.18 Temperature – heat transfer rate diagram for high superheated vapour at boiler exit.

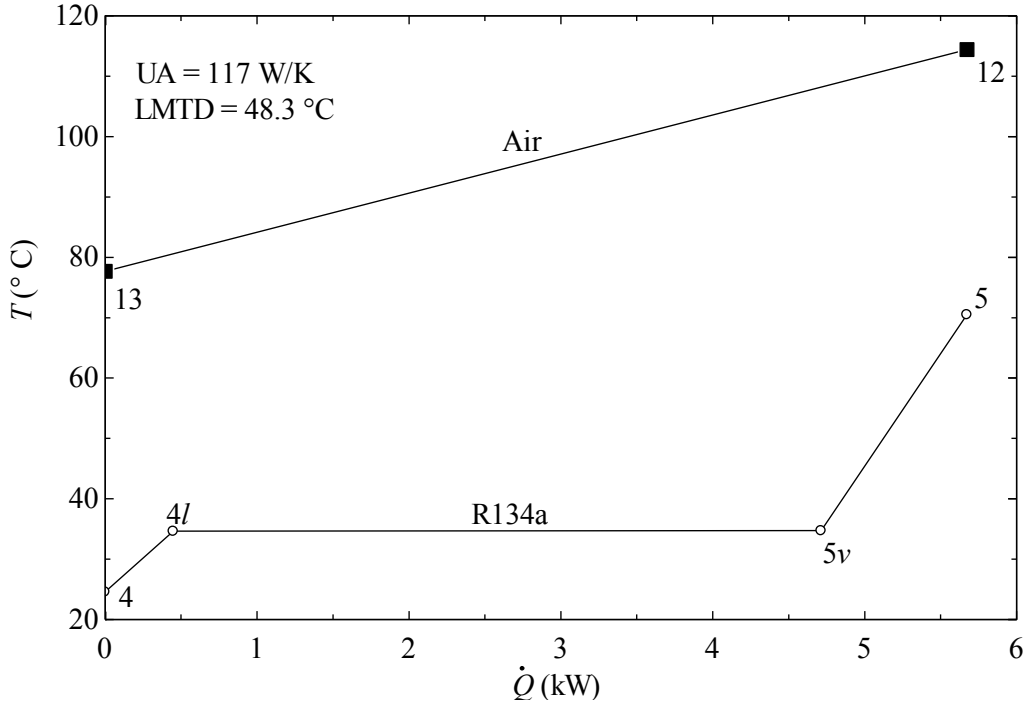

Figure 6.19 Temperature – heat transfer rate diagram for enhanced heat transfer case at boiler due to installation of a better blower ($\dot{\mathbf{Q}} = \mathbf{5.7\ kW}$).

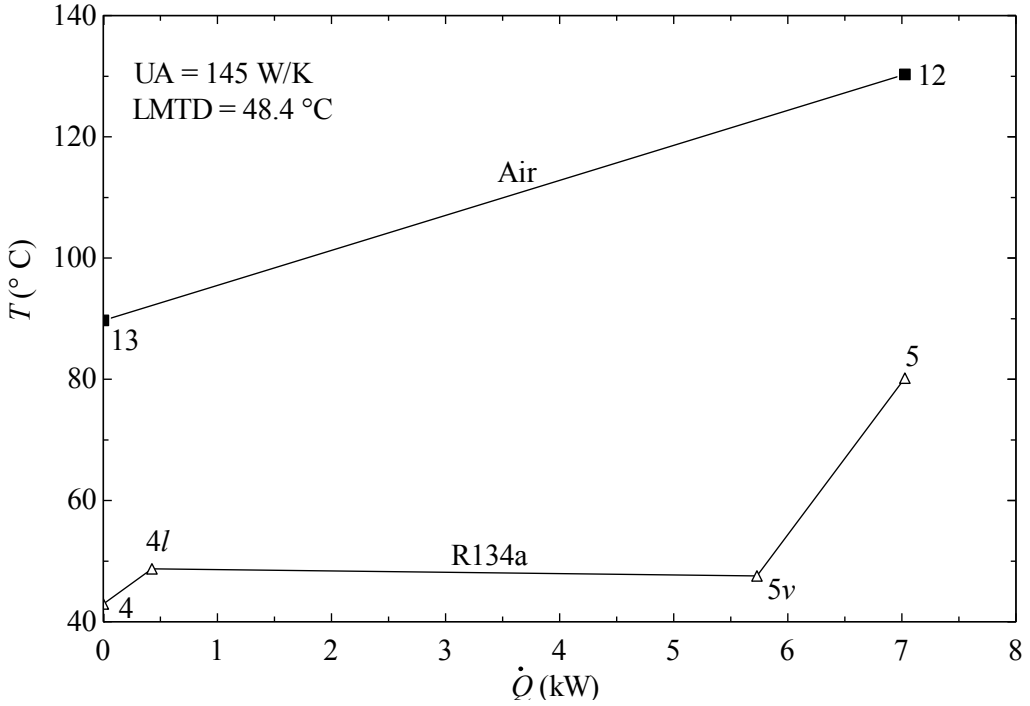

Figure 6.20 Temperature – heat transfer rate diagram for the experiment run when the achieved boiler duty is the highest ($\dot{Q} = 7$ kW).

6.1.3 Expander measurements

The expansion process with the selected scroll machine (Bitzer) has been investigated for both two-phase and superheated vapour case. The experimental measurements for the expansion process are summarized in Figure 6.21 which represents those in the *T-s* diagram. For each case the isentropic efficiency of the expander is determined based on energy balance. The results regarding the isentropic efficiency are reported in Figure 6.22. Isentropic efficiencies of over 0.8 were obtained, especially at operation in two-phase. However, for higher pressure ratios and in the superheated region the isentropic efficiency degrades to about 40% as it can be observed on the same figure. The typical current-voltage diagram of the expander-generator assembly – as obtained within this work based on the measurements – is indicated in Figure 6.23. The maximum developed power achieved with the current ORC test bench is around 150 W. Note that the expander-generator assembly can develop up to 10 times more power than that obtained during the present experiments. For the experimental case indicated in Figure 6.24 the maximum power is delivered at 8 V, while for the results from Figure 6.25 at 6.5 V.

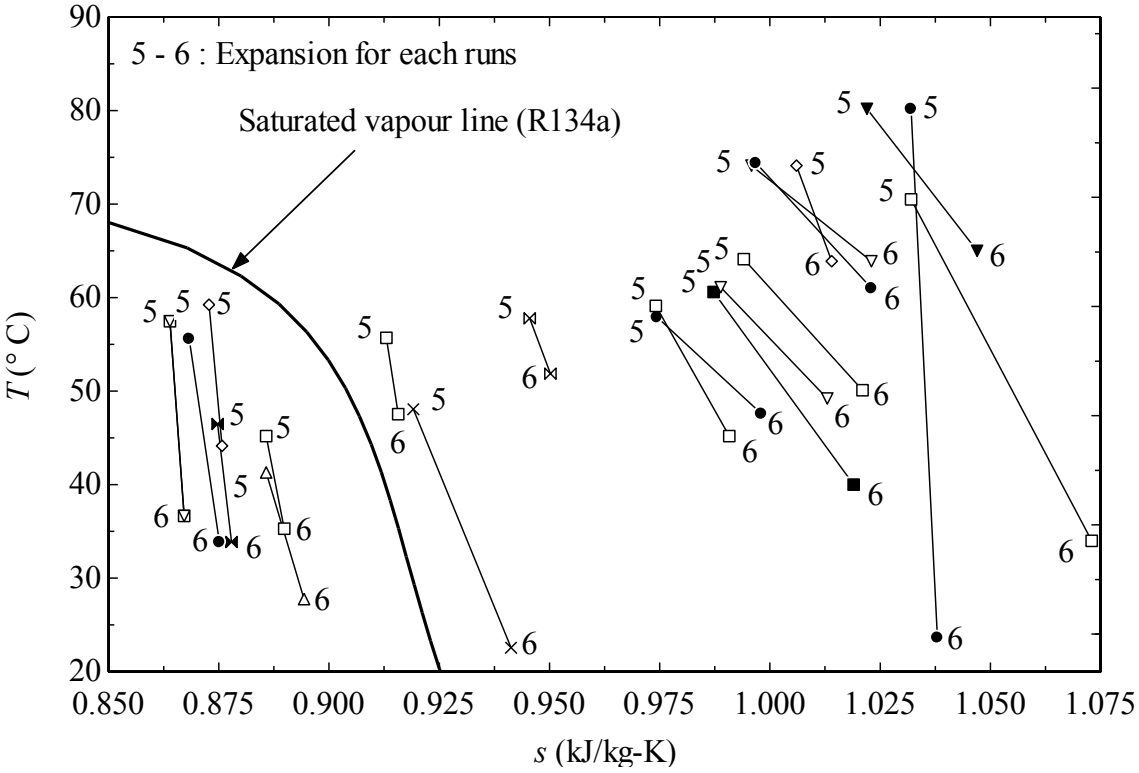

Figure 6.21 Summary of expansion (5-6) for each run in the *T-s* diagram.

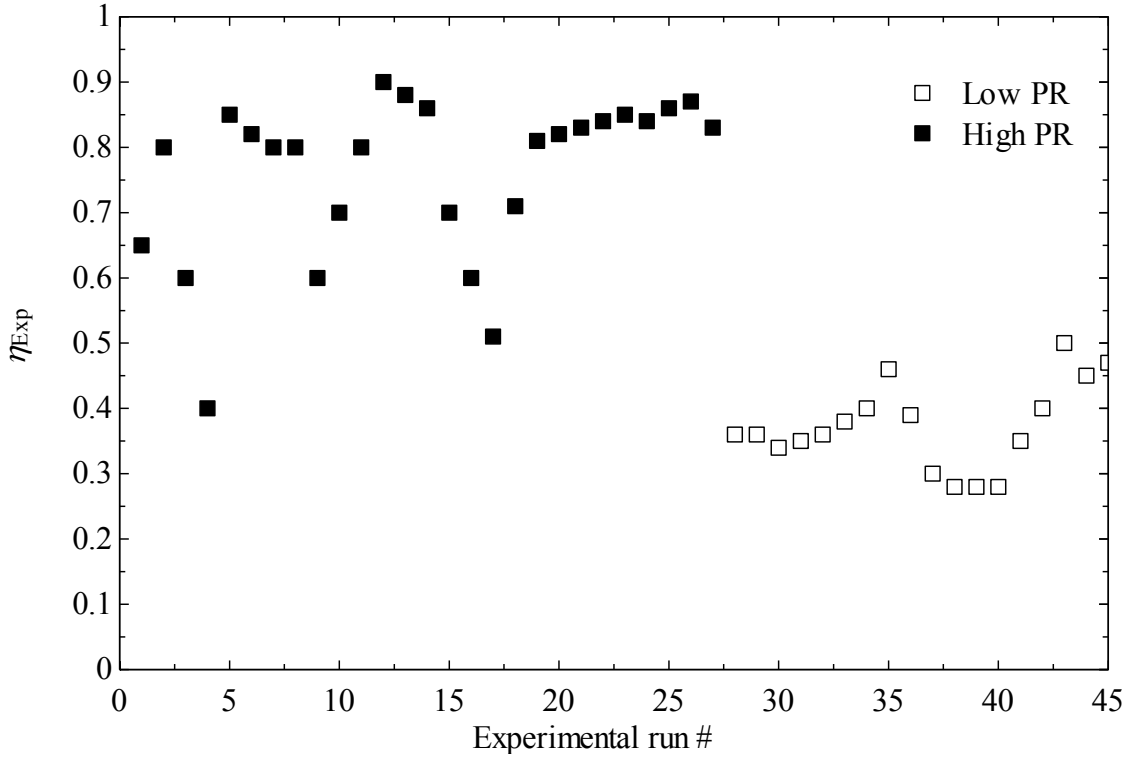

Figure 6.22 Isentropic efficiencies of scroll expander for each run.

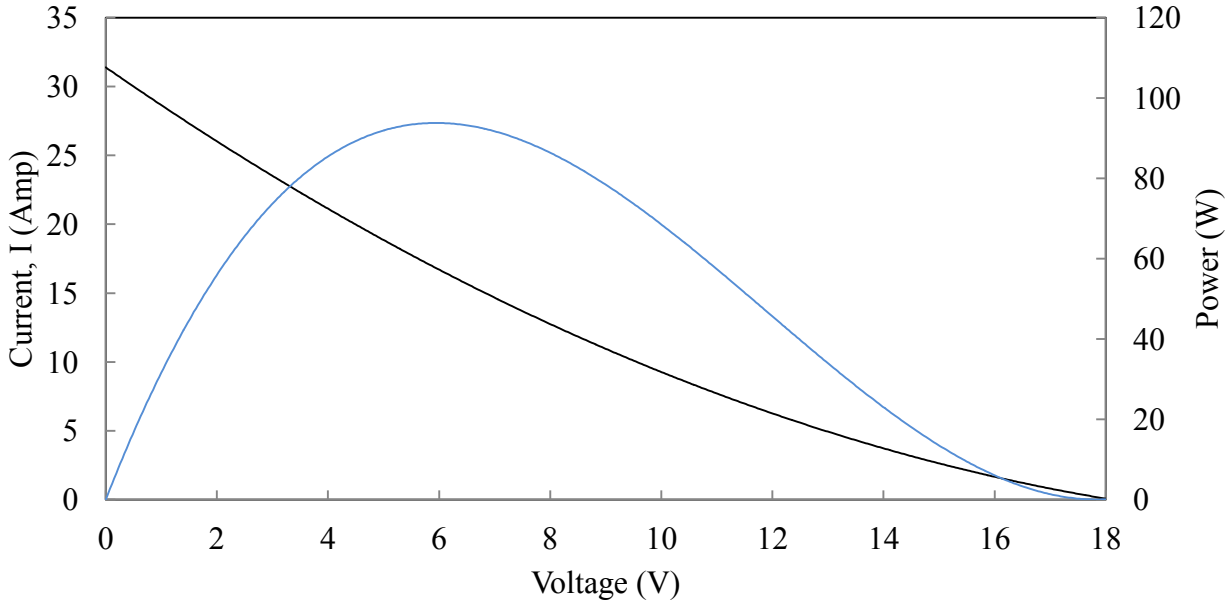

Figure 6.23 Experimental current, voltage, and power diagram for the expander-generator assembly.

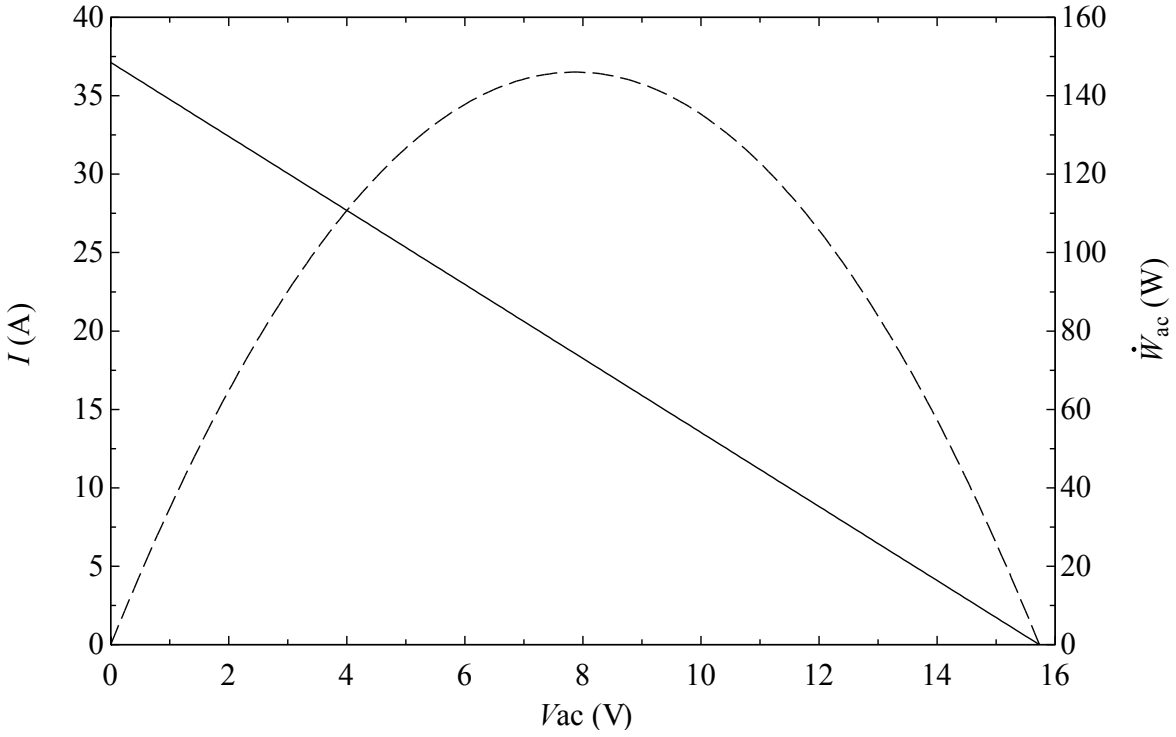

Figure 6.24 Current-voltage and power-voltage diagrams for the experimental run at 8 V.

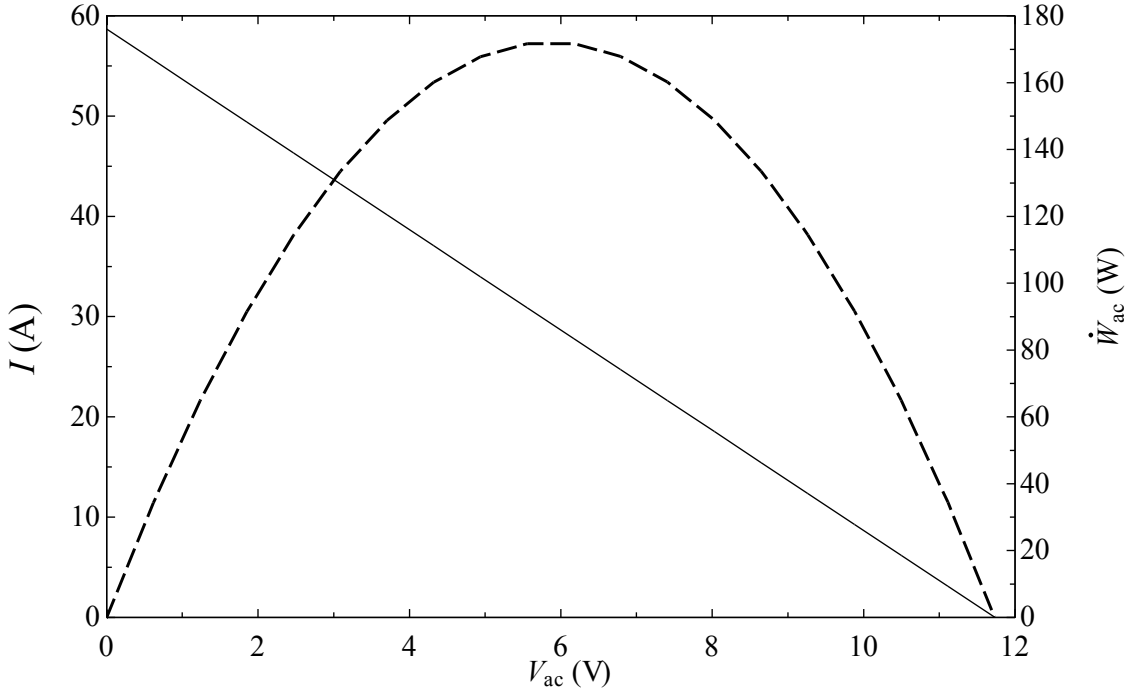

Figure 6.25 Current-voltage and power-voltage diagrams for the experimental run at 6.5 V.

The current-voltage diagram of the expander-generator assembly is in correspondence to the flow rate vs enthalpy difference diagram for the expander. In this diagram, the flow rate through the expander is correlated to the enthalpy difference between the inlet and outlet states. The $\dot{m} - \Delta h$ correlation – for the case presented as I-V diagram in Figure 6.25 is demonstrated with the help of Figure 6.26. This plot shows that the maximum expansion work is developed for an enthalpy difference of 10.5 kJ/kg and an optimum power delivered at 6.5 V. Note that this situation represents only one experimental situation in which nothing has been changed from the engine settings, except the electrical load at the generator attached to the expander. The optimum mass flow rate is 19.5 g/s. The pressure difference across the expander varies in direct proportion with the enthalpy difference as indicated in Figure 6.27. It results that the optimum pressure difference is 535 kPa. This study demonstrate that there always must be an optimal load which allows for maximum power generation for imposed boundary conditions at the heat engine source and sink

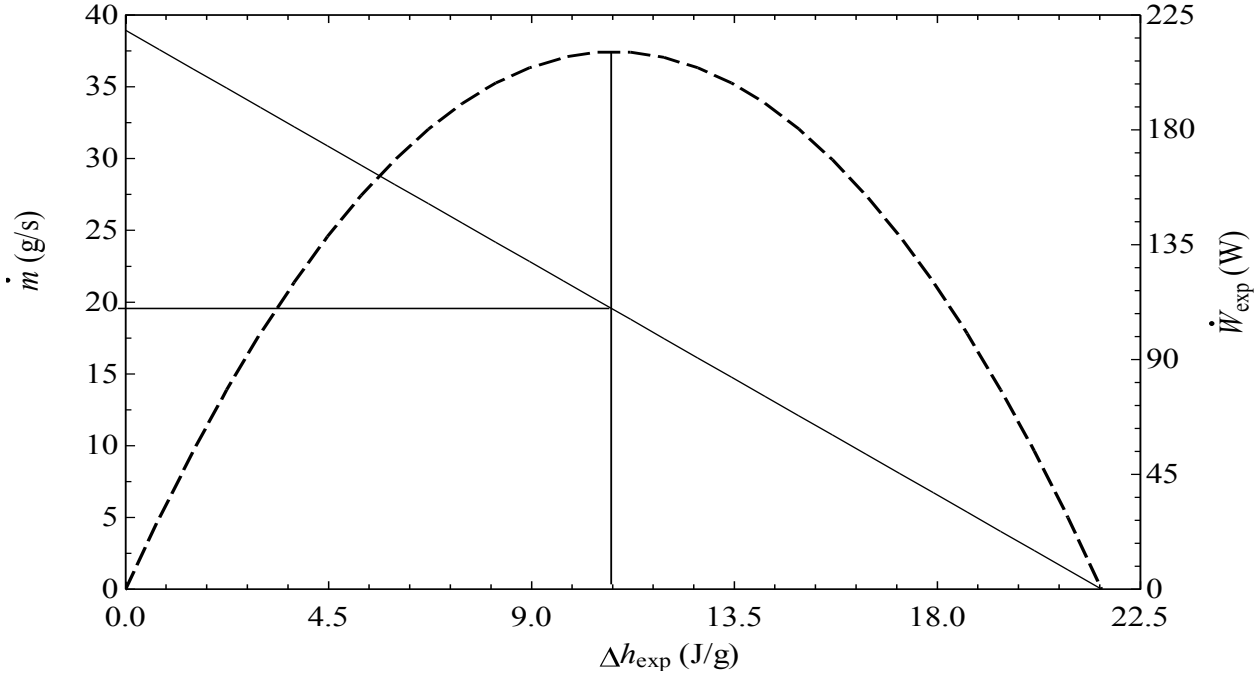

Figure 6.26 The correlation between mass flow rate and enthalpy difference over the expander.

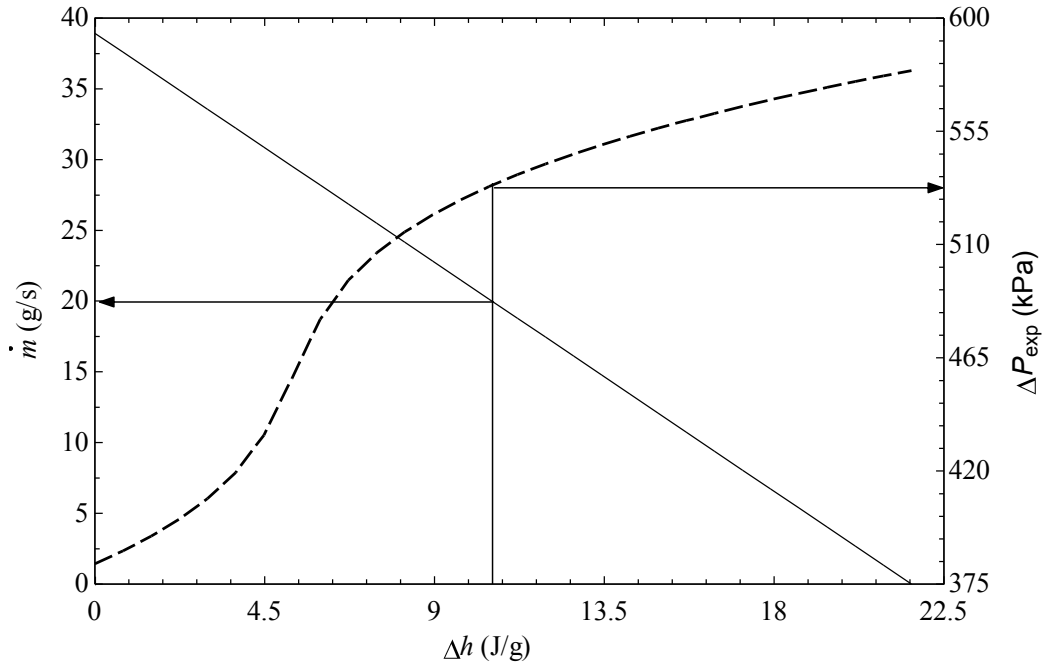

Figure 6.27 The optimum mass flow rate, pressure difference and enthalpy difference across the expander.

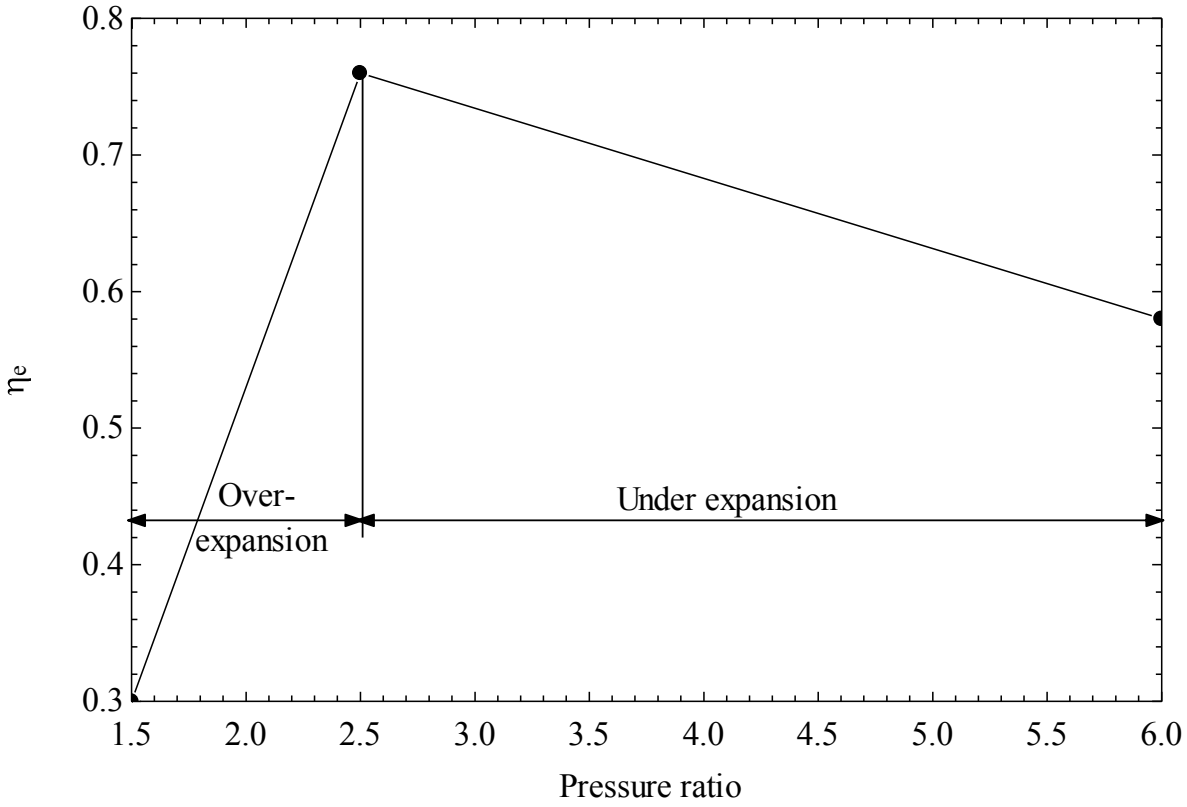

Figure 6.28 The correlation between pressure ratio and isentropic efficiency of the expander.

The last experimental study for the expander is shown in Figure 6.28 and refers to the optimal expansion with respect to the pressure ratio. In the positive displacement expanders, the pressure ratio of the expanded flow is correlated to the built-in volume ratio. In this regard, the pressure ratio between the higher and lower side of the Rankine cycle, must be correlated to the built-in volume ratio. If they are not, then the expander operation is non-optimal. In Figure 6.28 it is shown that the variation of the isentropic efficiency of the expander with the pressure ratio, for selected experimental runs in which the thermodynamic state at expander intake (pressure, enthalpy) are about the same.

The pressure ratio in horizontal axis represents the ratio between the highest and the lowest pressures, before and after the expander respectively. If this pressure ratio is lower than the one that correspond to the built-in volume ratio for the given operating condition, then the flow over-expands in the expander and then it must be recompressed to reach the pressure boundary condition at the lower side. This recompression consumes shaft work from the expander itself. The isentropic efficiency hardly degrades. If the pressure at expander exit

is lower such that the pressure ratio is higher than the one corresponding to the built-in volume ratio, then the working fluid expands too little within the expander, and it has to reduce its pressure by throttling at the exit port in order to reach the pressure boundary condition. This process represents an additional irreversibility, because the fluid pressure is wasted. The isentropic efficiency degrades slowly in this regime.

6.1.4 Experimented ORCs

The ORC testing system developed in this work allows for determination of boiler and expander operation in their joint operation within the Rankine cycle. The heat source is hot air. As explained in the System Description section, there is no condenser and pump installed on the system. Rather, the working fluid is pressurized using a condensing unit that comprises of a compressor and condenser. An additional heat exchanger is installed to cool the working fluid prior to boiling. Therefore, the experimentation allows for measurements of the preheating, boiling, superheating and expansion processes. Based on this experimental information, it is possible to determine the energy and exergy efficiency of the Rankine cycle. In this respect, it is assumed that after the expander outlet, a condenser is installed that sub-cools the working fluid with 5°C.

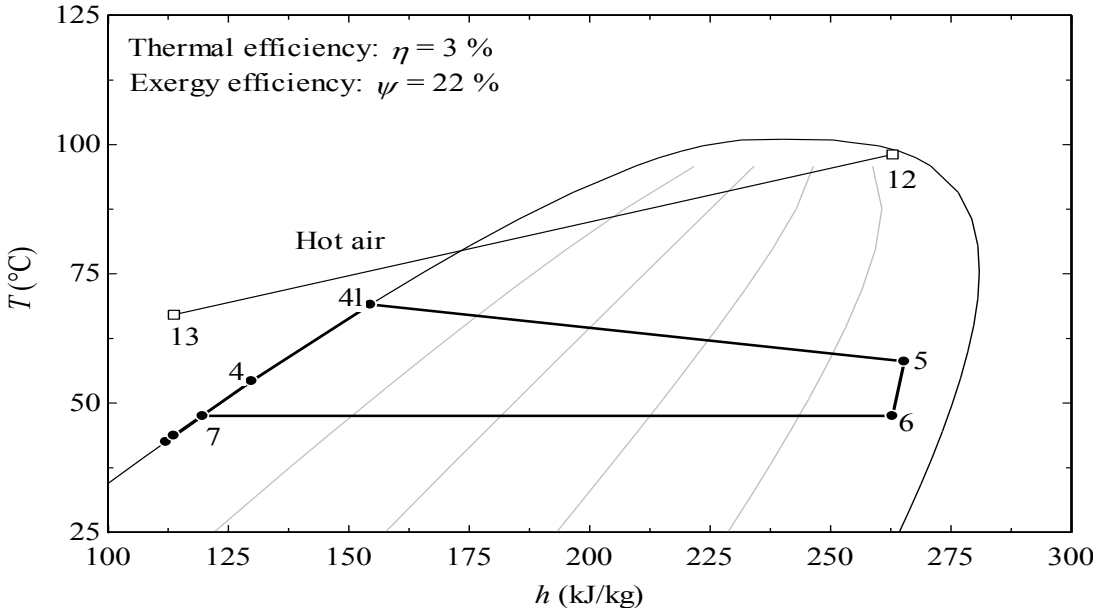

Figure 6.29 The ORC with two-phase expansion.

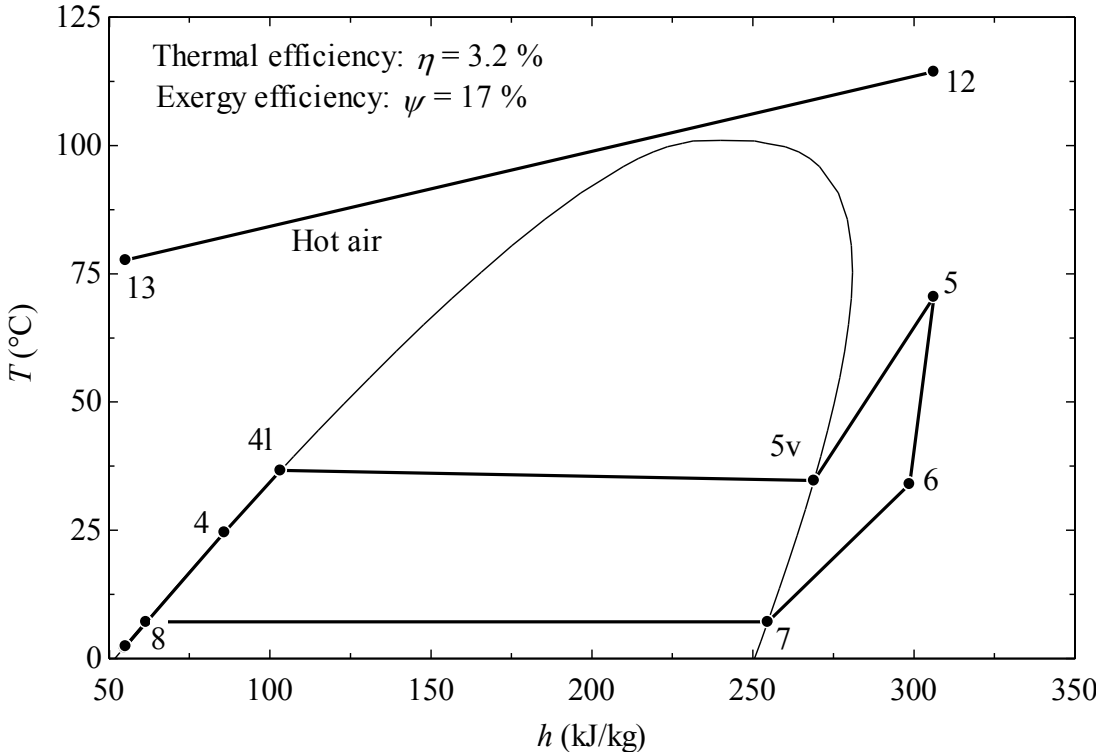

Figure 6.30 The ORC with superheated flow expansion.

The sub-cooling is necessary to allow for a better pump operation. The isentropic efficiency of the pump is assumed, conservatively, as 0.5. Two cycles are presented in Figures 6.29 and 6.30.

It is interesting to remark that both the two phase and superheated cycles have the same energy efficiency as calculated by

$$\eta = \frac{\dot{W}_{\text{exp}} - \dot{W}_{\text{pump}}}{\dot{Q}_{\text{in}}} \tag{6.5}$$

where, $\dot{Q}_{\text{in}}$ represents the total heat added to the cycle for preheating and boiling.

The efficiency is 3% in both cases. However, the exergy efficiency is higher for the two-phase expansion case with respect to the expansion of the superheated vapour. The two-phase cycle has 5% gain of exergy efficiency. The equation used for exergy efficiency calculation becomes

$$\psi = \frac{\dot{W}_{\text{exp}} - \dot{W}_{\text{pump}}}{\dot{m}_{\text{air}} \times [(h_{12} - h_{13}) - T_0 \times (s_{12} - s_{13})]} \tag{6.6}$$

where the specific enthalpies and entropies correspond to hot air at inlet (12) and outlet (13).

It is also important to observe that for the two phase expansion case, the pressure drop in the boiler is remarkably high. This is probably due to the fact that the load of the generator was not enough for the actual experiment, which resulted in a rather low pressure difference over the expander; consequently, the pressure drop over the boiler was high.

6.2 Case study

Modern society requires many types of commodities to maintain a certain standard of living; electricity, hot water, space heating, synthetic fuels, materials, etc. Traditional methods of producing these commodities are primarily driven by combustion of fossil fuels, which is a major contributor to pollution.

There is a worldwide initiative to develop cleaner, more efficient production methods which are able to replace, or supplement, traditional processes by incorporating sustainable energy sources such as; solar, wind, geothermal, ocean heat, bio-fuels, biomass, municipal waste, recovered industrial waste heat and so on. Most of these sources are available in small capacities in distributed locations. They can be converted to heat and power by using adequate heat engines.

Heat engines using an external heat supply are one of the most promising methods of generating power by utilising the above mentioned sources. In such heat engines, a heat exchanger is used to transfer heat from the external source to the working fluid. This type of heat engine is able to be coupled with a variety of heat sources, is capable of cogeneration, and may be designed for a wide range of generation capacities. In particular, low power capacity heat engines are of interest because of the ability to be coupled with on site renewable sources.

It is important to note that internal combustion heat engines, though available in market from low to high capacities, are limited to a narrower spectrum of heat sources (liquid or gas fuels), as opposed to externally supplied heat engines which are able to use any combustible material, or non-combustible heat sources. However, externally supplied heat engines (ESHE's) are not commercially available in a low capacity power range, though the existing

components specific to refrigeration and HVAC industries create an opportunity to make the ESHE available as a cost-effective, fully assembled, cogeneration unit.

Refrigeration and HVAC (automotive, other) are mature industries which produce a variety of systems such as; building and automotive air conditioners, heating, refrigerators, freezers, etc. These systems utilise components and working fluids applicable to Organic Rankine Cycles (ORCs): evaporators, condensers, expanders, compressors, hermetic pumps, fans, etc. For example, refrigerants such as R134a, and others, can be used as working fluids for low temperature heat sources in ORCs. Evaporators from air conditioners can be used as boilers in ORCs, heated with hot flue gases derived from biomass or bio-fuel combustion. Air cooled condensers from refrigerators can be used as air-cooled condensers in ORCs with cogeneration (i.e. space heating). Scroll and screw compressors can be operated in reverse and applied as expanders with minimal modification. Those are widely available in parts from various suppliers in a variety of arrangements and capacities at competitive pricing. Consequently, low-capacity ORCs may be built as assembled systems for heating and power generation without requiring the design of new components, thus avoiding associated increased costs.

Low-capacity ORCs have the potential to create a parallel to the economy of scale of "many and small" as opposed to "few and large" generators that exist in typical power generation infrastructures. Large scale power plants; coal, nuclear, hydro-electric, etc., generate power to supply a large region, and require a distribution grid to transmit electricity to consumers. Low capacity ORCs are able to generate power locally, and in most cases do not require a grid transmission system. Additionally, these do not require delivery of fuels, combustion materials, etc. at the generation site(s). For example: biomass availability in farming applications, solar heating, geothermal, and industrial waste heat, which are often available on site. Such systems can reduce pollution for a cleaner environment, are immune to black-outs, can be used to charge electric vehicles, and reduce the load on the grid.

It appears that there is a niche market for environmentally responsible power generation on an individual level. Low power ORC cogeneration units using components from the

refrigeration and HVAC industries have potential to fill this niche by providing or proposing a system which may be adapted at this individual level based on locally available heat sources.

In this case study, a low-capacity ORC cogeneration unit running with R134a is demonstrated and can be applied to produce power (1-2 kW) as well as low temperature heat (10-20 kW). The assumed heat source is a hot gas derived from biomass/bio-fuel/bio-gas combustion or heat recovery from exhaust gases. The specific application considered here refers to pool heating and critical power for a community centre.

Additional applications include residential; electrical power up to 24 kWh per day, and heating commodities such as water and space heating, greenhouse heating, crop drying for farming, seasonal thermal storage in summer for various winter heating applications including radiant floor heating, driveway heating, and so on.

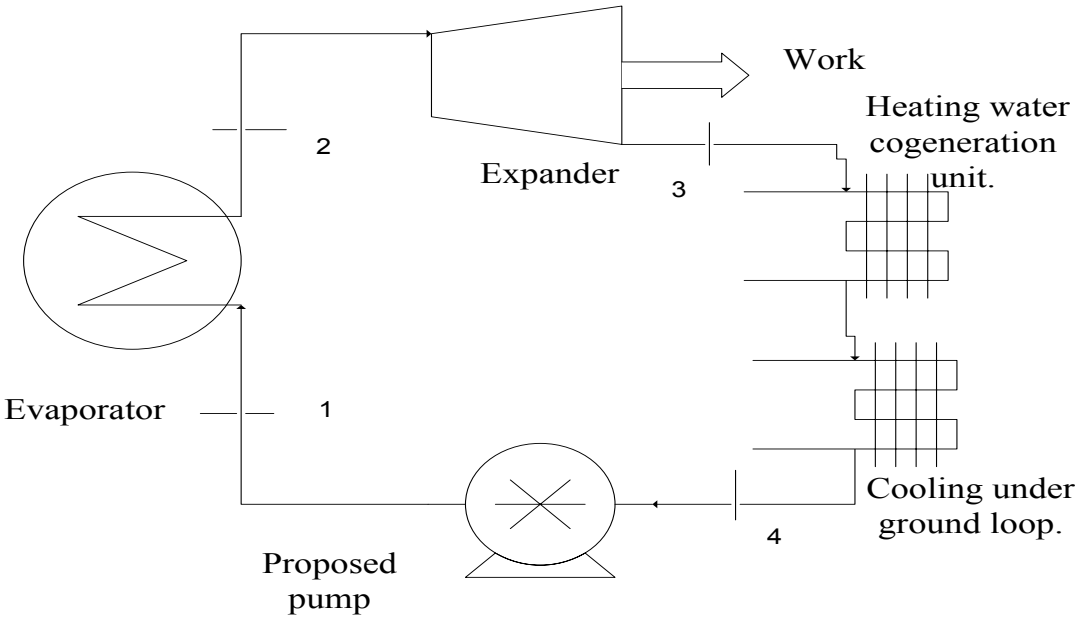

Figure 6.31 ORC cycle with reciprocating pump.

Table 6.7 List of ORC components and their characteristics.

Equipment	Manufacturer/Model	Characteristics
Pump	Hydra-Cell® D-03-B	- Positive disp. Reciprocating pump - Flow range: 0.1-1.1 Gpm (0.4-4.2 Lpm) - Shaft speed: 100-1750 RPM - Max. Discharge pressure = 1200 psi (70 bar)
	Hydra-Cell® M100TE18F3P143T	- Footed, 3 phase - Horsepower, Hp = 1 hp - 10:1 turndown ratio
Boiler		- Finned-tube, cross flow heat exchanger - 13 fpi - Fin thickness = 0.008 in - Overall heat transfer coefficient, US = 0.0436 kW/K (based on 3.6 kW source)
Expander	Bitzer ECH209Y-02G	- reversed-operation Scroll compressor - Optimal pressure ratio (experimental), $p_r = 2.5$ - built in vol ratio - generator info
Condenser	Scmidt SB5-20	- Brazed plate heat exchanger - Max. Capacity = 5 tons (17.58 kW) - Overall heat transfer coefficient, US = 1.927 kW/K

At present, an ORC test bench has been built with a compressor, condenser, evaporator and expander with other required accessories and piping. The specification of the compressor, condenser, evaporator (boiler) and expander has been described in detail in Chapter 4. As per the scope of the test bench design and selected design parameters, the overall cycle analysis has been done in the Chapter 5.

In this section, the case study will be done with proposed reciprocating pump which may replace the presently used compressor unit as shown in the Figure 6.31. Also presently used hot air will be replaced with exhaust gas, which could be derived from an engine exhaust, biomass combustible, industrial waste gas and so on. The heating properties of the exhaust will be little bit higher than the hot air. Presently, we can assume the heat input considering

with engineering judgement. The list of the main component of the ORC cycle is presented in Table 6.7.

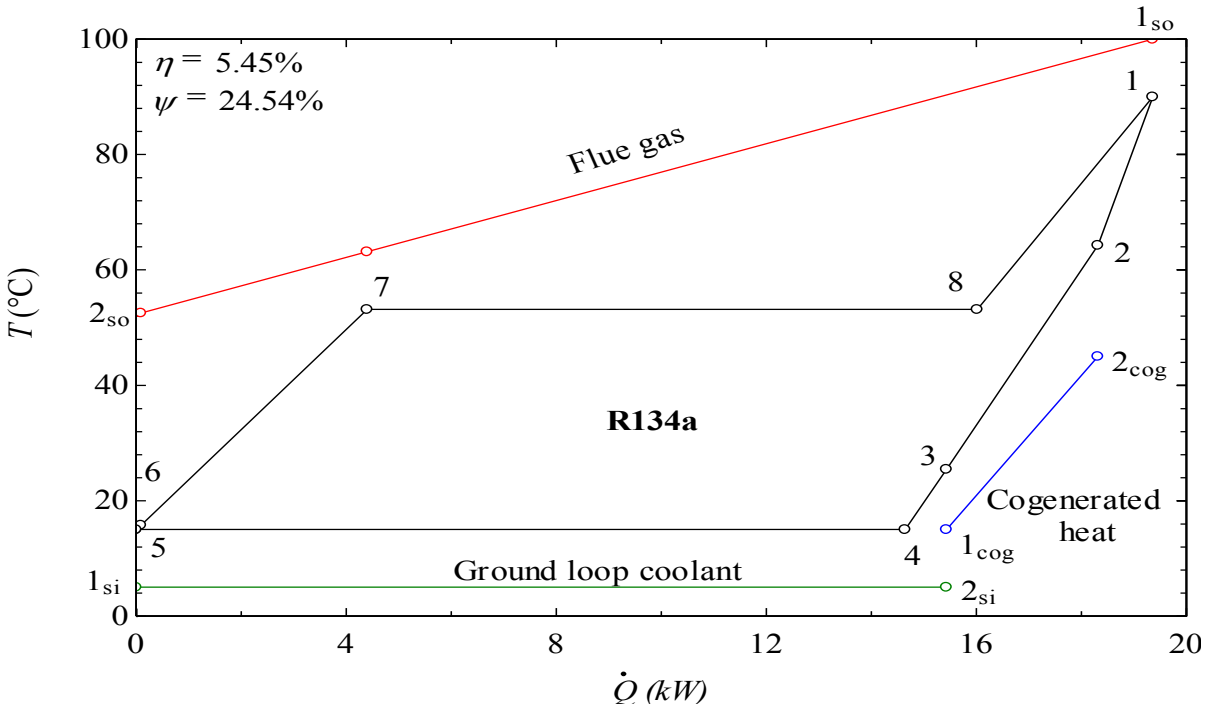

Figure 6.32 *T*-$\dot{\boldsymbol{Q}}$ diagram for the case study.

Pump: A positive displacement reciprocating pump with a variable speed motor will control the volumetric flow rate of the working fluid. The variable speed operation will be achieved by including a variable frequency drive in order to control the rotational speed of the motor shaft. The pump speed is directly controlled by the shaft speed of the motor.

Considering the state properties value from Table 5.4 and heat and work values of the components in Table 5.5, the following heat and work duties were calculated:

- Total heater input in the system: $\dot{Q}_{exhaust}$ = 39.6 kW
- Heat input to boiler: $\dot{Q}_{boiler}$ = 32.4 kW
- Pump work: $\dot{W}_{pump}$ = 0.20 kW
- Condenser: $\dot{Q}_{cond}$ = 34.14 kW (cogenerated)
- Heat exchanger: $\dot{Q}_{h.ex}$ = 2.033 kW
- Expander work: $\dot{W}_{exp}$ = 1.28 kW

- Net work output: $\dot{W}_{\text{net}}$=1.18 kW

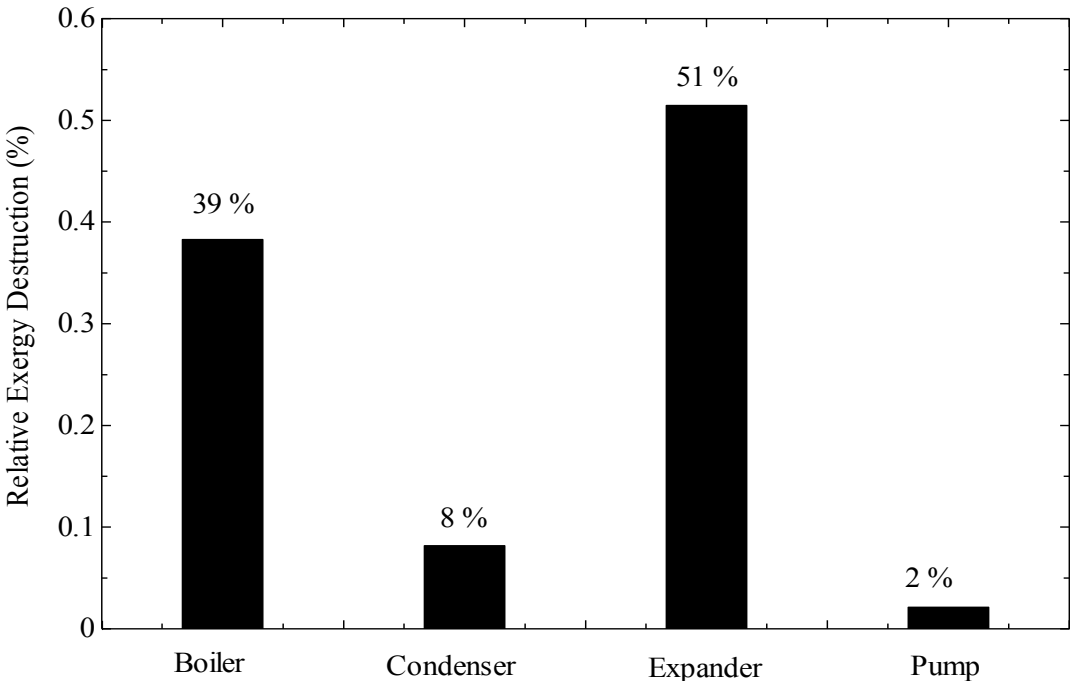

Figure 6.33 Relative exergy destruction for each component of the heat engine.

The thermodynamic cycle and the energy and exergy efficiency is indicated in Figure 6.32. The exergy destructions for each component are indicated in a bar chart in Figure 6.33. The maximum exergy destruction occurs at the expander with 51% and the second maximum is at the boiler with 39%. The exergy destruction at the condenser and boiler are reasonably low.

CHAPTER 7: CONCLUSIONS AND RECOMENDATION FOR FUTURE WORK

7.1 Conclusions

The experimental investigation of the ORC with external multi-pass finned tube type heat exchanger (boiler) to boil the working fluid R134a and modified scroll type expander has been performed in a optimised designed closed loop air duct test bench. The test bench set-up made it possible to acquire a set of well-defined experimental data with a variable electric load, working fluid flow rate, cooling water flow rate heating source and air flow rate. A total number of forty-fives experiments have been conducted; twenty eight of them were with 2400 watt heating source, eight experiments with 6303 watt heating source and nine experiment performed with 7800 heating source.

Some of the tests were done with small air blower in the closed loop air duct and others are with a bigger blower.

Some data was collected with working fluid sub cooling on and some of them sub cooling off. The working fluid flow rate was controlled with the by-pass valve during the experiments. During the test, the electric load was changed as required.

The collected data set represents a very interesting relationship with the air temperature and working fluid temperature with the quality level.

The Organic Rankine Cycle test bench was designed in a unique configuration that implied a wide range of operating parameters to evaluate the performance of the scroll expander more precisely. The parameters that influence the expander operation are inlet temperature, inlet pressure, mass flow rate, degree of superheat, and electrical load to the generator. The experimental result shows a maximum isentropic efficiency of 80% and an overall energy efficiency of maximum 3% at boiler LMTD 40°K, while the exergy efficiency is about 20%. These test results show that two phase region expansion is more appropriate than that of the superheated region.

Initially, difficulties arose in controlling the boiler working fluid temperature with the small air blower, which was changed and further tests and investigations were conducted. Another problem met was in measuring the working fluid flow rate with the flow meter. The flow meter creates a tremendous pressure drop in the piping system. As a result, it was disassemble6d from the test bench and the flow rate was calculated analytically.

Despite the few difficulties, the overall performance of the blower, boiler and expander in the Rankine cycle was in good agreement with the modelled and the predicted value.

7.2 Recommendation for future work

A few recommendations are brought to the attention of future researchers for further investigation and improvement of such systems:

- There is a strong need to work for improvement of experimental set up with the sizing of the air duct and air blower.
- For higher power output, more heating sources and electric loads can be added for further investigation.
- An automated airflow and temperature measurements will help give more accurate results.
- Replacing the compressor with a suitable pump will give an opportunity for further improvement of the system performance.
- Further work is required to select more suitable working fluids for two phase region expansion tests.

REFERENCES

ASES. 2007. ASES Report: Renewable Energy Can Curb Global Warming by 2030. Internet source http://www.renewableenergyworld.com/rea/news/article/2007/02/ases-report-renewable-energy-can-curb-global-warming-by-2030-47351, accessed at June 19th , 2011.

Badr O., O'Callaghan P.W., Hussein M., Probert S.D. 1984. Multi-vane expanders as prime movers for low-grade energy organic Rankine-cycle engines. Applied Energy 16:129-146.

Boehm C., Starflinger J., Schulenberg T., Oeynhausen H. 2005. Supercritical Steam Cycle for Lead Cooled Nuclear Systems. Proceeding of GLOBAL Conference, Tsukuba, Japan paper #035.

Bombarda P., Invernizzi C.M., Pietra C. 2010. Heat recovery from Diesel engines: A thermodynamic comparison between Kalina and ORC cycles. Applied Thermal Engineering 30:212-219.

Borsukiewicz-Gozdur A., Nowak W. 2007. Comparative analysis of natural and synthetic refrigerants in application to low temperature Clausius–Rankine cycle. Energy 32:344-352.

Brasz J.J., Biederman B.P., Holdman G. 2005. Power production from a moderate-temperature geothermal source. GRC Annual Meeting, Reno NV, September 25-28.

Bush J.W., Beagle W.B. 1992. Derivation of general relationship governing the conjugacy of scroll profiles. Proceedings of International Compressor Engineering Conference at Purdue 1079-1088.

Chen Y., Halm N.P., Groll E.A., Braun J.E. 2002. Mathematical modeling of scroll compressors-part I: compression process modeling. International Journal of Refrigeration 25:731-750.

Chen, Y., Lundqvist, P., Johansson, A., Platell, P. 2006. A comparative study of the carbon dioxide transcritical power cycle compared with an organic Rankine cycle with R123 as working fluid in waste heat recovery. Applied Thermal Engineering 26:2142-2147.

Colonna P., Nannan N.R., Guardone A., Lemmon E.W. 2006. Multiparameter equations of state for selected siloxanes. Fluid Phase Equilibria 244:193–211.

Colonna P., Guardone A., Nannan N.R., Zamfirescu C. 2008. Design of the dense gas flexible asymmetric shock tube, Journal of Fluids Engineering. 130/034501:1-6.

Congress G.C. 2010. Hyundai Introduces New Tucson/ ix35 Hydrogen Fuel Cell Electric Vehicle. Internet source http://www.greencarcongress.com/2010/03/hyundai-fcev-20100304.html, accessed at February 9th, 2011.

Corman J.C., Bjorge R.W., Kalina A. 1995. Kalina cycle looks good for combined cycle generation. MPS Review 19–22.

Dai Y., Wang J., Gao L. 2009. Parametric optimization and comparative study of organic Rankine cycle (ORC) for low grade waste heat recovery. Energy Conversion and Management 50:576–582.

Declaye S. 2009. Design, optimisation and modelling of an Organic Rankine Cycle for waste heat recovery. BSc thesis University of Liege, Belgium.

Delgado-Torres M.A., Garcia-Rodriguez L. 2010. Analysis and optimization of the low-temperature solar organic Rankine cycle (ORC). Energy Conversion and Management 51:2846-2856.

Desideri U., Bidini G. 1997. Study of possible optimization criteria for geothermal power plants. Energy Conversion and Management 38:1681–1691.

Dincer I., Al-Muslim H. 2001. Thermodynamic analysis of reheat cycle steam power plants. International Journal of Energy Research 25:727-739.

Dincer I., Rosen M.A. 2007. Exergy: energy, environment and sustainable development. Elsevier Science, London.

Engin T., Ari V. 2005. Energy auditing and recovery for dry type cement rotary kiln systems – A case study. Energy Conversion and Management 46:551–562.

Fraas, A. 1982. Engineering evaluation of energy systems. New York: McGraw-Hill.

Harada K. 2007. Development of a small scale scroll expander. Master of Science Thesis. Oregon State University.

Harinck J., Turunen-Saaresti T., Colonna P, van Buijtenen J. 2010. Computational study of a high-expansion ratio radial ORC turbine stator. Journal Engineering of Gas Turbines and Power 132:054501.

Harr H., Gallagher G., Kell K. 1984. NBS/NRC Steam Tables, Hemisphere Publishing Co.

Hettiarachchi H.D., Golubovic M., Worek W.M., Ikegami Y. 2007. The Performance of the Kalina Cycle System 11(KCS-11) With Low-Temperature Heat Sources. Journal of Energy Resources Technology 129:243.

Hung T. 1997. A review of organic Rankine cycles (ORCs) for the recovery of low-grade waste heat. Energy 22:661-667.

Hung T.C. 2001. Waste heat recovery of organic Rankine cycle using dry fluids. Energy Conversion and Management 42: 539-553.

Husband W.W., Beyene A. 2008. Low-Grade Heat-Driven Rankine Cycle, A Feasibility Study. International Journal of Energy Research 32:1373-1382.

Hyland H., Wexler W. 1983. Formulations for the Thermodynamic Properties of the Saturated Phases of H2O from 173.15 K to 473.15 K, ASHRAE Transactions, Part 2A, Paper 2793 (RP-216).

Infante Ferreira C.A., Zamfirescu C., Zaytsev D. 2006. Twin screw oil-free wet compressor for compression–absorption cycle. International Journal of Refrigeration 29:556–565.

Jaffe L.D. 1989. Test Results on Parabolic Dish Concentrators for Solar Thermal Power Systems. Solar Energy 42:173-187.

Kalina A. 1984. Combined-cycle system with novel bottoming cycle. Journal of engineering for gas turbines and power. 106:737-742.

Kalina A.L., Tribus M., El-Sayed Y.M. 1986.A Theoretical Approach to the Thermophysical Properties of Two-Miscible-Component Mixtures For the Purpose of Power-Cycle Analysis. Proceedings of the Winter Annual Meeting ASME, Anaheim, California, December 7-12, paper 86-WA/HT-54.

Kane M., Larrain D., Favrat D., Allani Y. 2003. Small hybrid solar power system. Energy 28:1427-1443.

Kim H. J., Lee E.S., Joo N.S., Rha P.C. 2001. Design of scroll expander. In: Proceedings of the 3rd International Compressor Technique Conference, Wuxi City 261–267.

Khennich M., Galanis N. Performance Limits of Power Cycles Using Low Temperature Heat Sources. Proceedings of the 5th IASME/WSEAS International Conference on Energy and Environment, University of Cambridge UK, February 23-25, 124-128.

Klein S.A. 2010. Engineering Equation Solver (EES). F-Chart Software.

Koji T., Suguru F., Kiyoshi S., Tooru S., Hirotoshi S., Mitsunobu M. 2004. Heat Recovery Power Generation by Rankine Cycle with Ammonia Working Fluid. Hitachi Zosen Technical Review 65:6-9.

Kongtragool B., Wongwises S. 2003. A review of solar-powered Stirling engines and low temperature differential Stirling engines. Renewable and Sustainable Energy Reviews 7:131–154.

Lariola J. 1995. Electricity from industrial waste heat using high speed organic Rankine cycle (ORC). International Journal of Production Economics 41:227-235.

Latour S.R., Menningmann J.G., Blaney B.L. 1982. Waste Heat Recovery Potential in Selected Industries. US Environmental Protection Agency – Industrial Environmental Research Laboratory Report # EPA-600/S7-82-030.

Lemmon E.W., Jacobsen R.T., Penoncello S.G., Friend D. 2000. Thermodynamic Properties of AIr and Mixtures of Nitrogen, Argon, and Oxygen from 60 to 2000 K at Pressures to 2000 MPa. J.Phys.Chem. Ref. Data, Vol. 29, No. 3.

Lemort V., Quoilin S., Cuevas C., Lebrun J. 2009. Testing and modeling a scroll expander integrated into an Organic Rankine Cycle. Applied Thermal Engineering 29:3094–3102

Mago P.J., Chamra L.M., Somayaji C. 2007. Performance analysis of different working fluids for use in organic Rankine cycles. Proceedings of the Institution of Mechanical Engineers, Part A: Journal of Power and Energy 221:255-263.

Mago P.J., Chamra L.M., Srinivasan K., Somayaji C. 2008. An examination of regenerative organic Rankine cycles using dry fluids. Applied thermal engineering 28:998-1007.

Manolakos D., Papadakis G., Kyritsis S., Bouzianas K. 2007. Experimental evaluation of an autonomous low-temperature solar Rankine cycle system for reverse osmosis desalination. Desalination 203:366-374.

Manolakos D., Kosmadakis G., Kyritsis S., Pa G. 2009. Identification of behaviour and evaluation of performance of small scale, low-temperature Organic Rankine Cycle system coupled with a RO desalination unit. Energy 34:767-774.

Marston C.H. 1990. Parametric analysis of the Kalina cycle. Journal of Engineering for Gas Turbines and Power 112:107–116.

Mathias J.A., Johnston J.R.Jr., Cao J., Priedeman D.K, Christensen R.N. 2009. Experimental Testing of Gerotor and Scroll Expanders Used in, and Energetic and ExergeticModeling of, an Organic Rankine Cycle. Journal of Energy Resources Technology 131/012201:1-9.

Maurer T., Zinn T. 1999. Experimentelle Untersuchung von Entspannungsmaschinen mit mechanischer Leistungsauskopploung für die transkritische CO_2-Käeltemaschine. DKV-Tagungsbericht 26.

McNicol B.D., Rand D.A.J., Williams K.R. 2001. Fuel cells for road transportation purposes-yes or no? Journal of Power Sources100: 47-59.

Miller E.W., Hendricks T.J., Peterson R.B. 2009. Modeling energy recovery using thermoelectric conversion integrated with an organic Rankine bottoming cycle. Journal of Electronic Materials 38:1206-1213.

Mustafah M., Yamada N. 2010. Efficiency of Compact Organic Rankine Cycle System with Rotary-Vane-Type Expander for Low-Temperature Waste Heat Recovery. Journal of Thermal Science and Technology 5:61-74.

Md. Ali Tariq, 2010, Thesis on Experimental Investigation of Scroll Based Organic Rankine Systems, UOIT.

Nagatomo S., Ootaka T., Morishima A. 1999. Effects of operating conditions on expander performance characteristics. Transaction of Japanese Society of Refrigeration and Air Conditioning Engineers 16:59-66.

NRC. 2009. Canmet ENERGY. Natural Resources Canada. Internet source http://canmetenergy-canmetenergie.nrcan-rncan.gc.ca/eng/renewables/wind_energy/trm.html, accessed at February 9th , 2011.

NRC. 2010. Renewable energy. Natural Resources Canada. Internet source http://www.nrcan.gc.ca/eneene/renren/aboaprren-eng.php, accessed at February 9th , 2011.

Oralli E., Tarique Md.A., Zamfirescu C., Dincer I. 2010. Modeling and Analysis of Scroll Compressor conversion into Expander for Rankine Cycle. Second International Conference on Nuclear and Renewable energy resources. Ankara July 4-7.

Oralli E., Tarique Md.A., Zamfirescu C., Dincer I. 2010b. A Study on Scroll Compressor Conversion into Expander for Rankine Cycles. International Journal of Low Carbon Technology, In Press.

Papadopoulos A.I., Stijepovic M., Linke P. 2010. On the systematic design and selection of optimal working fluids for Organic Rankine Cycles. Applied Thermal Engineering 30:60–769.

Park Y.M., Sontag R.E. 1990. A preliminary study of the Kalina power cycle in connection with a combined cycle system. International Journal of Energy Research 14:153–162.

Peterson R.B., Wang H., Herron T. 2008. Performance of a small-scale regenerative Rankine power cycle employing a scroll expander. Proceedings of the Institution of Mechanical Engineers, Part A - Journal of Power and Energy 222/A3:271-82.

Pouraghaie M., Atashkari K., Besarati S.M., Nariman-zadeh N. 2010. Thermodynamic performance optimization of a combined power/cooling cycle. Energy Conversion and Management 51:204–211.

Prins J., Zaytsev D. 2001. Prediction of Injection Flow Rates in Twin-Screw Compressor Systems. IMechE Conference Transactions 7th International Conference on Compressors and their Systems, City University, London, UK 43-51.

Puff R., Krueger M. 1992. Influence of the main constructive parameters of a scroll compressor on its efficiency. Proceedings of the International Compressor Engineering at Purdue 107-118.

Quoilin S. 2007. Experimental study and modelin of a low temperature Rankine cycle for small scale cogeneration. BSc Thesis, Liege University, Belgium.

Quoilin S., Lemort V., Lebrun J. 2010. Experimental study and modeling of an Organic Rankine Cycle using scroll expander. Applied Energy 87:1260–1268.

Rajput P. K. 2007. Engineering thermodynamics 3rd Eds. Laxmi Publications, Boston.

Roy P., Desilets M., Galanis N., Nesreddine H., Cayer E. 2009. Thermodynamic analysis of a power cycle using a low temperature source and a binary NH_3–H_2O mixture as working fluid. International Journal of Thermal Sciences 49:48–58.

Saitoh T., Yamada N., Wakashima S. 2007. Solar Rankine Cycle System Using Scroll Expander. Journal of Environment and Engineering 2:708-719.

Saleh B., Koglbauer G., Wendland M., Fischer J. 2007. Working fluids for low temperature organic Rankine cycles. Energy 32:1210-1221.

Schuster A., Karellas S., Kakaras E., Spliethoff H. 2009. Energetic and economic investigation of Organic Rankine Cycle applications. Applied thermal engineering 29:1809 -1817.

Schuster A., Karellas S., Aumann R. 2010. Efficiency optimization potential in supercritical Organic Rankine Cycles. Energy 35:1033-1039.

Sesto E., Casale C. 1998. Exploitation of wind as an energy source to meet the world's electricity demand. Journal of Wind Engineering and Industrial Aerodynamics 74-76:375-387.

Simon T.W., Seume J.R. 1990. The Stirling Engine: An Engine that Requires High-Flux Heat Exchange under Oscillating Flow Conditions. Compact Heat Exchangers, R.K. Shah, A.D. Kraus, and D. Metzger, eds. Hemisphere Publishing, New York, 567-626.

Smith I.K., Stosic N., Aldis I.K. 1996. Development of the trilateral flash cycle system Part 3: The design of high efficiency two-phase screw expanders. Proceedings of Institute of Mechanical Engineering, Part A, 210(A2):75-93.

Suefuji K., Shiibayashi M., Tojo K. 1992. Performance analysis of hermatic scroll compressor. Proceedings of the International Compressor Engineering at Purdue 75-84.

Shah 1981 Fundamental of heat exchanger design by Ramesh K. Shah and Dusan P. Sekulic.

Tchanche B.F, Papadakos G. Lambrinos, G. Frangoudakis, A. 2008. Criteria for working fluids selection in low-temperature solar organic Rankine cycles. Proceedings of Eurosun Conference, Lisbon, Portugal, 7–10 October.

Thombare D.G., Verma S.K. 2008. Technological Development in the Stirling Cycle Engines. Renewable and Sustainable Energy Reviews 12:1-38.

Tillner-Roth R., Baehr H.D. 1994. An International Standard Formulation for the Thermodynamic Properties of 1,1,1,2-Tetrafluoroethane (HFC-134a) for Temperatures from 170 K to 455 K and Pressures up to 70 MPa, J. Phys. Chem, Ref. Data, Vol. 23, No. 5.

Tojo K., Igekawa M., Maeda N., Machiela S., Shiibayashi M., Uchikiawa N. 1986. Computer modeling of scroll compressor with self-adjusting back-pressure mechanism. Proceedings of the International Compressor Engineering at Purdue 872-886.

Tsiklauri G., Talbert R., Schmitt B., Filippov G., Bogoyavlensky R., Grishanin E. 2005. Supercritical steam cycle for nuclear power plant. Nuclear Engineering and Design 235:1651–1664.

Uehara H., Ikegami Y. 1993. Parametric performance analysis of OTEC using Kalina cycle. Joint Solar Engineering Conference, ASME:203-207.

UOC-UCCP. 2009. Non-renewable energy sources. Internet source http://cnx.org/content/ m16730/1.2, accessed at February 9th , 2011.

Wagar W.R., Zamfirescu C., Dincer I. 2010. Thermodynamic Performance Assessment of an Ammonia-Water Rankine Cycle for Power and Heat Production. Energy conversion and management 51:2501-2509.

Wang B., Li X., Shi W. 2005. A general geometrical model of scroll compressors based on discretional initial angles of involute. International Journal of Refrigeration 28:958-966.

Wang C., Chi K., Chang C. 2000. Heat transfer and friction characteristics of plain fin-and-tube heat exchangers, part II: Correlation. In: International Journal of Heat and Mass Transfer, Volume 43, Pages 2693-2700.

Wang X., Zhao L., Wang J., Zhang W., Zhao X., Wu W. 2010. Performance evaluation of a low-temperature solar Rankine cycle system utilizing R245fa. Solar Energy 84:353-364.

Yamaguchi H., Zhang X.R., Fujima K., Enomoto M., Sawada N. 2006. Solar energy powered Rankine cycle using supercritical CO_2. Applied Thermal Engineering 26:2345-2354.

Yamamoto T. 2001. Design and testing of the organic Rankine cycle. Energy 26:239-251.

Yanagisawa T., Shimizu T., Fukuta M., Handa T. 1988. Study on fundamental performance of scroll expander. Japanese Society of Mechanical Engineers 54:2798-2803.

Yougub W., Doherty P., Riffat S. 2006. Solar energy gas-driven micro-CHP system for an office building. Applied thermal engineering 26:1604-1610.

Zamfirescu C., Dincer I. 2008. Thermodynamic analysis of a novel ammonia-water trilateral Rankine cycle. Thermochimica Acta 477:7-15.

Zamfirescu C., Guardone A., Colonna P. 2008. Admissibility region for rarefaction shock waves in dense gases. Journal Fluid Mechanics 599:363–381.

Zamfirescu C., Dincer I., Stern M., Wagar W.R. 2010. Exergetic, environmental and economic analyses of small-capacity concentrated solar-driven heat engines for power and heat cogeneration. International Journal of Energy Research DOI: 10.1002/er.1811.

Zanelli R., Favrat D. 1994. Experimental investigation of a hermetic scroll expander-generator. In: Proceedings of International Compressor Engineering Conference, Purdue, 459–46.

APPENDIX: EES code for test runs.

```
//Fig6.5 - boiler with not enough air flow, worse regime
R$='R134a'
T4=46.4
T5=41.3
T12=93
T13=51.3
P2=(174+14.7)*convert(psi,kPa)
P5=(140+14.7)*convert(psi,kPa)
P6=(90+14.7)*convert(psi,kPa)
P7=(65+14.7)*convert(psi,kPa)
Qheater=2.4
Vdc=8.5
I=6.8

//Assumed heat lost by the air
Qlost=z*Qheater
z=0.1
//heat transferred to the working fluid
Qtransf=Qheater-Qlost
//Heat balance on air side
Qtransf=mAir*dhAir
dhAir=h12-h13
h12=enthalpy(air_ha,T=T12,P=Po#)
h13=enthalpy(air_ha,T=T13,P=Po#)
rhoAir13=density(air_ha,T=T13,P=Po#)
VdotAir=mAir/rhoAir13
Vair=VdotAir/Aduct
Aduct=10^2*convert(in^2,m^2)
//State at refrigerant outlet
Tsat5=T_sat(R$,P=P5)
//dT wall fluid at boiler outlet
dTwOut=Tsat5-T5
//if dTwOut is lower than ~1 then saturated flow
//Assume P4 between P2 and P5
Tsat2=T_sat(R$,P=P2)
//Assume saturation in 4
P4=P_sat(R$,T=T4)
//Estimate pressure drop across the

//Throttling after expander + heat addition (1.1)
h6=h7
T6=T_sat(R$,P=P6)
x6=quality(R$,P=P6,h=h6)
//Balance on expander
Wdc=Vdc*I
etaRect=Vdc/(Vdc+1.2)
Wac*etaRect=Wdc
etaELM=0.9
Wexp*etaELM=Wac/1000
//Energy Balance on boiler+heater
m*(h6-h4)=Qtransf-Wexp
//energy balance on boiler, refrigerant side
m*(h5-h4)=Qtransf
x5=quality(R$,P=P5,h=h5)
//condenser duty
Qcond=m*(h1-h2)
h2=enthalpy(R$,P=P2,x=0)
VdotAirCond=4*10^2*convert(in^2,m^2)
mDotAirCond=VdotAirCond*density(air_ha,T=25,P=Po#)
Qcond=mDotAirCond*dhAirCond
dhAirCond=h2AirCond-enthalpy(air_ha,T=25,P=Po#)
T2AirCond=temperature(air_ha,P=Po#,h=h2AirCond)

//Boiler heat transfer
dTb1=T12-T5
dTb2=T13-T4
dTbMax=max(dTb1,dTb2)
dTbMin=min(dTb1,dTb2)
LMTD*ln(dTbMax/dTbMin)=dTbMax-dTbMin
Qtransf=UAboiler*LMTD

//Show the cycle
//compressor suction
T[1]=T7
s[1]=s7
//compressor discharge
T[2]=T1
s[2]=entropy(R$,P=P2,T=T1)
//Sat vapor
T[3]=Tsat1
```

```
boiler
dPboiler=P4-P5
//Calculate h4 for saturation
h4=enthalpy(R$,T=T4,x=0)
//Assume a value for superheating
at compressor discharge
dTsupC=10
Tsat1=T_sat(R$,P=P2)
T1=Tsat1+dTsupC
//Compressor discharge
h1=enthalpy(R$,T=T1,P=P2)
v1=enthalpy(R$,T=T1,P=P2)
//Compressor suction
s7=entropy(R$,P=P7,h=h7)
h1s=enthalpy(R$,P=P2,s=s7)
h1s-h7=etaC*(h1-h7)
etaC=0.6
T7=temperature(R$,P=P7,h=h7)
Tsat7=T_sat(R$,P=P7)
x7=quality(R$,P=P7,h=h7)
Wcomp=m*(h1-h7)
s[3]=entropy(R$,P=P2,x=1)
//Sat liq
T[4]=T4
s[4]=entropy(R$,T=T4,x=0)
//Bolier out
T[5]=T5
s[5]=entropy(R$,P=P5,h=h5)
//Expander out
T[6]=T6
s[6]=entropy(R$,P=P6,h=h6)
//Compressor inlet
T[7]=T7
s[7]=s7

//T-Q diagram boiler
Q[1]=0
Q[2]=Qtransf
Tb[1]=T[4]
Tb[2]=T[5]
Ta[1]=T13
Ta[2]=T12
```